Observations of particulate organic carbon and particulate assemblages from remote sensing in contrasted coastal waters

Trung Kien Tran

To cite this version:

Trung Kien Tran. Observations of particulate organic carbon and particulate assemblages from remote sensing in contrasted coastal waters. Earth Sciences. Université du Littoral Côte d'Opale, 2020. English. NNT : 2020DUNK0589 . tel-03328588

HAL Id: tel-03328588
https://theses.hal.science/tel-03328588

Submitted on 30 Aug 2021

THÈSE
DE L'UNIVERSITÉ DU LITTORAL CÔTE D'OPALE

Laboratoire d'Océanologie et de Géosciences

Présentée par
TRUNG KIEN TRAN

Pour obtenir le grade de Docteur en
SCIENCES DE LA TERRE, DE L'UNIVERS ET DE L'ESPACE: TERRE SOLIDE ET ENVELOPPES SUPERFICIELLES

Sujet de thèse

Observation du carbone organique particulaire et des assemblages de particules par télédétection dans les eaux côtières contrastées.

Soutenue le 16 Juin 2020
devant le jury composé de

Mr. David Doxaran, CNRS, LOV, France	Rapporteurs
Mr. Robert Frouin, CASPO, SIO, UC San Diego, USA	Rapporteurs
Mr. Bertrand Lubac, Université de Bordeaux, EPOC, France	Membres de jury
Mr. François Schmitt, CNRS, LOG, France	Membres de jury
Mr. Hubert Loisel, ULCO, LOG, France	Directeur de thèse
Mme. Lucile Duforêt-Gaurier, ULCO, LOG, France	Co-Directeur de thèse

DISSERTATION
UNIVERSITÉ DU LITTORAL CÔTE D'OPALE
Laboratoire d'Océanologie et de Géosciences

By
TRUNG KIEN TRAN

Submitted in partial fulfillment of the requirements for the degree of Doctor in
IN SCIENCES OF EARTH AND UNIVERSE, SPACE: SOLID EARTH AND SURFACE ENVELOPMENT

Subject
Observations of particulate organic carbon and particulate assemblages from remote sensing in contrasted coastal waters.

Defended on 16th June 2020
for the dissertation committee composed of

Mr. David Doxaran, CNRS, LOV, France	Reporter
Mr. Robert Frouin, CASPO, SIO, UC San Diego, USA	Reporter
Mr. Bertrand Lubac, Université de Bordeaux, EPOC, France	Reviewer
Mr. François Schmitt, CNRS, LOG, France	Committee member
Mr. Hubert LOISEL, ULCO, LOG, France	Promoter
Ms. Lucile Duforêt-Gaurier, ULCO, LOG, France	Co-Promoter

Acknowledgements

First and foremost, I would like to express my sincere thanks to my supervisors Professor. Hubert Loisel, Assistant Professor Lucile Duforêt-Gaurier for their ongoing encouragement, patience, careful guidance, and invaluable advice to enable me to complete this work. They have generously given their time and support for my PhD studies.

My PhD research program would not have been possible without the financial support from the Université du Littoral-Côte d'Opale and the Hauts-de-France region. This study was realized with the support from the French Space Agency (CNES) through the COYOTE project (CNES/TOSCA program).

I thank the members of the dissertation committee: Vincent Vantrepotte, Hervé Claustre, Bertrand Lubac for their time and constructive advices. I would like to thank Bertrand Lubac, David Doxaran, Robert Frouin for evaluating and reviewing this work.

My special thanks go to all administrative staff of LOG and the Doctoral School of The Université du Littoral-Côte d'Opale for their helpful support. I also wish to acknowledge the supports of Physical Oceanography, Transport, and Remote Sensing team of LOG: Cedric Jamet, Xavier Mériaux, Arnaud Cauvin, David Dessailly, and Daniel Schaffer Ferreira Jorge.

The authors are grateful to all the people that contributed to data provided by the Service d'Observation en Milieu Littoral (SOMLIT), INSU-CNRS. We thank also our many colleagues, who participated in the collection of various datasets cited in this study. We thank the PIs of the AERONET sites for their continuous efforts in providing high quality measurements. Special thanks go to GlobCoast project (ANR 2011 BS56018 01) for supporting and providing satellite products.

I have always received encouragement and support from friends and colleagues during my PhD research program Bonelli Ana Gabriela, Rachik Sara, and Ngoc Dat Dinh, friends, who have shared their experience and provided invaluable advice for my research.

Last but not least, my huge thanks to my wife Phương for taking care of my family, my children in Viet Nam during my PhD's time in France.

Abstract

Inversion of ocean color radiometry satellite data allows the estimation of a variety of biogeochemical parameters. Past studies have for instance demonstrated the possibility to estimate the concentration of particulate organic carbon (POC) in the open ocean at global scale with a satisfying accuracy. Estimating POC concentration in coastal waters is a more difficult task than in open waters considering the optical complexity of these contrasted environments, generally characterized by high loads of particles and dissolved substances of mixed (terrestrial and oceanic) origin. The first objective of this work was to develop a novel approach to estimate POC concentration in coastal waters at global scale. For that purpose, an extensive in situ data set covering contrasted bio-optical environments and a large range of POC concentration was used. Twelve existing algorithms were tested. The results show that the performance of historical algorithms depends on the type of water, with an overall low performance observed for mineral-dominated waters. None of the tested algorithms provided satisfactory results over the whole POC range. A novel approach was thus developed based on a maximum band ratio of remote-sensing reflectance (R_{rs}). The performance of this new coastal POC algorithm was found higher than that of the methods previously documented. The large applicability of the developed method was further illustrated at regional scale on the Louisiana continental shelf where the MERIS derived average POC concentrations with the new inversion algorithm were found consistent with those derived from a regional specific model (Le et al., 2016). The second objective of this work was to examine coastal waters classification through different approaches. First, a coastal water type definition based on the shape of the reflectance spectra was proposed using an extended dataset of coincident optical and biogeochemical parameters based on hyperspectral $R_{rs.}$ Six optical water classes were defined providing a finer representation of coastal waters optical properties than that provided with past studies using the same method (e.g. 4 classes by Vantrepotte et al., 2012). Interestingly, a clear definition of the bio-optical/biogeochemical environments associated with the 6 optical classes was obtained, which can be associated with a dilution gradient from the turbid to the clear water environments, is in that respect more clear than the results obtained from 4 classes in Vantrepotte et al. (2012). Another classification of the coastal water masses based on the ratio of POC to suspended particulate matter (POC/SPM) concentration (as proposed by Wozniak et al., 2010) was also re-examined. In practice, new POC/SPM threshold were defined from our extended coastal data set in order to provide a finer partition of the coastal ocean into 3 water types based on the particulate matter pool quality (i.e. mineral-dominated, organic-dominated and mixed waters). The two revised classification approaches were applied to MERIS data over the period 2002-2012 for the Eastern English Channel and Southern North Sea. The spatio-temporal dynamics of the optical water types still remains highly relevant when facing the seasonal changes occurring in the water masses.

Keywords: Particulate organic carbon, ocean color, remote-sensing, coastal waters, bio-optical algorithm, Optical classification, particle assemblage.

Résumé

L’inversion des données issues de la radiométrie couleur de l’eau permet l’estimation d’une variété de paramètres biogéochimiques depuis l’espace. Les études passées ont démontré par exemple, la possibilité d’estimer la concentration en carbone organique particulaire (POC) dans l’océan ouvert avec une précision satisfaisante. Estimer le POC dans les eaux côtières est une tâche plus ardue que dans les eaux du large car il faut considérer la complexité d’environnements contrastés, caractérisés par d’importants contenus en matière particulaire et dissoute d’origines variées (terrestre et océanique). Le premier objectif de cette thèse était de développer un algorithme pour estimer la concentration de POC dans les eaux côtières. Dans ce contexte, nous avons rassemblé des mesures in situ afin de disposer d’un vaste jeu de données couvrant des environnements bio-optiques contrastés et une large gamme de concentrations de POC. Douze algorithmes déjà existants, ayant été développés pour des régions précises, ont été testés. Les résultats montrent que la performance des algorithms existants dépend du type d’eau, avec globalement une performance faible pour les eaux dominées par les minéraux. Aucun des algorithmes testés ne fournit une précision satisfaisante sur l’ensemble de la gamme de concentrations de POC. Une nouvelle approche a ainsi été développée; elle est basée sur le maximum du rapport de réflectance (R_{rs}) dans deux bandes spectrales. La performance du nouvel algorithme est supérieure aux méthodes existantes précédemment documentées. L’applicabilité de la nouvelle méthode a été illustrée à l’échelle régionale sur les côtes de Louisiane. Les concentrations de POC estimées avec le nouvel algorithme, à partir des données MERIS, sont cohérente avec celle précédemment estimées à partir d’un algorithme régional (Le et al., 2016). Le deuxième objectif de ce travail était d’examiner la classification des eaux côtières à travers deux approches. Premièrement, une classification basée sur la forme du spectre de réflectance hyperspectrale a été proposée à partir d’un jeu de données in situ complet. Six classes d’eau ont été définies fournissant ainsi une représentation plus fine des propriétés optiques des eaux côtières que ce qu’avait établies des études précedentes utilisant la même méthode (e.g. 4 classes par Vantrepotte et al., 2012). Une définition claire des environnements bio-optiques et biogéochimiques associés aux 6 classes a été réalisée. Ces 6 classes peuvent être associées à un gradient de dilution allant des eaux turbides aux eaux claires. Ceci aboutit à une caractérisation plus fine que ce qui avait été mis en évidence à partir des 4 classes définies par Vantrepotte et al. en 2012. Deuxièmement, une autre classification des eaux côtières basée sur le rapport de la concentration de POC et de la matière particulaire en suspension, telle que proposée par Wozniak et al., 2010, a été ré-examinée. En pratique, des nouveaux seuils ont été établis sur le rapport POC/SPM pour fournir une partition plus précise de l’océan côtier en terme de 3 catégories simples basée sur la qualité de la matière particulaire. Ces trois classes sont les eaux dominées par les minéraux, par le phytoplancton et les eaux mélangées. Les deux méthodes de classification ont été appliquées aux données MERIS pour la période 2002-2012 pour la Manche Orientale et le sud de la Mer du Nord. La dynamique spatio-temporelle des types d’eaux est cohérente en regard des changements saisonniers observés.

Mots clés: Carbone organique particulaire, couleur de l'océan, télédétection, eaux côtières, algorithme bio-optique, classification optique, assemblage de particules.

TABLE OF CONTENTS

List of symbols

Parameter	Description	Unit
POC	Particulate organic carbon	$\mu g\ L^{-1}$
a(λ)	Absorption coefficient	m^{-1}
a_{CDOM}	colored dissolved organic matter absorption coefficient	m^{-1}
a_d(λ)	Absorption coefficient of detritus	m^{-1}
a_g(λ) or a_{CDOM}(λ)	Absorption coefficient of gelbstoff (CDOM)	m^{-1}
a_{NAP}(λ)	Non-algal particulate matter absorption coefficient	m^{-1}
a_p(λ)	Particulate absorption coefficient	m^{-1}
a_{ph}(λ)	Absorption coefficient of pigments of living phytoplankton	m^{-1}
a_w(λ)	Absorption coefficient of pure water	m^{-1}
b(λ)	Scattering coefficient	m^{-1}
b_b(λ)	Backward scattering coefficient	m^{-1}
b_{bp}(λ)	Particulate backscattering coefficient	m^{-1}
b_f(λ)	Forward scattering coefficient	m^{-1}
b_p(λ)	Scattering coefficient of particle	m^{-1}
b_w(λ)	Scattering coefficient of sea water	m^{-1}
c(λ)	Beam attenuation coefficient	m^{-1}
Chla	Chlorophyll-a concentration	$\mu g\ L^{-1}$
c_p	Particle attenuation coefficient	m^{-1}
$E_d(0^+,\lambda)$	Above water down-welling irradiance	$W\ m^{-2}$
λ	Wavelength	nm
$L_u(0^-,l)$	Upwelling radiance below sea surface	$Wm^{-2}sr^{-1}$
R_{rs}	Remote sensing reflectance	sr^{-1}
SPM	Suspended particulate matter concentration	$\mu g\ L^{-1}$
Δ_T^2	Chi-Square value	dimensionless
Δ_M^2	Mahalanobis distance	dimensionless
R	Irradiance reflectance	dimensionless
β	Volume scattering function	$m^{-1}sr^{-1}$
$\tilde{\beta}$	Scattering phase function	sr^{-1}

List of Figures

List of Tables

Introduction

The ocean plays an important role in the climate system by storing carbon and so allows the regulation of the amount of carbon dioxide (CO_2) in the atmosphere. The amount of carbon storage in the ocean is around 50 times more important than in the atmosphere (Siegenthaler and Sarmiento 1993). The total active pool of carbon at the Earth's surface for 10,000 years durations is about 40,000 Gt C. About 95% (~38,000 Gt C) is stored in the ocean, mainly in the form of inorganic carbon dissolved in seawater (Falkowski et al. 2000; Schlesinger and Bernhardt 2013). The oceanic carbon cycle is composed of processes that exchange carbon among oceanic pools between the atmosphere, Earth interior, and the seafloor. The main processes (or pumps) that ensure the circulating role are: biological pump which transfers surface carbon towards the seabed via the food web, and the physical pump which results from ocean circulation. Microorganisms as phytoplankton are major actors of the biological pump. By photosynthesis, phytoplankton fix the dissolved inorganic carbon (DIC) and nutrients and produce, among other things, particulate (POC) and dissolved (DOC) organic carbon. This process is named primary production. Note that POC and DOC are also produced by degradation of organic matter by the microbial loop. The particulate organic carbon contributes a small part in ocean carbon pool: 0.43 Gt C (Gardner et al. 2006) at the surface, around 2.28 Gt C in the 200 m layer (Stramska 2009), and are 0.39 Gt C and 1.19 Gt C, over the first penetration and euphotic depth, respectively (Duforêt-Gaurier et al. 2010). Despite its relatively small stock in open ocean waters, its high turnover rate makes POC a central component of the oceanic carbon cycle. Knowledge of the POC concentration distribution and dynamics is indeed a key parameter to study the biological export of carbon from the surface to the deep ocean but also the transfer of carbon throughout the marine food web.

Although coastal zones cover only 7% of the oceanic surface area, they represent productive and dynamic systems with about 20% of the total oceanic organic matter production (Barrón and Duarte 2015). Coastal zones also are well acknowledged as 75-90% of the global sink of suspended river load in which about 15% of the primary production occurs (Loisel et al. 2013). Coastal zones include marine, estuarine, riverine, and marsh areas. The coastal area receives organic carbon inputs from the terrestrial reservoirs mainly through rivers, groundwater discharge, and small inputs of precipitation (Burnett et al. 2003; Cauwet 2002; Willey et al. 2000). Riverine organic carbon inputs to the coastal ocean were estimated at about 426 Tg C yr^{-1}, in which 58.7% is delivered as DOC and 41.3% as POC (Cauwet 2002). Organic carbon can be exported from the coastal to the open ocean as POC and DOC. Coastal waters are of a particular interest, as they are active exchange zones between the terrestrial and oceanic reservoirs.

Various shipboard samplings have been carried out during the international programs and times-series programs to better characterize the standing stock of POC and DOC in open or coastal waters. However, as in situ measurements are limited to sampling performed in some parts of the ocean, the determination of particulate and dissolved organic stocks and flux distributions at a global scale must be established from the extrapolation of field data performed at various spatio-temporal scales. Previous studies have shown that this is a very difficult task because the assessed carbon contents are in many cases only representative of the spatial and temporal context of their acquisition (Platt and Sathyendranath 1988).

In the past few years, inversions of data from ocean color satellite radiometry (OCR) have allowed to derive biogeochemical parameters from space. A primary goal of ocean-colour remote sensing was initiated to produce synoptic fields of chlorophyll a concentration, an index of phytoplankton biomass. Since the first ocean colour sensor, CZCS (Coastal Zone Color Scanner Experiment) launched in 1978, the ocean colour sensors have been increased in number and also in complexity design to satisfy requests of the scientific community. Nowadays, satellite sensors provide high frequency measurements now with a sufficiently fine spatial resolution. They are very useful and valuable tools as they provide a unique opportunity to assess the seasonal and inter annual variability of biogeochemical parameters at global scale.

Over the past few years, the scientific community in ocean-color has made progress to develop bio-optical algorithms to derive biogeochemical parameters other than the chlorophyll concentration. Concerning the particulate organic carbon, few empirical or semi-empirical algorithms have been established to derive POC concentration at both the surface (Gardner et al. 2006; Loisel et al. 2002; Mishonov et al. 2003; Pabi and Arrigo 2006; Son et al. 2009; Stramska 2009; Stramski et al. 2008; Stramski et al. 1999) and within the euphotic (Duforêt-Gaurier et al. 2010) or mixed oceanic layers (Stramska 2009; Świrgoń and Stramska 2015). These algorithms were dedicated to open waters and rely on the fact that the variability of the inherent optical properties is driven by phytoplankton and its associated material (heterotrophic bacteria, detritus, and colored dissolved organic matter). The performance of different available POC algorithms for oceanic waters has recently been evaluated (Evers-King et al. 2017) showing that empirical approaches based on band ratios (Stramski et al. 2008) and semi-analytical approaches based on the backscattering coefficient (b_{bp}) and chlorophyll-a concentration (Chla) (Stramski et al. 2008) performed the best. While the application of these algorithms to OCR observations allowed to study the spatio-temporal variability of POC in open waters, such information is still not available for global coastal waters, which are more complex bio-optical environments (Loisel et al. 2013). To overcome this limitation on our understanding of the POC dynamics, some purely empirical approaches were recently developed from in situ measurements performed in offshore and coastal waters (Hu et al. 2016; Le et al. 2018a; Liu et al. 2015; Woźniak et al. 2016) or exclusively from measurements collected mainly in river-dominated systems (Le et al. 2016) to estimate the surface POC concentration from OCR. However, these algorithms were almost all developed from limited datasets gathered in specific regions. This dictates that the results and performance of these approaches at a global scale may be strongly conditioned by the representativeness of the dataset used for their development. In other words, these algorithms may be not suitable to catch the large POC variability encountered in optically contrasted coastal areas.

In this context, the first objective of the PhD (Chapter 2) aimed at improving the retrieval of POC concentration for global scale applications in coastal waters (i.e., over large POC concentration range). In practice, the particulate organic carbon is defined as particulate carbon from organic origin retained by a Whatman GF/ F filter according to the JGOFS (Joint Global Ocean Flux Study) protocol (Knap et al. 1996). The POC is then composed of particles (autotrophic organisms, heterotrophic bacteria, and detritus) with a diameter between 0.4 and 200mm, a pre-filtration usually being performed.

As explained above, coastal waters present a very high optical complexity and the analysis of the spectral signature is a tedious and difficult task. Moreover, the development of satellite observation of coastal environments has to face other key issues as the high spatio-temporal variability of hydrodynamic and biological processes. In this context, regional algorithms were developed; each regional algorithm being established from in situ measurements of optical and biogeochemical parameters sampled in a given area. Regional approaches are convenient but present limitations as they depend on the dataset used for their development. It results that some algorithms developed from in situ measurements sampled in specific areas can show good performance for some type of waters and bad performance for others. To summarize, regional algorithms are conditioned to the representativeness of their dataset and are potentially not suitable for global scale applications. The influence of the optical characteristics of the water mass on the relative performance of bio-optical algorithms was clearly demonstrated (Brown et al. 2008; Loisel et al. 2011; Woźniak et al. 2010). An alternative approach aims at partitioning waters with similar optical features and aims in developing a specific bio-optical algorithm for each water class (Monolisha et al. 2018; Moore et al. 2009; Vantrepotte et al. 2012). It implies that coastal waters located in different regions can present similar bio-optical characteristics and leads the way potentially to applications at large scale. Promising approaches were developed to identify optical water types from a framework within each different water type is automatically distinguished, from each other, by examining remotely sensed data, as for example the remote-sensing reflectance (R_{rs}) (Vantrepotte et al. 2012). Vantrepotte et al., 2012 developed a classification-based approach based on R_{rs} to retrieve the concentration of suspended particulate matter. Their work highlights the potential of class-based approach to increase the performance of the SPM inversion. The suspended particulate matter is composed of particles including both organic (autotrophic organisms, heterotrophic bacteria, and detritus) and mineral, with diameter above 0.5–0.7 mm (Loisel et al. 2007). In their conclusions, the authors specified that their results need to be confirmed from larger data set. This is the main objective of chapter 3. In this context, we dispose of a large dataset of coincident optical and biogeochemical parameters to apply an optical classification, based on hyperspectral $R_{rs,}$ to identify optical water types present in the coastal ocean.

Information about the composition of the particle assemblage can also be obtained from the POC to SPM ratio, that represents the fraction of the organic matter to the total suspended particulate matter assemblage (Babin et al. 2003b; Emmerton et al. 2008; Koestner et al. 2018; Lubac and Loisel 2007; Neukermans et al. 2016; Reynolds and Stramski 2019; Reynolds et al. 2016; Stramski et al. 2007; Stramski et al. 2008; Woźniak 2014; Woźniak et al. 2016; Woźniak et al. 2011; Woźniak et al. 2010). From in situ data in the near-shore marine environment at Imperial Beach, California, Woźniak et al. 2010 set threshold values on POC to SPM ratio to identify changes in the particulate assemblage from the dominance of mineral particles to the dominance of organic particles, considering also waters composed of mixed particles. These categories represent arbitrary divisions but provide a useful mean to classify particle assemblages and from parameters now available in coastal waters from satellite sensors. The objective of Chapter 4 is to re-examine the pertinence of POC/SPM thresholds on an extensive in situ data set covering a wider range of optical and biogeochemical variability than the previous dataset used by Woźniak et al. 2010. Then, we will study the nature of the particle assemblage from MERIS data over two coastal areas: the English Channel and Black Sea known for their high variability in particle assemblage and dynamics. POC concentrations will be derived using the algorithm developed in Chapter 2, whereas SPM concentrations will be estimated using the recently developed algorithms of Han et al., 2016.

To summarize, this dissertation is organized as follows:

The chapter 1 will introduce the formalism used in marine optics and will present all the parameters used in this study with their respective acronyms. The chapter 2 investigates performance of historical POC algorithms for coastal water and introduces the new POC algorithm for coastal water. In chapter 3, optical classification is applied to identify optical water types present in the coastal ocean. In chapter 4, we re-examine the use of the POC to SPM ratio to partition. The overall conclusions and perspectives of this work are summarized in Chapter 5.

This work resulted in 1 peer-reviewed publication, which is available in open access:

Tran, T.K., Duforêt-Gaurier, L., Vantrepotte, V., Jorge, D.S.F., Mériaux, X., Cauvin, A., Fanton d'Andon, O., & Loisel, H. (2019). Deriving Particulate Organic Carbon in Coastal Waters from Remote Sensing: Inter-Comparison Exercise and Development of a Maximum Band-Ratio Approach. Remote Sensing, 1111(23), 2849; https://doi.org/10.3390/rs11232849.

Chapter 1: Sea water constituents, inherent and apparent optical properties: definitions

1.1. Sea water constituents and ocean color

Natural seawater constituents in the water column are water molecules and dissolved salt, dissolved organic material (also called gelbstoff, yellow substance or Colored Dissolved Organic Matter - CDOM) and Suspended Particulate Matter (SPM). SPM include both inorganic (minerals) and organic particles (phytoplankton, detrital particles, bacteria and viruses) (IOCCG 2000). The organic and inorganic fractions of SPM are POM and PIM, respectively. While numerous studies have been performed to assess the optical properties of SPM (Babin et al. 2003b; Babin et al. 2003c; Loisel et al. 2007) only few studies were dedicated to the study of IOPs of POM and PIM (see for example (Snyder et al. 2008)).

The size range of the different seawater constituents are provided in Figure 1.1. For a given size, they all differ according to their shapes, internal structures and refractive indexes, parameters which control how the interact with them.

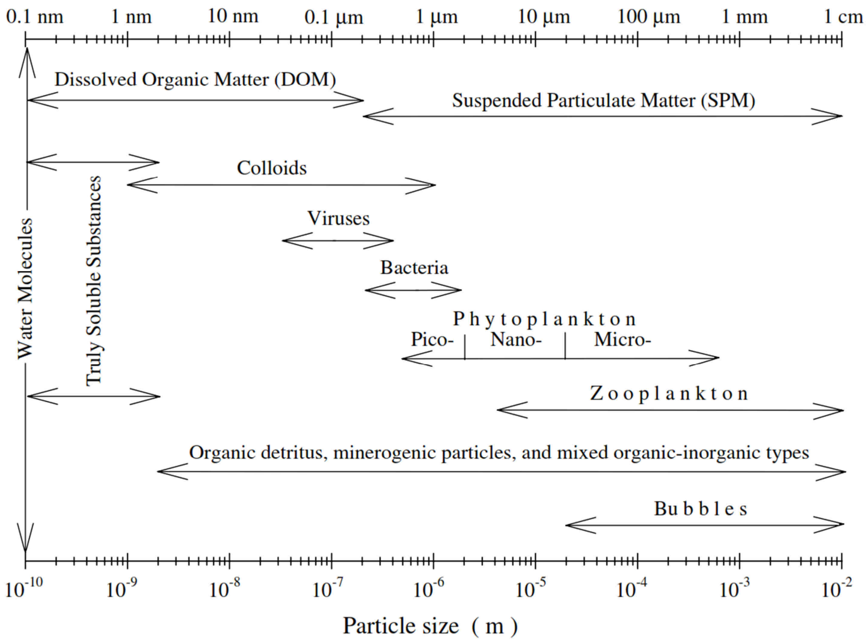

Figure 1.1. Schematic diagram showing the size ranges of various seawater constituents from molecular (10^{-10} m) to large particles (1 cm) (Stramski et al. 2004)

The presence of these constituents and variations of their concentration and physicochemical properties (internal structure, chemical composition, size distribution) changes the color of the water. Indeed, water color is determined by scattering and absorption of the light field in the visible part of the spectrum (400-700 nm) (IOCCG 2006). The spectral variations which bring qualitative and quantitative information about the water constituents can be measured by radiometers thus providing the basis for spectral radiometry, also known as ocean-colour radiometry (OCR) or simply ocean colour (IOCCG 2008). The ocean-colour radiometry is used to deduce information about marine ecosystems through the estimates of proxies, such as the chlorophyll concentration. Optical properties of water are divided into two classes: inherent and apparent optical properties. The relationship of these properties and water constituents are described in Figure 1.2.

Inherent optical properties (IOPs) are properties that depend only upon the medium, and therefore are independent of the ambient light field within the medium. The two fundamental IOPs are the absorption coefficient and the volume scattering function. **Apparent optical properties (AOPs)** are those properties that (1) depend on the medium (the IOPs) and (2) on the geometric (directional) structure of the radiance distribution. Commonly used AOPs are irradiance and remote-sensing reflectances, average cosines, and diffuse attenuation coefficients (Mobley et al. 2010).

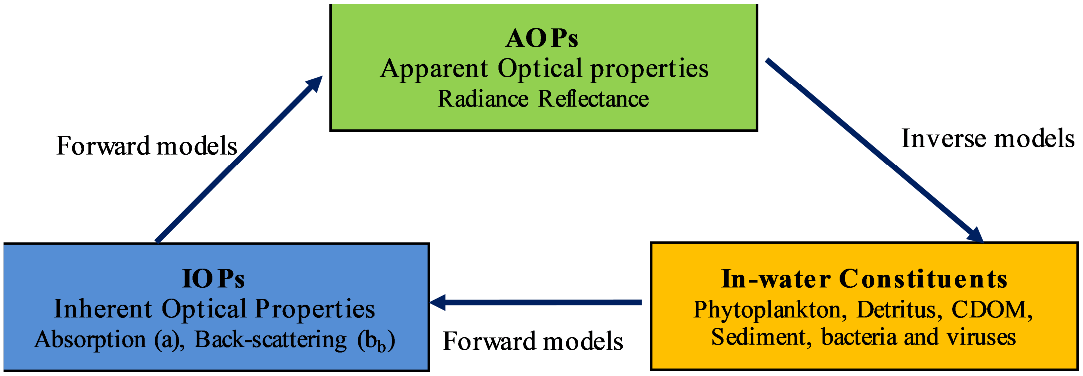

Figure 1.2. Schematic diagram showing the interrelationships between apparent optical properties, in-water constituents and inherent optical properties (IOCCG 2000).

1.2. IOP description

Figure 1.3. describes the interaction of incident light (spectral radiant power in W nm^{-1}) Φ_i at wavelength λ with a medium or sea water mass described by volume Δv of thickness Δr. During the traveling route of $\Phi_i(\lambda)$, some energy $\Phi_a(\lambda)$ is absorbed by the water mass, and some part is scattered ($\Phi_s(\lambda)$) at an angle ψ. The remaining part $\Phi_t(\lambda)$ is transmitted thought the water mass with unchanged direction. Based on the conservation of energy, Φ_i is the sum of total energyΦ_a, Φ_s and Φ_t. The absorptance A(λ) is the fraction of incident energy which is absorbed within the volume (equation 1.1). Likewise, the scatterance B(λ) is the fractional part of the incident power that is scattered out of the beam into all directions (equation 1.2) and the transmittance T(λ), the fraction of the incident power that passes through the volume without interacting with the medium (equation 1.3)

$$A(\lambda) = \Phi a(\lambda) / \Phi i(\lambda), \tag{1.1}$$

$$B(\lambda) = \Phi s(\lambda) / \Phi i(\lambda), \tag{1.2}$$

$$T(\lambda) = \Phi t(\lambda) / \Phi i(\lambda), \tag{1.3}$$

where $A(\lambda)+B(\lambda)+T(\lambda) = 1$

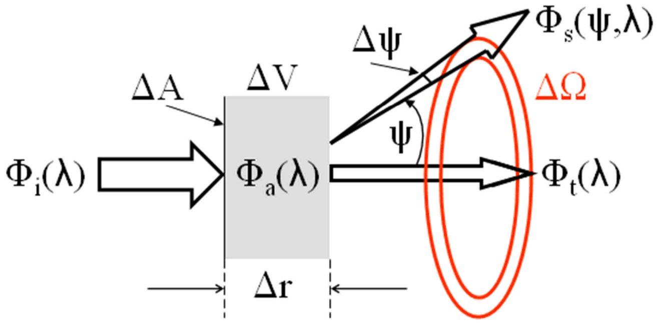

Figure 1.3. Geometry used to define inherent optical properties (Mobley et al. 2010).

The inherent optical properties in optical oceanography are the absorption and scattering *coefficients*, which are respectively the absorptance and scatterance *per unit distance* in the medium (Mobley 1994; Mobley et al. 2010). In the **Figure 1.3**, let the thickness Δr approach zero, in which case only a decreasingly small fraction $\Delta A(\lambda)$ ($\Delta B(\lambda)$) of the incident power is absorbed (scattered). The *absorption coefficient* $a(\lambda)$, the scattering *coefficient* $\mathrm{b}(\lambda)$ and the beam attenuation coefficient $\mathrm{c}(\lambda)$ is then defined by equations 1.4, 1.5 and 1.6 respectively.

$$\mathrm{a}(\lambda) \equiv \lim_{\Delta \mathrm{r} \to 0} \left(\frac{\Delta \mathrm{A}(\lambda)}{\Delta \mathrm{r}} \right) = \frac{\mathrm{dA}(\lambda)}{\mathrm{dr}}, (\mathrm{m}^{-1}) \qquad 1.4$$

$$\mathrm{b}(\lambda) \equiv \lim_{\Delta \mathrm{r} \to 0} \left(\frac{\Delta \mathrm{B}(\lambda)}{\Delta \mathrm{r}} \right) = \frac{\mathrm{dB}(\lambda)}{\mathrm{dr}}, (\mathrm{m}^{-1}) \qquad 1.5$$

$$\mathrm{c}(\lambda) = \mathrm{a}(\lambda) + \mathrm{b}(\lambda)\ (\mathrm{m}^{-1}), \qquad 1.6$$

The IOPs depend on the concentration of particles and dissolved substances but also on the chemical composition of the particulate pool and dissolved substances, the particle size distribution, the internal structure and shape of particles.

For spherical particles or randomly oriented non-spherical particles, the scattering process is assumed azimuthally symmetric. It results that the scattering depends only on the zenith angle ψ. $\beta(\psi, \lambda)$ is refered as the *fraction* of incident power scattered out of the beam through an angle ψ into a solid angle $\Delta\Omega$ centered on ψ. The solid angle $\Delta\Omega$ includes all directions within the two red rings shown in the **Figure 1.3**, corresponding to all directions between scattering angles ψ and $\psi + \Delta\psi$. $\beta(\psi, \lambda)$ is then estimated:

$$\beta(\psi, \lambda) \equiv \lim_{\Delta \mathrm{r} \to 0} \lim_{\Delta \Omega \to 0} \left(\frac{\mathrm{B}(\psi, \lambda)}{\Delta \mathrm{r} \Delta \Omega} \right) \qquad 1.7$$

$$\beta(\psi, \lambda) = \lim_{\Delta \mathrm{r} \to 0} \lim_{\Delta \Omega \to 0} \left(\frac{\Phi_s(\psi, \lambda)}{\Phi_\mathrm{i}(\lambda) \Delta \mathrm{r} \Delta \Omega} \right) (\mathrm{m}^{-1}\mathrm{sr}^{-1}) \qquad 1.8$$

$\beta(\psi, \lambda)$ is the **volume scattering function** (commonly abbreviated as VSF). Integrating $\beta(\psi, \lambda)$over all directions (solid angles) gives the scattering coefficient:

$$\mathrm{b}(\lambda) = \int_{\Xi} \beta(\psi, \lambda) \mathrm{d}\Omega = 2\pi \int_0^{\pi} \beta\,(\psi, \lambda) \sin\psi \mathrm{d}\psi\ (\mathrm{m}^{-1}) \qquad 1.9$$

This integration is often divided into forward scattering, $0 \leq \psi \leq \pi/2$, and backward scattering, $\pi/2 \leq \psi \leq \pi$. The corresponding forward $b_f(\lambda)$ and backward $b_b(\lambda)$ scattering coefficients are, respectively,

$$b_f(\lambda) \equiv 2\pi \int_0^{\frac{\pi}{2}} \beta(\psi,\lambda) sin\psi d\psi \text{ (m}^{-1}\text{)} \qquad 1.10$$

$$b_b(\lambda) \equiv 2\pi \int_{\frac{\pi}{2}}^{\pi} \beta(\psi,\lambda) sin\psi d\psi \text{ (m}^{-1}\text{)} \qquad 1.11$$

Practically, it is not possible to measure the absorption properties of each individual absorbing component and thus the individual components can be grouped into similarly absorbing constituents based upon similarity in their optical properties and/or analytically-based groupings:

$$\begin{gathered} a(\lambda)= a_w(\lambda) + a_p(\lambda) + a_g(\lambda) \\ \text{with } a_p(\lambda) = a_{phy}(\lambda) + a_d(\lambda) \end{gathered} \qquad 1.12$$

where: a_w, a_p, a_{ph}, a_d, a_g is absorption coefficient of pure water, particulate, living phytoplankton, detritus, and gelbstoff (or yellow substances) with units of m^{-1}.

Likewise, the scattering coefficient is defined as:

$$b(\lambda) = b_w(\lambda) + b_p(\lambda) \qquad 1.13$$

The water molecules have a high absorption coefficient in the shorter wavelengths close the ultraviolet, low absorption in the visible and high towards the longer wavelengths of the near infrared spectral region. For a given temperature, salinity, and wavelength, a_w and b_{bw} are used as constants in the bio-optical models and are parameterized using laboratory measurements and theoretical formulations (Morel and Prieur 1977; Twardowski et al. 2001; Zhang et al. 2009).

The Coloured dissolved organic matter (**CDOM**) as known as chromophoric DOM, yellow substance, gelbstoff and gilvin, is the fraction of the dissolved organic matter (DOM) (<0.2 µm) that interact with light due to absorption. The CDOM spectral absorption (a_g) can be described by an exponential law function of wavelength, that decreases toward longer wavelengths (Annick Bricaud 1995; Babin et al. 2003c; Bricaud et al. 1998).

The Suspended Particulate Matter (SPM) can be defined as the material retained on a 0.2µm pore-sized filter (Mueller et al. 2003; Stramski et al. 2004). Particulate IOP properties are known as particulate absorption (a_p), scattering (b_p) or backscattering (b_{bp}) coefficients (all in m^{-1}). In the other hand, TSM can be divided into organic and inorganic matters.

The particulate absorption coefficient is the sum of the detritus (a_d) fraction, also referred to as non-algal particles (NAP), and phytoplankton absorption (a_{phy}). The NAP term defines a higher range of living and non-living particles, besides the organic detritus such as, heterotrophic bacteria and minerals. a_{phy} can be modeled as function of chlorophyll (Annick Bricaud 1995; Babin and Stramski 2004; Babin et al. 2003c; Bricaud et al. 1998) and a_{NAP} can adequately be parameterized as a function of SPM (Babin et al. 2003c).

The detritus represent the coloured particulate organic matter (a_d), and have a similar spectral behavior as CDOM (Babin et al. 2003c). These two components: CDOM and detritus are commonly combined in a single absorption coefficient a_{cdm}, albeit having spectral similarities and being part of degradation products in the carbon cycle, they are regulated by different biogeochemical processes and may vary independently in the ocean layers.

In open water, scattering and backscattering properties varies nonlinear with Chla and POC, and the dependences of b_p have been modeled to estimate Chla and POC from OCR (Loisel et al. 2001; Loisel and Morel 1998; Loisel et al. 2002).

1.3. AOP description

Apparent optical properties are described by the reflectances, averaged cosines, and attenuation coefficients. In the frame of the present study we will only work with reflectances which are now briefly described. The spectral irradiance reflectance or irradiance ratio, R(λ,z) is a measure of how much the radiance (direct solar radiance + diffuse skylight radiance) traveling in all downward directions is reflected upward into any direction, as measured by a cosine collector Figure 1.4 Thus, R(λ,z), is estimated as follows (equation 13):

$$R(\lambda, z) = \frac{E_u(\lambda,z)}{E_d(\lambda,z)} \qquad 1.14$$

where $E_u(\lambda, z)$ is the upwelling irradiance at wavelength λ and depth □; $E_d(\lambda, z)$ (W m^{-2}) is the down-welling irradiance at the same wavelength λ and depth □

The remote-sensing reflectance is a measure of how much of the down-welling irradiance that is incident onto the water surface in any direction is eventually returned through the surface into a small solid angle ΔΩ centered on a particular direction (θ, ϕ), as illustrated in Figure 1.4. The spectral remote-sensing reflectance R_{rs} is computed as:

$$R_{rs}(\lambda) \equiv \frac{L_w(air,\theta,\phi,\lambda)}{E_d(air,\lambda)} (sr^{-1}) \qquad 1.15$$

R_{rs} is evaluated using the water-leaving radiance L_w and E_d in the air, just above the water surface.

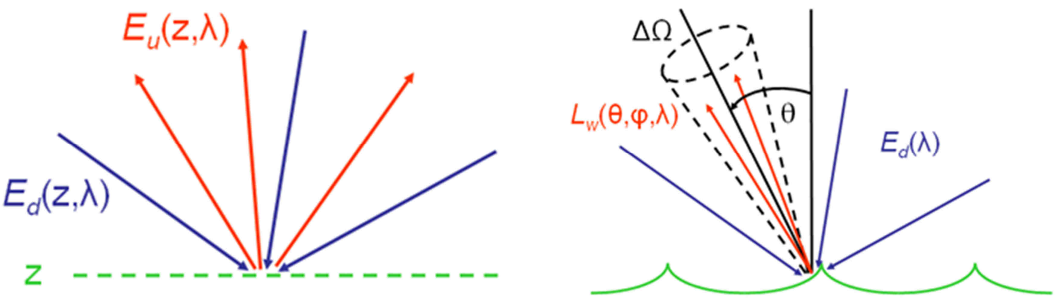

Figure 1.4. Illustration of light rays contributing to the irradiance reflectance R (left) and contributing to the remote-sensing reflectance Rrs (right) (Mobley et al. 2010)

Chapter 2: Deriving Particulate Organic Carbon in Coastal Waters from Remote Sensing: Inter-Comparison Exercise and Development of a Maximum Band-Ratio Approach

2.1. Introduction

Carbon is unevenly distributed in the biosphere among three major reservoirs: atmospheric, oceanic, and terrestrial (on land in vegetation, soils and freshwaters). Knowledge of the carbon exchanges between the different reservoirs is a key issue for better understanding the carbon cycle in the biosphere (Keller et al. 2018; Ward et al. 2017). Although coastal waters represent only 7% of the oceanic surface area, this domain is of a particular interest, being an active exchange zone between the terrestrial and oceanic reservoirs. A significant amount of terrestrial carbon is transported from soils to river headstreams. A fraction of this carbon returns to the atmosphere via degassing occurring in inland waters, a fraction is stored in freshwater organic sediments, and the remaining amount is delivered by estuaries to the coastal waters as dissolved inorganic carbon (DIC), dissolved organic carbon (DOC) and particulate organic (POC) and inorganic (PIC) carbon (Cole et al. 2007; Raymond et al. 2013; Tranvik et al. 2009). Besides this pool of terrestrial carbon origin, marine coastal ecosystems are also productive areas where dissolved and particulate organic carbon may be locally produced and degraded due to complex biogeochemical and physical processes. For a better understanding of the role of coastal waters in the carbon cycle, the spatiotemporal evolution of the different carbon compartment (POC, DOC, PIC, DIC) and their respective standing stocks, must be evaluated and analyzed (Bauer et al. 2013).

POC is one of the main pools of ocean organic carbon, which is composed of living material (heterotrophic bacteria, phytoplankton, zooplankton) and detritus (i.e., non-living cells). Despite its relatively small stock in open ocean waters, its high turnover rate makes POC a central component of the oceanic carbon cycle. Knowledge of the POC concentration distribution and dynamics is indeed a key parameter to study the biological export of carbon from the surface to the deep ocean but also the transfer of carbon throughout the marine food web. Indeed, being the first level of the trophic chain, the production of organic matter (and organic carbon) by phytoplankton supports higher trophic levels and marine diversity. Thus, the amount of POC is an indicator of productivity in the euphotic zone, and can also be used as an indicator of pollution events in coastal areas impacted by human activities.

Over the past few years, many bio-optical algorithms have been developed to derive the POC concentration at both the surface (Gardner et al. 2006; Loisel et al. 2002; Mishonov et al. 2003; Pabi and Arrigo 2006; Son et al. 2009; Stramska 2009; Stramski et al. 2008; Stramski et al. 1999) and within the euphotic (Duforêt-Gaurier et al. 2010) or mixed oceanic layers (Stramska 2009; Świrgoń and Stramska 2015) from ocean-color radiometry (OCR). These algorithms were developed for open waters and rely on the fact that the variability of the inherent optical properties is driven by phytoplankton and its associated material (heterotrophic bacteria, detritus, colored dissolved organic matter (CDOM)). The performance of different available POC algorithms for oceanic waters has recently been evaluated (Evers-King et al. 2017) showing that empirical approaches based on band ratios (Stramski et al. 2008) and semi-analytical approaches based on the back scattering coefficient (b_{bp}) and chlorophyll-a concentration (Chla) (Loisel et al. 2002) performed the best. While the application of these algorithms to OCR observations allowed the pool of POC over the open ocean to be estimated (about 0.4 and 1.2 Pg. C in the first attenuation and euphotic layers, respectively), (Duforêt-Gaurier et al. 2010), such information is still not available for global coastal waters, which are more complex bio-optical environments (Loisel et al. 2013). To overcome this limitation on our understanding of the POC dynamics, some purely empirical approaches were recently developed from in situ measurements performed in offshore and coastal waters (Hu et al. 2016; Le et al. 2018b; Liu et al. 2015; Woźniak et al. 2016) or exclusively from measurements collected in coastal waters (mainly in river-dominated systems) (Le et al. 2016) to estimate the surface POC concentration from OCR. However, these algorithms were almost all developed from limited datasets gathered in specific regions. This dictates that the results and performance of these approaches at a global scale may be strongly conditioned by the representativeness of the dataset used for their development. In other words, these algorithms may be not suitable to catch the large POC variability encountered in optically contrasted coastal areas.

This study emerged in this context and aimed at improving the retrieval of POC concentration for global scale applications in coastal waters (i.e., over large POC concentration range). For this purpose, a large number of in situ measurements performed at low, medium, and high latitudes were first gathered to constitute an extended dataset attesting to the high diversity of physical and biological coastal environments. Different existing algorithms built on different approaches and assumptions were tested over this in situ dataset. A new empirical algorithm involving a maximum band ratio was then developed. Finally, the new approach was applied to a dataset of the medium resolution imaging spectrometer (MERIS) and a coastal region was selected, where the spatial changes of POC concentrations were discussed.

2.2. Data & Methods

2.2.1. In Situ data

The in-situ dataset includes the concentration of biogeochemical parameters (POC, Chla, and suspended particulate matter, SPM) and remote sensing reflectance spectra $R_{rs}(\lambda)$ where λ is the wavelength. Measurements were collected by different contributors and instruments undoubtedly introducing uncertainties, which are not necessarily well characterized (Table 2.1). The field measurement protocols and data processing are described in detail in related papers listed in Table 2.1. Measurements were sampled between 1997 and 2015 in various coastal regions (Figure 2.1): European coastal waters (Babin et al. 2003b; Babin et al. 2003c; Lubac and Loisel 2007; Lubac et al. 2008; Neukermans et al. 2012; Novoa et al. 2017), French Guiana

(Vantrepotte et al. 2015), Eastern Viet Nam Sea (Loisel et al. 2014; Loisel et al. 2017), coastal waters of South East Pacific (Claustre et al. 2008) and North Canada (Bélanger et al. 2008). The particulate organic carbon is here considered as particulate carbon from organic origin retained by a Whatman GF/F filter according to the JGOFS (Joint Global Ocean Flux Study) protocol (Knap et al. 1996). The POC is then composed of particles with a diameter between 0.4 and 200 µm, with pre-filtration usually performed.

The highest POC values are observed in French Guiana 5744 µg L^{-1} and Mekong River 4623 µg L^{-1}. The lowest POC concentrations (< 100 µg L^{-1}) are associated with the Chilean upwelling system sampled during the Biosope campaign (Leblanc et al. 2018). The Chilean upwelling system was identified as coastal waters on criteria based on bathymetry (4000 m), distance to the coast (200 km), and Chla concentration (> 0.8 µg L^{-1}) (Loisel et al. 2017). Biosope upwelling data were included in our dataset in order to consider the transition zone between coastal and open waters.

Among the $R_{rs}(\lambda)$ spectra considered, about 69% were obtained from hyperspectral measurements performed from 310 to 950 nm with a 3 nm spectral resolution, while the remaining 31% were obtained from multispectral measurements at the standard spectral bands of ocean color sensors. Hyperspectral data were interpolated to obtain $R_{rs}(\lambda)$ at every nanometer, to be able to test the different published algorithms considering their specific input spectral bands. Quality controls were applied on $R_{rs}(\lambda)$ spectra based on criteria developed in (Han et al. 2016) (unusual spectral shape, negative values in the near-infrared, strong deviation in the Rrs vs. SPM relationship in the red). The whole dataset (named DSW) consists of 606 measurements of POC concentrations (N_{POC}) associated with hyperspectral (73%) and multispectral (27%) $R_{rs}(\lambda)$ spectra. Note that, for some of the 606 POC measurements, coincident Chla and SPM concentrations are missing so $N_{POC} > N_{Chla} > N_{SPM}$. The POC, Chla, and SPM concentrations vary from 45.37 to 5744 μg L^{-1}, 0.034 to 48.66 μg L^{-1}, and 207.4 to 2626 x 10^3 μg L^{-1}, respectively (Table 2.1 and Figure 2.2).

The large ranges of POC, SPM, and Chla concentrations attest to the high diversity of physical and biological coastal environments (river plumes, phytoplankton blooms, and areas affected by bottom sediment re-suspension, land-ocean exchange, and upwelling) sampled at low (tropical), medium, and high latitudes (Arctic). Because POC represents a significant fraction of the particulate organic matter, the POC to SPM ratio (POC/SPM) can be used as a rough proxy of the relative contribution of organic particles to the total suspended particulate matter (Loisel et al. 2007; Stavn and Richter 2008; Stramski et al. 2008; Woźniak et al. 2010). Woźniak et al. 2010 (Woźniak et al. 2010) identified three types of waters according to the POC/SPM level. Waters are considered as mineral-dominated if POC/SPM<0.06, organic-dominated if POC/SPM>0.25, and mixed if 0.06≤POC/SPM≤0.25. According to these criteria, which may not be adapted for all water types while giving a rough approximation of the nature of the particulate assemblage, about 50% of the measurements of our dataset were sampled within mineral-dominated waters, 10% within organic-dominated waters, and 40% within mixed waters (Figure 2.3a). The whole dataset (DSW, N_{POC} = N = 606) was randomly split (Monte Carlo method) into a development dataset (DSD) and a validation dataset (DSV), which represent 67.8% (N=411) and 32.2% (N=195) of DSW, respectively. DSD and DSV cover about three orders of magnitude in terms of POC concentration (Figure 2.4) being representative of the large natural variability of coastal environments. The ranges of R_{rs} (490), R_{rs} (555), and R_{rs} (665) and proportion of mineral-dominated, organic-dominated, and mixed waters are quite similar for DSW, DSD, and DSV (Figure 2.3).

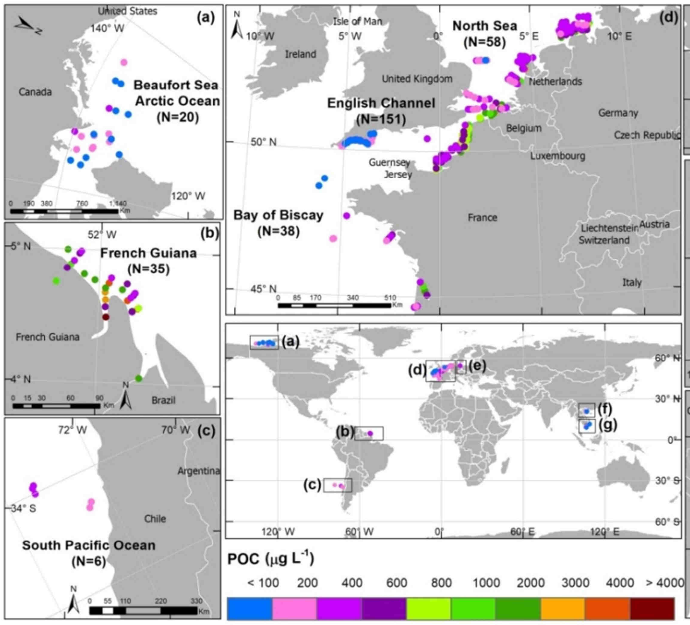

Figure 2.1. Geographical distribution of the 606 in situ coincident measurements of POC and R_{rs} listed in Table 2.1. The color scale corresponds to surface POC concentrations (in µg L^{-1}).

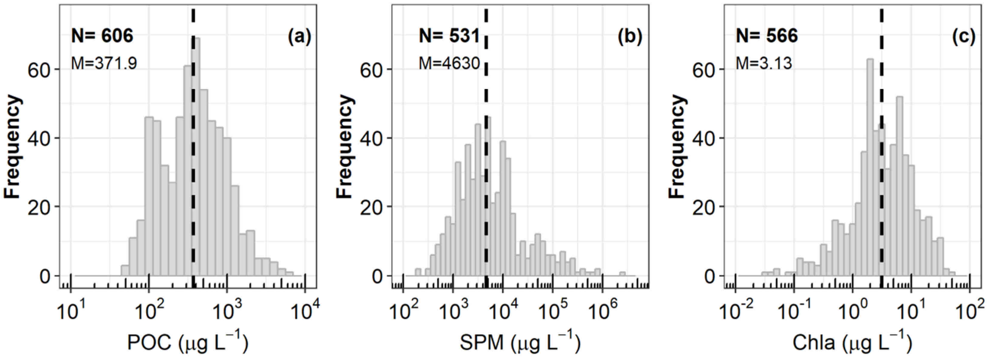

Figure 2.2. Frequency distribution of (a) POC, (b) SPM, and (c) Chla concentration. Dashed lines stand for the median values (M) of each parameter.

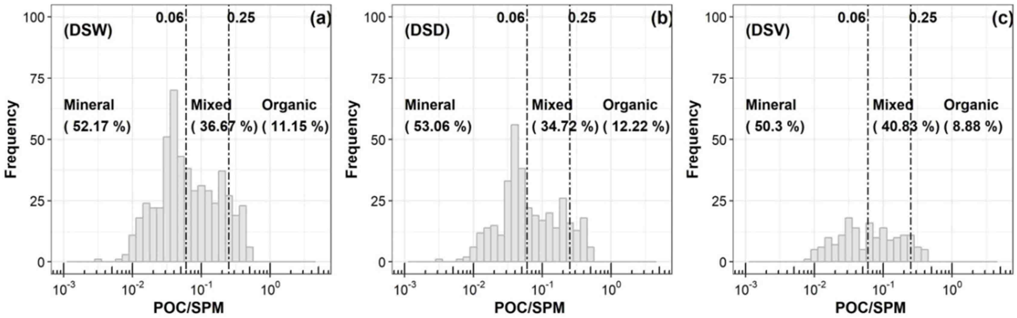

Figure 2.3. Frequency distribution of the POC to SPM ratio for (a) DSW, (b) DSD, and (c) DSV. Dot-dashed lines represent the values, which delimit the POC/SPM ranges for the mineral-dominated, mixed, and organic-dominated waters according to (Woźniak et al. 2010). The percentages between brackets indicate the percentage of in situ data for each type of water.

Table 2.1. Information on the in-situ data used in this study: number of data (N), minimum (Min), maximum (Max), mean, and standard deviation (StdDev) values of POC concentrations (µg L^{-1}). M and H stand for multispectral and hyperspectral data, respectively.

Region	**Year**	**N_{POC}**	**N_{Rrs}**	**Min**	**Max**	**Mean**	**StdDev**	**Reference**	**Multispectral (M) or Hyperspectral data (H).**
Baltic Sea	1998	33	33	330.0	1990	823.3	339.7	(Babin et al. 2003a; Babin et al. 2003c)	M
Bay of Biscay-France	2012	38	38	157.0	3930	1225	1056	(Novoa et al. 2017)	H
Beaufort Sea Arctic Ocean	2004	20	20	49.80	319.7	120.8	64.15	(Bélanger et al. 2008)	M
East Sea Viet Nam	2010	14	14	188.0	1248	485.1	365.6	(Loisel et al. 2014; Loisel et al. 2017)	H
	2011	125	125	68.90	1203	283.7	200.4		H
	2013	37	37	221.0	1858	649.5	248.1		H
	2014	72	72	65.41	4623	588.3	816.9		H
	2015	17	17	45.37	144.5	99.98	36.92		H
English Channel	1997	47	47	60.00	221.0	119.4	41.53	(Babin et al. 2003a; Babin et al. 2003c)	M
	2004	84	84	214.7	2262	754.0	388.2	(Lubac et al. 2008) (Lubac and Loisel 2007)	H
	2010	20	20	110.2	2159	331.6	276.9	(Koji et al.) (Neukermans et al. 2012)	H
French Guiana	2012	35	35	216.0	5744	1406	1309	(Vantrepotte et al. 2015) (Vantrepotte et al. 2012)	H
North Sea	1998	58	58	190.0	2470	505.8	390.5	(Babin et al. 2003a; Babin et al. 2003c)	M
South Pacific Ocean	2004	6	6	112.9	277.8	192.6	62.79	(Claustre et al. 2008)	M
Overall		**606**	**606**	**45.37**	**5744**	**575.6**	**662.5**		

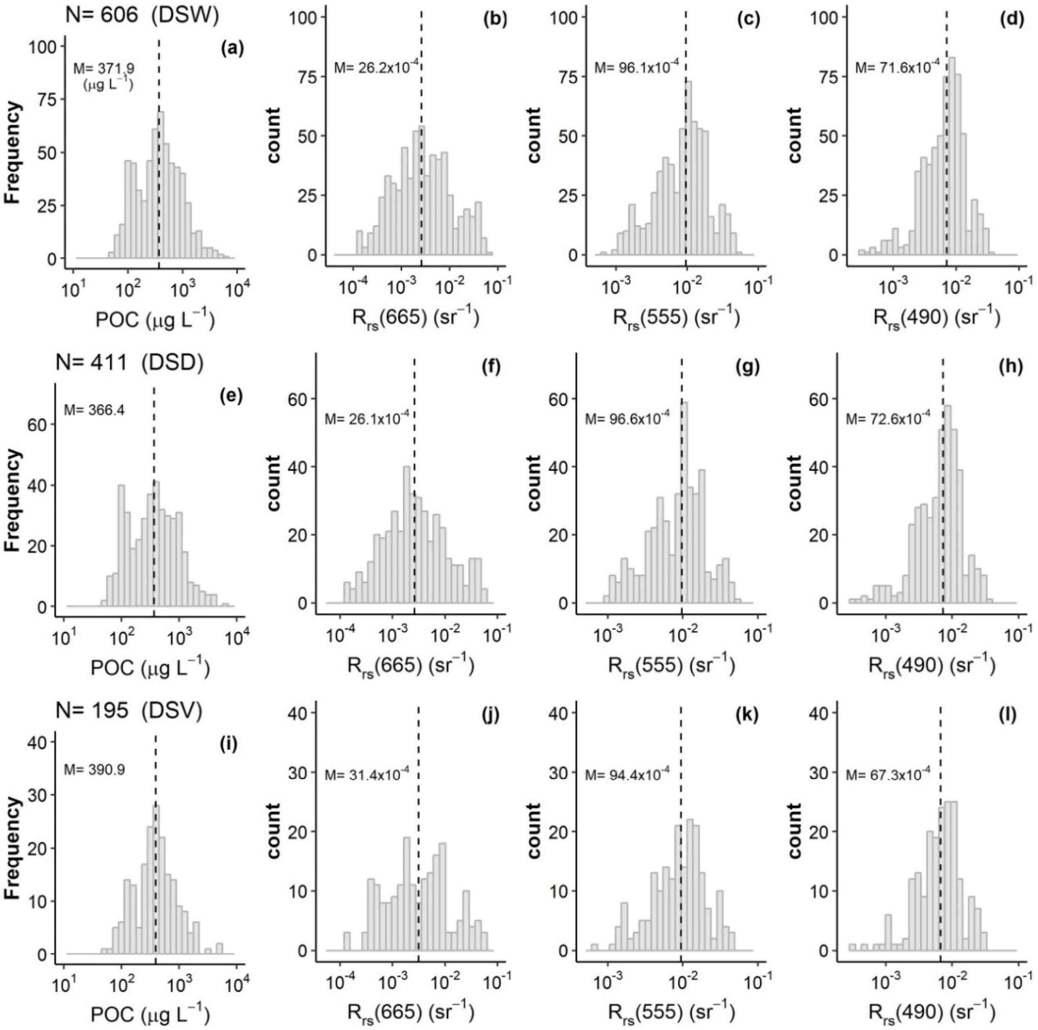

Figure 2.4. POC and R_{rs} values at 665, 555 and, 490 nm for the whole (a-d), development (e-h), and validation dataset (i-l) named DSW, DSD and DSV, respectively. Dashed lines display the median values, M.

2.2.2. Satellite-in situ matchup data base

The matchup dataset is composed by in situ measurements of POC collected in the frame of the French Coastal Monitoring Network (SOMLIT, Service d'Observation en Milieu LITtoral, http://somlit.epoc.u-bordeaux1.fr/fr/) nearly simultaneously with the overpass of the MERIS onboard the European Space Agency (ESA)'s Envisat platform. The SOMLIT network gathers several coastal stations along the French coastline (Eastern English Channel, Atlantic Ocean, and Mediterranean Sea) sampled bi-monthly since 1995 (Figure 2.5). MERIS level 1 data were processed using the polymer atmospheric correction algorithm (Steinmetz et al. 2011), which was adapted for coastal waters in the frame of the GlobCoast project funded by the French Research National Agency (Vincent et al.). From daily MERIS images, a total of 336 in situ data points were extracted during the satellite lifetime (2002–2012). The criteria considered for the matchup selection were: (1) selection of a 3 × 3 pixel window centered on matchup location, (2) a time difference between in situ measurements and satellite overpass lower than 3 hours (a time window of one hour also was tested with no significant differences in the results), (3) spatial homogeneity in the satellite pixels (coefficient of variation of $R_{rs}(\lambda)$, ratio of the standard deviation to the mean computed over the pixel window, lower than 30%), and (4) number of valid pixels per pixel window greater than 6. After the application of all these criteria, the final matchup dataset is then composed of 154 matched points (Table 2). For the matchup dataset, POC concentrations are between 26.58 and 658.2 μg L^{-1}, Chla ranges from 0.04 to 10.04 μg L^{-1}, and SPM from 80 to 20,270 μg L^{-1}, respectively (Figure 2.6). According to the value of the in situ POC/SPM ratio, 38.31%, 15.58%, and 46.1% of matchups concern mineral-dominated, organic-dominated, and mixed waters, respectively.

Table 2.2. In situ data from the French SOMLIT network (DSM dataset) sampled simultaneously with MERIS overpass.

Station	Location	Distance to coastline (km)	Number of in situ POC data	Number of matchups
S 01	Wimereux, North of France (Channel Sea)	1.6	30	6
S 02	Wimereux, North of France (Channel Sea)	8.1	56	11
S 03	Roscoff, Brittany (Channel Sea)	3.5	42	30
S 10	Banyuls-sur-Mer (Mediterranean Sea)	0.8	92	78
S 11	Marseille (Mediterranean Sea)	4.8-6.4	69	28
S 12	Villefranche-sur-Mer, French Riviera, (Mediterranean Sea)	0.5	44	
S 17	Luc-sur-Mer, Normandy, (Channel Sea)	0.175	1	
S 18	La Rochelle, Bay of Biscay (Atlantic Ocean)	8.046	2	1
	Total		**336**	**154**

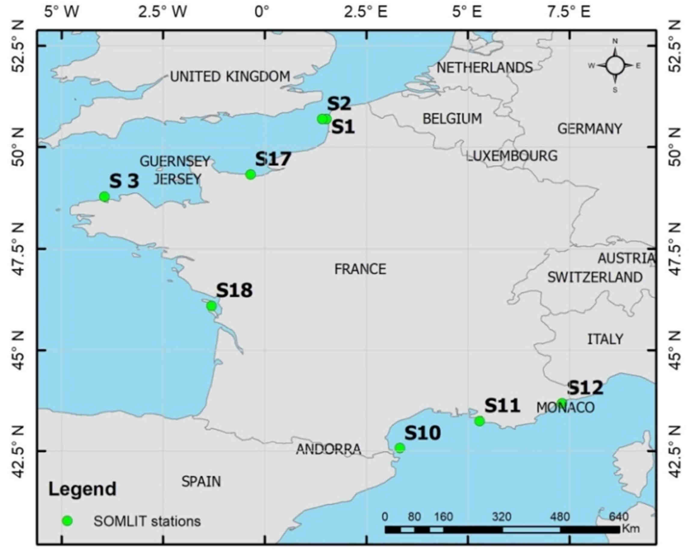

Figure 2.5. Map of SOMLIT stations location around France, presented for divers' type of waters in coastal area.

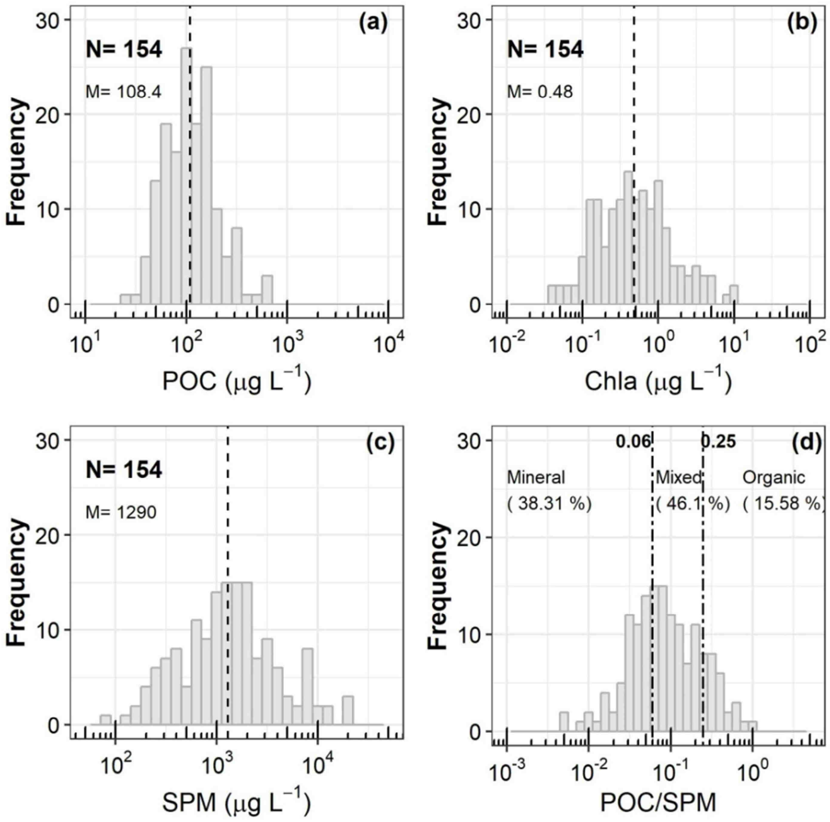

Figure 2.6. Frequency distribution of the biogeochemical measurements for the matchup dataset (DSM). (a) POC, (b) Chla, (c) SPM concentration (μg L^{-1}), and (d) POC/SPM. The dashed lines in (a), (b), and (c) display the median values (M). The dot-dashed lines in (d) delimit the POC/SPM range for the mineral-dominated, mixed and organic-dominated waters according to (Woźniak et al. 2010).

2.2.3. Candidate Algorithms

Many bio-optical algorithms have been developed to derive the near-surface concentration of POC from satellite measurements (Gardner et al. 2006; Loisel et al. 2002; Mishonov et al. 2003; Pabi and Arrigo 2006; Son et al. 2009; Stramska 2009; Stramski et al. 2008; Stramski et al. 1999) and an inter-comparison exercise was recently performed to test their respective performances (Evers-King et al. 2017). These algorithms were developed for open ocean waters and rely on the dominance of phytoplankton biomass in the total POC concentration. More recently, some purely empirical approaches were developed from in situ measurements performed in offshore and coastal waters (Hu et al. 2016; Le et al. 2018a; Liu et al. 2015; Woźniak et al. 2016) or exclusively from measurements collected in coastal waters (mainly in river-dominated systems) (Le et al. 2016). These algorithms are all empirical because the use of a semi-analytical algorithm to estimate POC requires a perfect knowledge of the spectral specific POC-IOPs properties, which are not available as yet.

These latter coastal and offshore-coastal algorithms, which were almost all developed for specific regions (Table 2.3), were all considered for the inter-comparison exercise. In addition, we selected Stramski et al., (2008) algorithm that was implemented by the NASA Ocean Biology Processing Group to derive POC from MODIS at global scale. Because this algorithm is dedicated to open waters, the discussion on its performance is limited to organic-dominated waters. The selected models are representative of the different approaches found in the literature: purely empirical approaches using $R_{rs}(\lambda)$ (Le et al. 2016), R_{rs} band ratios (Hu et al. 2016; Liu et al. 2015; Stramski et al. 2008; Woźniak et al. 2016), or color index (Le et al. 2018b) as input parameters.

Table 2.3. Candidate algorithms used for the inter-comparison exercise. The four last columns provide relevant information on the algorithms: inputs of algorithm, region where the data were collected, the range of POC, and number of data used for the development of the algorithm.

Authors	Abbreviation	Inputs	Region	POC range (μg L^{-1})	N
Band ratio-based algorithms					
Stramski et al. 2008	S08-1 S08-2	$R_{rs}(443)$ / $R_{rs}(555)$ $R_{rs}(490)$ / $R_{rs}(555)$	Eastern South Pacific	10 – 270	53
Woźniak et al. 2016	W16-1 W16-2	$R_{rs}(555)$ / $R_{rs}(589)$, R_{rs} (490) / $R_{rs}(625)$	Baltic Sea Gulf of Gdańsk (Poland)	145-2370	73
Hu et al. 2015	Hu15-1 Hu15-2 Hu15-3	$R_{rs}(443)$ / $R_{rs}(555)$ $R_{rs}(490)$ / $R_{rs}(555)$ $R_{rs}(510)$ / $R_{rs}(555)$	China Sea	17.59 - 687.5	120
Liu et al. 2015	Liu15	$R_{rs}(678)$ / $R_{rs}(488)$ & $R_{rs}(748)$ / $R_{rs}(412)$	Pearl River Estuary, (China)	113-1402	103
R_{rs} based algorithm					
Le et al. 2016	Le16-1	$R_{rs}(488)$, $R_{rs}(532)$, $R_{rs}(547)$, R_{rs} (667), $R_{rs}(678)$	Louisiana & Mobile Bay (Gulf of Mexico)	11.5 - 230	230
	Le16-2	$R_{rs}(490)$, $R_{rs}(510)$, $R_{rs}(550)$, R_{rs} (670)			
Color index algorithm					
Le et al. 2018	Le18-1 Le18-2	$R_{rs}(490)$ & $R_{rs}(555)$ & $R_{rs}(665)$, $R_{rs}(443)$ / $R_{rs}(555)$	Global ocean*	52.6 - 375.2	297

* *The algorithm was developed from satellite R_{rs} and coincident in situ POC measurements through a matchup exercise.*

2.2.3.1. Band ratio-based algorithms

S08 - Stramski et al., 2008 (Stramski et al. 2008) developed an empirical algorithm based on $R_{rs}(\lambda)$ ratios at two different wavelengths to derive POC concentration in open ocean waters. This algorithm was developed from in situ data (N=53) collected within oligotrophic and upwelling waters of the eastern South Pacific Ocean ($10 \leq$ POC ≤ 270 µg L^{-1}) during the Biosope campaign. This algorithm is based on an empirical power-law between near-surface POC and blue-to-green ratio of $R_{rs}(\lambda)$. Stramski et al. (2008) showed that the following two algorithms have the best performance for their dataset:

$$\mathrm{POC} = 203.2\left[\frac{\mathrm{R_{rs}}(443)}{\mathrm{R_{rs}}(555)}\right]^{-1.034} \tag{2.1}$$

$$\mathrm{POC} = 308.3\left[\frac{\mathrm{R_{rs}}(490)}{\mathrm{R_{rs}}(555)}\right]^{-1.639} \tag{2.2}$$

These two algorithms will be named S08-1 (equation 2.1) and S08-2 (equation 2.2) in the following.

W16- Woźniak et al. 2016 (Woźniak et al. 2016) proposed an empirical algorithm built from 73 in situ measurements collected during four field campaigns during spring and late summer within the open waters of the Southern Baltic and coastal regions of the Gulf of Gdańsk. POC measurements cover a wide range from 145 to 2370 µg L^{-1}. The authors tested correlations of POC concentrations with reflectance ratios at various spectral bands leading to the selection of the $R_{rs}(555)/R_{rs}(589)$ ratio:

$$\mathrm{POC} = 0.814\times\left[\frac{\mathrm{R_{rs}}(555)}{\mathrm{R_{rs}}(589)}\right]^{-4.42} \tag{2.3}$$

A good performance was also obtained with the $R_{rs}(490)/R_{rs}(625)$ ratio, which has benefits to consider the input R_{rs} close to bands potentially available from satellite observations:

$$\mathrm{POC} = 0.774\left[\frac{\mathrm{R_{rs}}(490)}{\mathrm{R_{rs}}(625)}\right]^{-1.18)} \tag{2.4}$$

Equations 2.3 and 2.4 will be further named W16-1 and W16-2, respectively. Note that the 589 nm spectral band is absent in all ocean color sensors, while the 625 nm band is only available for MERIS and OLCI (Ocean and Land Colour Instrument).

Hu16 - Hu et al., 2016 (Hu et al. 2016) developed a regional algorithm using coastal and offshore data (N=120) collected in the South China Sea mainly during the summer. The POC values range between 25.3 and 687.5 mg m^{-3}. Their algorithm is quite similar to the 2008 algorithm from Stramski et al. as it is based on a blue-to-green reflectance ratio. The authors examined the following band ratios:

$$\mathrm{POC} = 262.1730\left[\frac{\mathrm{R_{rs}}(443)}{\mathrm{R_{rs}}(555)}\right]^{-0.940} \tag{2.5}$$

$$\mathrm{POC} = 285.0929\left[\frac{\mathrm{R_{rs}}(490)}{\mathrm{R_{rs}}(555)}\right]^{-1.2292} \tag{2.6}$$

$$\mathrm{POC} = 243.8148\left[\frac{\mathrm{R_{rs}}(510)}{\mathrm{R_{rs}}(555)}\right]^{-2.4777} \tag{2.7}$$

They showed that the algorithm described by equation 2.5 provides the best performance. The equations 2.5–2.7 will be further named Hu16-1, Hu16-2, and Hu16-3, respectively.

Liu15 - Liu et al., 2015 (Liu et al. 2015) developed an algorithm for estimating surface POC concentration in the highly turbid waters of the Pearl River estuary in China. Their algorithm is based on band ratios of the equivalent reflectance computed for MODIS/AQUA (Moderate Resolution Imaging Spectro-radiometer) spectral bands (412, 443, 488, 531, 551, 667, 678 and 748 nm). The equivalent reflectance is defined by equation 2.8:

$$\mathrm{r_{equi}}(\lambda) = \int_{\lambda_{\min}}^{\lambda_{\max}} \mathrm{f}(\lambda)\mathrm{r}(\lambda)\mathrm{L}(\lambda)\mathrm{d}\lambda \Big/ \int_{\lambda_{\min}}^{\lambda_{\max}} \mathrm{f}(\lambda)\mathrm{L}(\lambda)\mathrm{d}\lambda \tag{2.8}$$

where $r_{equi}(\lambda)$ is the equivalent reflectance for a band with a central wavelength λ, $f(\lambda)$ is the spectral response function, available from the Ocean Color website (http://oceancolor.gsfc.nasa.gov/), $r(\lambda)$ is the in situ remote-sensing reflectance, $L(\lambda)$ is the solar irradiance at mean Earth-Sun distance, λ_{min} is equal to 350 nm, and λ_{max} is 800 nm. The authors selected an approach based on two different band ratios, and used an optimization approach to determine the best band combination:

$$\mathrm{POC} = \mathrm{b_0} + \mathrm{b_1}\frac{\mathrm{r_{equi}}(\lambda_1)}{\mathrm{r_{equi}}(\lambda_2)} + \mathrm{b_2}\frac{\mathrm{r_{equi}}(\lambda_3)}{\mathrm{r_{equi}}(\lambda_4)} \tag{2.9}$$

After testing all possible band combinations, the algorithm achieved the best fit with λ_1 = 678 nm, λ_2 = 488 nm, λ_3 = 748 nm, and λ_4 = 412 nm. The regression coefficients are $b_0 = 0.0078$, $b_1 = 1.3973$, and $b_2 = -1.2397$. Equation 2.9 is named Liu15. It was shown that the $R_{rs}(\lambda)$ values at the central bands are very similar to the equivalent reflectance values calculated using the band spectral response at all visible bands of the different OCR (Han et al. 2016). For this reason, the central remote-sensing reflectance at 678, 488, 748, and 412 nm are used instead of the equivalent reflectance in this inter-comparison exercise.

It is worth noticing that the two-step algorithm developed by Woźniak et al. in 2016 (Woźniak et al. 2016), based on the particulate absorption (a_p) coefficient at 570 and 675 and the concentration of SPM, was not tested because of the complexity in retrieving a_p in the green and in the red from OCR (Loisel et al. 2018).

2.2.3.2. Absolute Rrs-based algorithms

Le16- Using a dataset of in situ POC concentrations matched with satellite $R_{rs}(\lambda)$, Le et al., 2016 (Le et al. 2016) developed multiple regression algorithms for two river-dominated estuaries in the northern Gulf of Mexico (the Louisiana Continental Shelf and Mobile Bay). The multiple linear regression models which showed the lowest prediction error between log(POC) (log-transformed base 10) and $R_{rs}(\lambda)$ are given in equation 2.10 (named Le16-1) and in equation 2.11 (L16-2). L16-1 and L16-2 were developed using MODIS and SeaWiFS (Sea Viewing Wide Field of View Sensor) spectral bands, respectively.

$$\log(POC) = -126.22 \times R_{rs}(488) - 120.74 \times R_{rs}(531) + 245.42 \times R_{rs}(547) - 493.54 \times R_{rs}(667) + 489.3 \times R_{rs}(678) - 0.59 \quad (2.10)$$

$$\log(POC) = -115.69 \times R_{rs}(490) - 53.64 \times R_{rs}(510) + 172.13 \times R_{rs}(555) - 40.06 \times R_{rs}(670) - 0.54 \quad (2.11)$$

2.2.3.3. Color index algorithm

Le18 – In 2018, Le et al., (Le et al. 2018a) formulated two algorithms using in situ POC data from the SeaWiFS Bio-optical Archive and Storage System (SeaBASS) of NASA (https://seabass.gsfc.nasa.gov) and satellite $R_{rs}(\lambda)$ data obtained from matchups. This approach uses three spectral bands centered at 490 nm, 550 nm, and 670 nm to determine a color index (CI_{POC}, equation 2.12), from which the POC concentration is estimated (equations 2.13–2.14). This approach is named Le18-1.

$$CI_{POC} = R_{rs}(555) - (R_{rs}(490) + (555 - 490) / (670 - 490) \times (R_{rs}(670) - R_{rs}(490))) \quad (2.12)$$

$$CI_{POC} \leq -0.0005: \log(POC) = 185.72 \times CI_{POC} + 1.97 \quad (2.13)$$

$$CI_{POC} \geq -0.0005: \log(POC) = 485.19 \times CI_{POC} + 2.1 \quad (2.14)$$

Le et al. formulated another algorithm based on the blue-to-green ratio (equations 2.15–2.16). The color index (equation 2.12) is used to pick up a suitable relationship. Indeed, the authors indicated that equation 2.15 used when the CI_{POC} is less than –0.0005 is more suitable for open waters, whereas equation 2.16 used when CI_{POC} is greater than –0.0005 is suitable for coastal waters, respectively.

$$CI_{POC} \leq -0.0005: \log(POC) = -\,0.66 \times \log[R_{rs}(443) / R_{rs}(555)] + 2.06 \quad (2.15)$$

$$CI_{POC} \geq -0.0005: \log(POC) = -1.38 \times \log[R_{rs}(443) / R_{rs}(555)] + 2.31 \quad (2.16)$$

2.2.4. Statistical Indicators used for model development and validation

To assess the performance of the 12 selected algorithms, we use the graphical comparison of model predictions and observations as well as quantitative statistical metrics of differences between the corresponding predictions of model and observations. These indicators include the root mean square deviation for log-transformed data ($RMSD_{log}$) (equation 2.17), the root-mean-square deviation for un-transformed data (RMSD) (equation 2.18), and the median absolute percent difference (MAPD) (equation 2.19):

$$\mathrm{RMSD_{log}} = \left(\sum_{i=1}^{N} \left(\log\left(\mathrm{POC_i^{mod}}\right) - \log\left(\mathrm{POC_i^{obs}}\right) \right)^2 \Big/ N \right)^{1/2} \quad (2.17)$$

$$\mathrm{RMSD} = \left(\sum_{i=1}^{N} \left(\mathrm{POC}_i^{mod} - \mathrm{POC}_i^{obs}\right)^2 \Big/ \mathrm{N}\right)^{1/2} \tag{2.18}$$

$$\mathrm{MAPD} = \mathrm{median}\left[\left|\mathrm{POC}_i^{mod} - \mathrm{POC}_i^{obs}/\mathrm{POC}_i^{obs}\right|\right] \times 100 \tag{2.19}$$

where $\mathrm{POC_i}^{obs}$ and $\mathrm{POC_i}^{mod}$ are the in situ and model - derived POC concentration. The mean bias (MB) (equation 2.20) and the median ratio (MR) (equation 2.21) are also calculated:

$$\mathrm{MB} = \frac{1}{\mathrm{N}}\sum_{i=1}^{N}\left(\mathrm{POC}_i^{mod} - \mathrm{POC}_i^{obs}\right) \tag{2.20}$$

$$\mathrm{MR} = \mathrm{median}\left(\mathrm{POC}_i^{mod}/\mathrm{POC}_i^{obs}\right) \tag{2.21}$$

The statistical indicators obtained for the 12 algorithms are normalized to be compared graphically. For that purpose, the normalized statistical indicators for each algorithm are defined as follows:

$$\mathrm{MAPD}^{norma}(j) = \frac{\mathrm{MAPD}(j)}{\mathrm{maximum}(\mathrm{MAPD}(j), j = 1, k)} \tag{2.22}$$

$$\mathrm{RMSD}_{log}^{norma}(j) = \frac{\mathrm{RMSD}_{log}(j)}{\mathrm{maximum}\left(\mathrm{RMSD}_{log}(j), j = 1, k\right)} \tag{2.23}$$

$$\mathrm{MB}^{norma}(j) = \frac{|\mathrm{MB}(j)|}{\mathrm{maximum}(|\mathrm{MB}(j)|, j = 1, k)} \tag{2.24}$$

$$\mathrm{MR}^{norma}(j) = \frac{|\mathrm{MR}(j) - \mathrm{R}|}{\mathrm{maximum}(|\mathrm{MR}(j) - \mathrm{R}|, j = 1, k)} \tag{2.25}$$

where *j* identifies the algorithm (*j*=”S08-1”,”S08-2”, “W16-1”, “W16-2”, “Hu16-1”, “Hu16-2”, “Hu16-3”, “Liu-15”, “Le16-1”, Le16-2”, “Le18-1”, “Le18-2”) and *k* is the number of tested algorithms.

Radar charts are also used to compare the performance of the algorithms. A radar chart is a graphical method displaying multi parameters in the form of a two-dimensional chart. The radar plots in Figures 13 and Figure 2.14 give an overview of the statistical indicators by displaying the normalized MAPD, RMSDlog, MB and MR (equations 2.22–2.25). For the development of the new model, we also use a half-matrix representation of the determination coefficient (R^2) calculated between POC and $R_{rs}(\lambda i)/R_{rs}(\lambda j)$ as it does not matter which $R_{rs}(\lambda)$ is taken as a numerator or denominator.

2.3. Results and discussion

2.3.1. Development of a new algorithm for POC

As explained in Section 2.3.1, empirical algorithms based on band ratios at two different wavelengths were first developed for open waters. More recently, they were adjusted to coastal waters but from limited in situ datasets in terms of the number of samples or geographical distribution (Table 2.3). The objective of this section is to define a band ratio algorithm for coastal waters using the large DSD dataset. The use of band ratios allows the influence of potential errors due to atmospheric correction being minimized (Woźniak et al. 2016).

The performance of different color ratios is tested considering only the hyperspectral $R_{rs}(\lambda)$ measurements in DSD (N=298, representing 72.5% of DSD). For each spectrum, $R_{rs}(\lambda)$ in the visible part (400–700 nm) is measured at 300 different wavelengths ($R_{rs}(\lambda_i)$). Mathematically, the different $R_{rs}(\lambda)$ ratios, defined as $R_{rs}(\lambda_i)/R_{rs}(\lambda_j)$ where $i \neq j$, correspond to *k*-combinations ($R_{rs}(\lambda_i)$, $R_{rs}(\lambda_j)$) of the set composed of DSD hyperspectral $R_{rs}(\lambda)$. The number of *k*-combinations is equal to 44,850. It corresponds to the binomial coefficient calculated using the factorials according to:

$$\binom{n}{k} = \frac{n!}{k!\,(n-k)!} \tag{2.26}$$

where k=2 and n=300. So, 44,850 linear type II regressions were computed between POC and the different $R_{rs}(\lambda_i)/R_{rs}(\lambda_j)$ ratios. Both POC concentration and $R_{rs}(\lambda_i)/R_{rs}(\lambda_j)$ were log-transformed to base 10. Figure 2.7 summarizes through a half matrix representation the value of the coefficient of determination (R^2) for the 44,850 regressions. The highest R^2 values (about 0.68) are obtained for band ratios $R_{rs}(\lambda_i)/R_{rs}(\lambda_j)$ with λ_i ranging from 675 to 695 nm and λ_j ranging from 490 and 590 nm. It corresponds to red-to-blue, red-to-green, or red-to-yellow ratios. However, as the spectral region around 680 nm corresponds to the maximum of chlorophyll fluorescence (Gower et al. 2010; Xing et al. 2007), the $R_{rs}(\lambda)$ signal may be contaminated by light emission, which may bias the POC retrieval. Figure 2.7 shows that $R_{rs}(\lambda)$

between 660–670 nm and $R_{rs}(\lambda)$ between 490-560 are “statistically promising” spectral band combinations. The advantage is that many ocean color sensors have bands in the corresponding spectral region. These results are in agreement with those of Woźniak et al. in 2016, who obtained good performance for a blue-to-red ratio ($R_{rs}(490)/R_{rs}(625)$ (Equation 2.4). As MERIS data will be used in the matchup exercise, a focus is performed on bands for that sensor, selecting the following red-to-green and red-to-blue band ratios: $R_{rs}(665)/R_{rs}(555)$, $R_{rs}(665)/R_{rs}(510)$, $R_{rs}(665)/R_{rs}(490)$ (Table 2.4 and Figure 2.8). Note that these bands are also available on OLCI, SeaWiFS, and VIIRS (Visible Infrared Imaging Radiometer Suite).

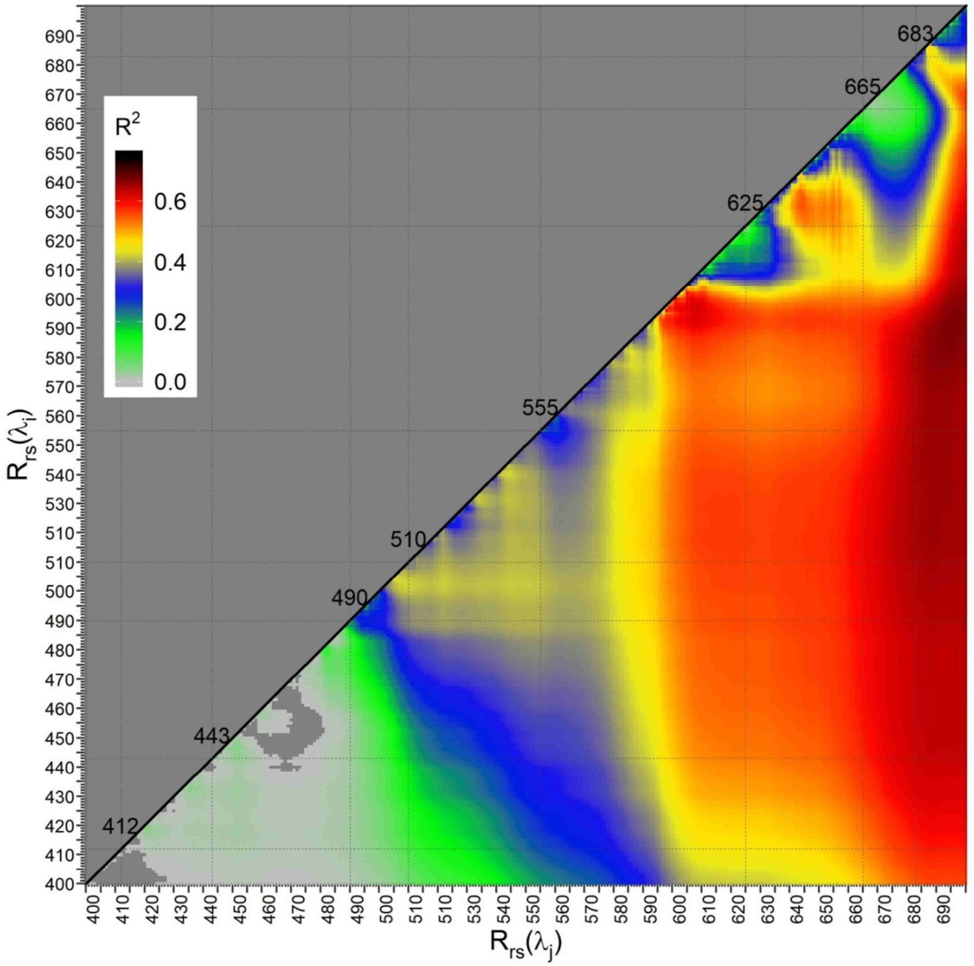

Figure 2.7. Coefficient of determination (R^2) for linear type II regression (in log space) between POC and band ratio defined as $R_{rs}(\lambda_i)/R_{rs}(\lambda_j)$. The dashed lines represent the central wavelength of MERIS spectral bands (units, nm).

Because of the slightly different statistics (in terms of R^2 and RMSD) observed between POC and the different latter band ratios (see Table 2.4), a linear type II regression (log-transformed data) based on the maximum band ratio (MBR) is also examined (Figure 2.9a). Considering both statistical and graphical criteria, the linear type II regression based on MBR presents rather better performance with linear type II regression based on a single band ratio. The coefficient of determination is a bit higher ($R^2 = 0.67$ instead of R^2 between 0.59 and 0.66) and the $RMSD_{log}$ is a bit lower ($RMSD_{log} = 0.242$ instead of $RMSD_{log}$ between 0.246 and 0.267) (Table 2.4). As already discussed by (O'Reilly et al. 1998) for Chla estimates from OC4 algorithm, the MBR allows to switch from a given band ratio to another, thereby avoiding, in some cases, a low and potentially noisy band ratio. Thus, in the context of satellite applications, it is expected that using MBR instead of a single band ratio allow maximization of the model precision over the entire range of POC. Among the three band ratios, $R_{rs}(665)/R_{rs}(490)$ and $R_{rs}(665)/R_{rs}(555)$ are maximal for POC above 500 µg L^{-1} and POC below 500 µg L^{-1}, respectively (Figure 2.10). The latter pattern can be explained by the fact that, over their broad range of variability, SPM and POC tend, at first order, to co-vary in coastal waters (R^2=0.63 on DSW). For instance, high SPM values increase R_{rs} in the red, while associated high POC values will increase absorption in the blue-green part of the spectrum, hence decreasing $R_{rs}(490)$. Although the $R_{rs}(665)/R_{rs}(510)$ ratio is maximum for only 4 data points over the present dataset, this ratio is more frequently selected as the MBR over the MERIS coastal archive (not shown here). As observed for OC4 (O'Reilly et al. 1998; O’Reilly et al.), there is an overlap, over the POC range, in the bands selected for the MBR definition, so there is a smooth transition for MBR around 0.2, which corresponds to POC concentrations between 100 and 500 µg L^{-1} (Figure 2.10). Second and third order polynomial regressions, which theoretically allow for a better account of specific spectral features, were tested. Statistical results obtained for the second-order polynomial are similar to those obtained for the type II linear regression (Figure 2.9b, Table 2.4) while those for the third polynomial regression do not show any improvements (not shown). Therefore, only the linear (Equation 2.27) and second-order polynomial (Equations 2.28-2.29) fits based on the maximum band ratio, named CPOC-1st and CPOC-2nd (Coastal POC), will be evaluated in the following section.

$$\mathrm{POC} = 10^{0.928\mathrm{X}+2.875} \tag{2.27}$$

$$\mathrm{POC} = 10^{0.025\mathrm{X}^2+0.945\mathrm{X}+2.873} \tag{2.28}$$

with:

$$\mathrm{X} = log_{10}\left[\mathrm{maximum}\left(\frac{\mathrm{R_{rs}}(665)}{\mathrm{R_{rs}}(490)}, \frac{\mathrm{R_{rs}}(665)}{\mathrm{R_{rs}}(510)}, \frac{\mathrm{R_{rs}}(665)}{\mathrm{R_{rs}}(555)}\right)\right] \tag{2.29}$$

Table 2.4. Statistical results for POC algorithms. The formulations are power function, $\mathrm{POC} = 10^{\mathrm{a_1X+a_0}}$ or second-order polynomial $\mathrm{POC} = 10^{\mathrm{a_2X^2+a_1X+a_0}}$(log is for decimal logarithm).

X	Functional form	a_o	a_1	a_2	R^2	$RMSD_{log}$
$\log(R_{rs}(665)/R_{rs}(555))$	Power	3.097	1.122		0.59	0.267
$\log(R_{rs}(665)/R_{rs}(510))$	Power	2.926	0.906		0.65	0.249
$\log(R_{rs}(665)/R_{rs}(490))$	Power	2.861	0.833		0.66	0.246
log(MRB)	Power	2.875	0.928		0.67	0.242
log(MRB)	Second-order polynomial	2.873	0.945	0.025	0.67	0.242

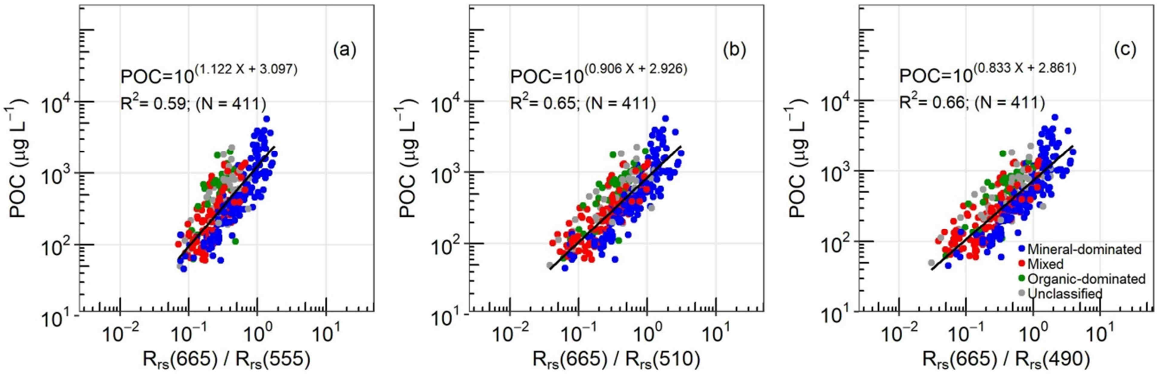

Figure 2.8. The relationship between POC and the different band ratios developed from the DSD dataset (N=411): (a) $R_{rs}(665)/R_{rs}(555)$, (b) $R_{rs}(665)/R_{rs}(510)$, and (c) $R_{rs}(665)/R_{rs}(490)$. Green, red and blue dots correspond to organic-dominated, mixed, and mineral-dominated waters; gray dots indicate the in-situ data points without information of SPM that cannot be classified according to POC / SPM ratio. The black line stands for the linear type II regression to log-transformed data. The letter “X” represents the band ratio.

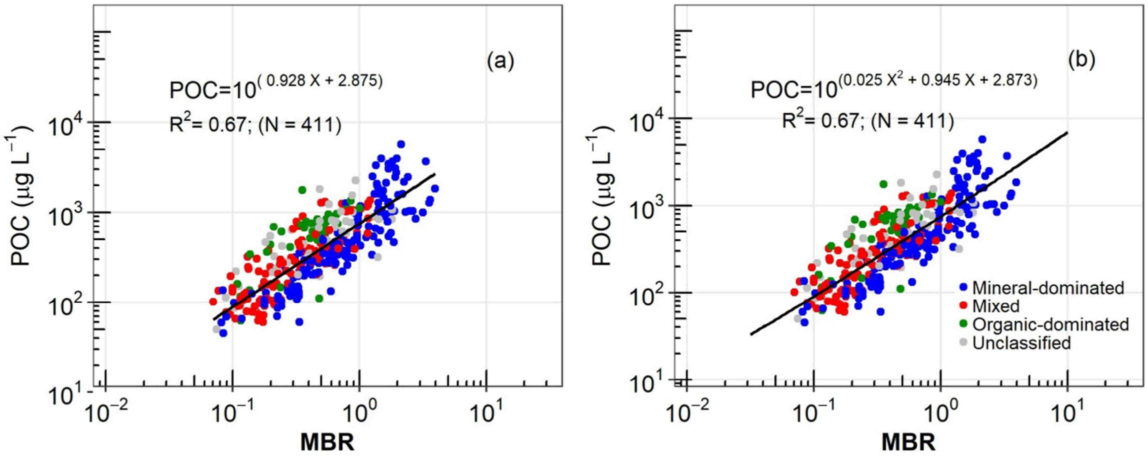

Figure 2.9. Relationships (in log-transformed) between POC and the maximum band ratio (MBR) developed from the DSD dataset (N=411). Green, red and blue dots correspond to organic-dominated, mixed and mineral-dominated waters; gray dots indicate the in-situ data points without information of SPM that cannot be classified according to POC / SPM ratio. The black line stands for (a) linear type II regression (b) second-order polynomial regression to log-transformed data. The letter "X" represents the MBR.

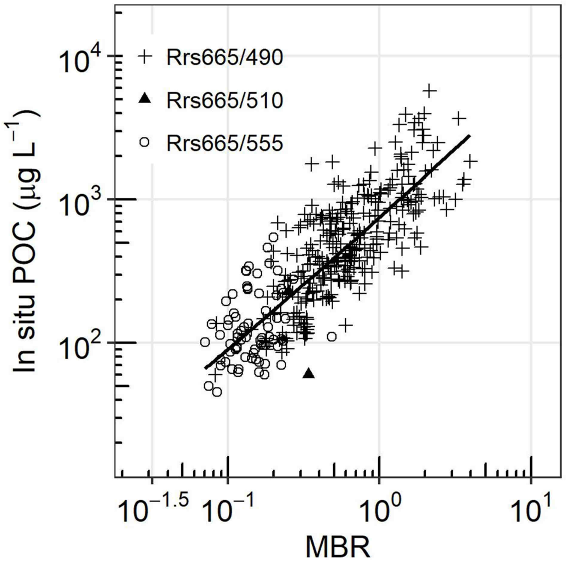

Figure 2.10. Relationships (log-transformed) between POC and the maximum band ratio (MBR) developed from the DSD dataset (N=411). Symbols indicate which ratio is maximal for each data point. For open circles, it is $R_{rs}(665)/R_{rs}(555)$, which is maximum, whereas for crosses and filled triangles, it is $R_{rs}(665)/R_{rs}(490)$ and $R_{rs}(665)/R_{rs}(510)$, respectively.

2.3.2. Inter-comparison exercise of existing algorithms

The inter-comparison exercise is carried out on DSV (N=195). Because some algorithms (W16, Le16 and Liu15) require $R_{rs}(\lambda)$ at wavelengths available from hyperspectral measurements only, multi-spectral measurements of DSV cannot be used for their evaluation.

The W16-1, W16-2, Le16-2, and Liu15 algorithms are therefore tested using 150, 146, and 144 data points, respectively. The number of used hyperspectral data changes based on the availability of the bands required by each algorithm. DSV was however not restricted to hyperspectral data to allow a wide representativeness of this validation dataset in terms of geographical distribution as well as biogeochemical and optical variability. The inter-comparison exercise is realized in two steps. First, the performance of the algorithms was assessed using hyperspectral and multispectral data (when possible) to cover a wide range of variability. Second, the inter-comparison exercise was performed on a consistent number of hyperspectral data (N=144) to observe if the number of data impacts the ranking of the algorithms' performance.

Figure 2.11 shows POC concentration derived from the different algorithms described in Section 2.3 and Table 2.3 against in situ POC measurements. Figure 2.12 compares the histograms of the frequency distribution of in situ and model-derived POC concentrations. Relevant statistical metrics are summarized in Table 2.5. The Le18-1 algorithm presents the highest MAPD, MB, $\mathrm{RMSD}_{\log}$ and MR values, and a much wider POC distribution compared to the in-situ ones (Figure 2.11f and 12f). For the organic-dominated waters, Le18-1 performs quite well as data points (green dots) are distributed along the 1:1 line. However, for mixed or organic-dominated waters, the variability in POC concentration is not reproduced and modeled POC values can be 100 times higher than in situ ones. In view of these results, this algorithm was excluded from further steps of the inter-comparison exercise. The statistical metrics (Table 2.5) provide a range of values among the 11 remaining algorithms for which the MAPD values vary between 38.83% and 64.40%, $\mathrm{RMSD}_{\log}$ between 0.27 and 0.44, MR between 1.04 and 1.59, and MB between –104.78 and 1237 µg L^{-1}. Note that the Liu15 algorithm generates 10 negative POC values, which were not considered within the log-scale statistics may be leading to an artificial increase in the algorithm performance. The radar plot in Figure 2.13 gives an overview of the statistical indicators by displaying the normalized MAPD, $RMSD_{log}$, MB and MR (Equations 20-23). The best performance, related to the smallest area in the normalized radar diagram (Figure 2.13), is obtained for the Hu15-3 algorithm. The Hu15-3 presents the smallest MAPD (38.87%), the smallest $RMSD_{log}$ (0.27), and an MR close to one (1.11) (Table 2.5). The Hu15-3 algorithm provides relatively good performance for organic-dominated (green dots close to the 1:1 line in Figure 2.11c). Data points sampled in mixed waters are scattered but follow the 1:1 line. However, for mineral-dominated waters, the Hu15-3 algorithm tends to underestimate high concentrations (POC > 1000 µg L^{-1}) (Figure 2.11c and 12c) and overestimates POC concentrations lower than 1000 µg L^{-1} (blue dots in Figure 2.11c). This results in the the regression slope between in situ and derived POC being lower than 1 (= 0.5). Similar observations can be made for the Hu15-2 and Hu15-1 algorithms.

The S08-1 and S08-2 algorithms provide accurate estimates at low concentrations for organic-dominated and mixed waters (around 100-200 µg L^{-1}), as it was developed mainly from data collected in open ocean waters. The performances of these algorithms are degraded at high concentrations, and for mineral dominated waters (blue dots in Figure 2.11h, i). Two Biosope data points in DSV were used previously by Stramski et al. (2008) to establish the S08-1 and S08-2 relationships and may artificially increase the performance of the S08-1 and S08-2. The performances of the S08 algorithms however do not change when removing these Biosope data points. The performance of the L18-2 algorithm is quite similar to the performance of the S08-1, 2 (Figure 2.11g, Tables 5 and S1). This was expected as Le18-2, S08-1 and S08-2 are based on a blue-to-green ratio.

Woźniak's algorithm W16-1 presents the best linear fit with a slope of 1.1. Both W16-1 and W16-2 algorithms overestimate POC concentration in mineral-dominated waters and underestimate POC concentration in organic-dominated and mixed waters (Figures 11k and 11l). For the W16-2 algorithm, data are less scattered and more accurate estimates of POC are achieved, especially for POC concentrations around 100 mg m^{-3}. This results in MAPD and RMSD_{log} being 61.32% and 0.337 for W16-2, respectively, against 64.08% and 0.427 for W16-1. The histograms in Figure 2.12k, l show that the shape of the frequency distribution of POC estimates and in situ data differ. The peak of frequency between 200 and 500 µg L^{-1} observed for the in-situ data is absent for modeled data.

Concerning the Liu15 algorithm, despite the fact that this algorithm was developed for highly turbid waters, it does not provide better POC retrievals over the mineral-dominated water dataset (Figure 2.11j and Table 2.5).

The second step of the inter-comparison exercise, performed on the same number of hyperspectral data (N=144), does not change the respective statistical results for the different algorithms, and Hu15-3 remains the best algorithm (Figure 2.S1 and Table 2.S1).

Table 2.5. Statistics obtained on DSV for the tested algorithms. The **best results for each statistic are shown in bold.**

Algorithms	**N**	**MAPD**	**MB**	**RMSD_{log}**	**RMSD**	**MR**	**R^2**	**Slope**	**Intercept**	**Negative Value**
CPOC - 1st	195	38.37	-2.77	**0.25**	**488.02**	1.03	**0.60**	0.78	0.58	**0**
CPOC - 2nd	**195**	**37.48**	**0.54**	**0.25**	489.88	**1.02**	0.60	0.78	0.58	**0**
Hu15-1	195	64.40	29.45	0.32	581.37	1.55	0.39	0.32	1.9	**0**
Hu15-2	195	38.83	-104.8	0.28	582.1	1.14	0.48	0.35	1.72	**0**
Hu15-3	195	38.87	-74.53	0.27	589.8	1.11	0.47	0.5	1.31	**0**
Le16-1	195	61.75	127.5	0.38	943.3	1.52	0.22	0.4	1.7	**0**
Le16-2	144	60.89	1237	0.44	4715	1.59	0.42	0.9	0.46	**0**
Le18-1	195	1781	1340760	1.76	13608584	18.81	0.08	**0.94**	1.48	**0**
Le18-2	195	68.94	157.7	0.35	651.5	1.63	0.39	0.48	1.52	**0**
Liu15	134	62.71	202.8	0.38	749.4	1.4	0.28	0.62	1.1	10
S08-1	195	45.09	-60.53	0.3	584.0	1.26	0.39	0.36	1.73	**0**
S08-2	195	49.19	44.14	0.29	590.4	1.41	0.48	0.47	1.51	**0**
W16-1	150	64.29	214.9	0.44	842.5	1.04	0.48	1.13	**-0.33**	**0**
W16-2	146	61.32	247.5	0.34	715.1	1.48	0.53	0.91	0.35	**0**
S08-1*	193	45.46	-61.03	0.30	587.0	1.26	0.38	0.35	1.75	**0**
S08-2*	193	49.19	44.47	0.30	593.5	1.41	0.48	0.46	1.52	**0**

**Removed Biosope data*

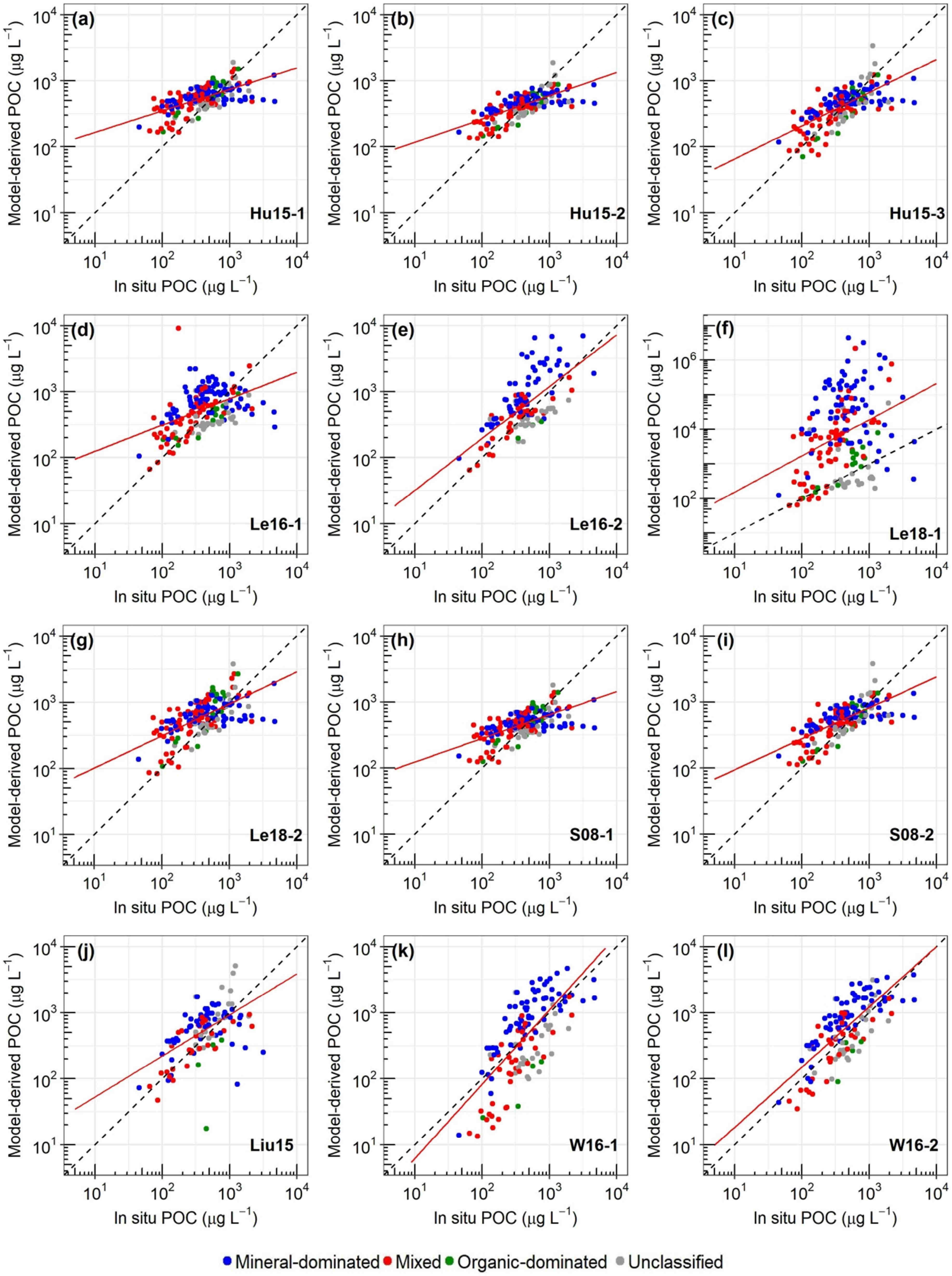

Figure 2.11. Comparison of in situ and model-derived POC for the selected algorithms (log-transformed data). Green, red, and blue dots correspond to organic-dominated, mixed, and mineral-dominated waters, respectively. Gray dots indicate the in situ data points without information of SPM that cannot be classified according to the POC/SPM ratio. The black dashed line is the 1:1 line, and the solid red line is the type II linear regression.

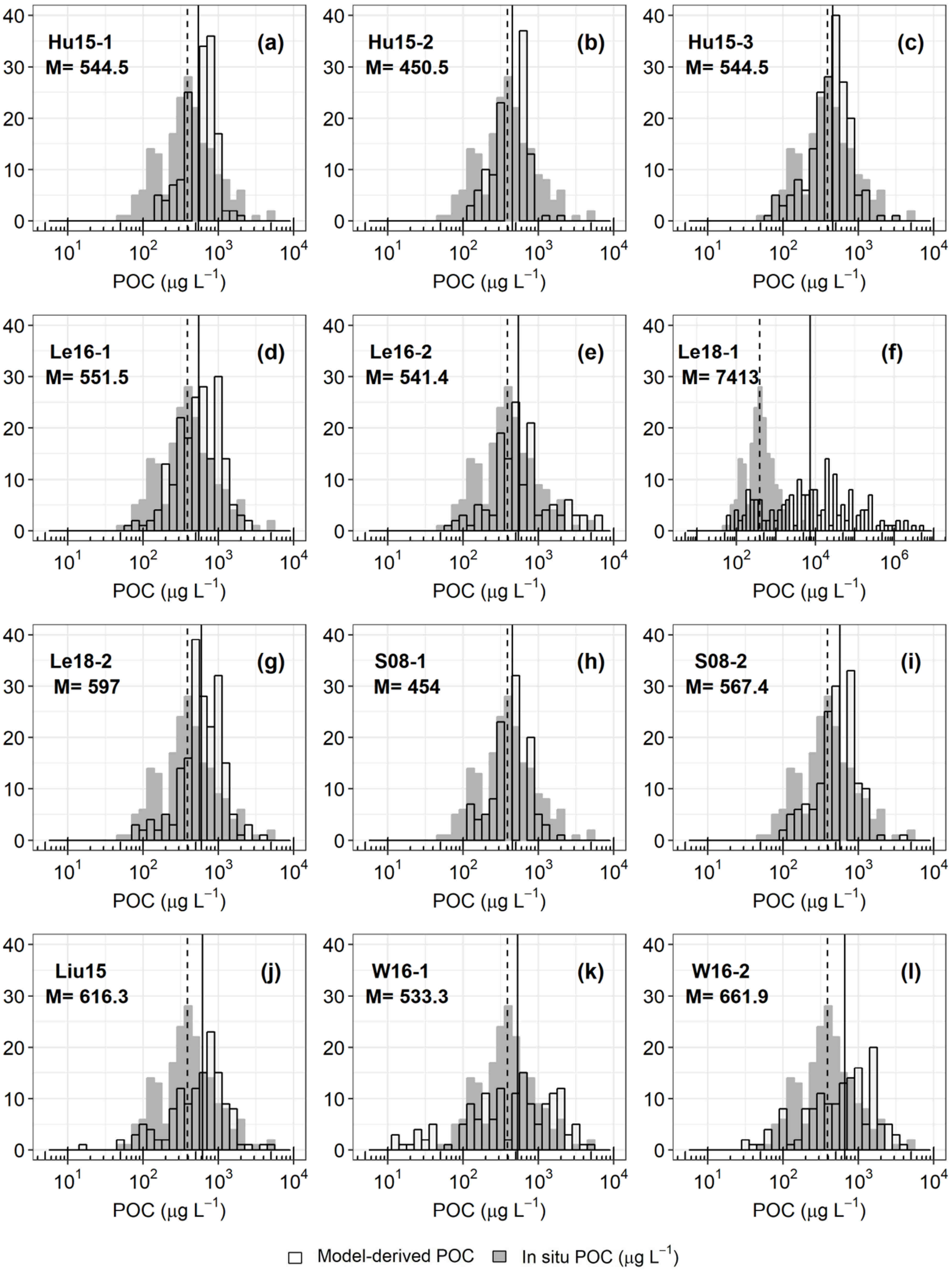

Figure 2.12. Frequency distribution of in situ (grey) and model-derived (white) POC. The dashed lines represent the median of in situ POC measurements for DSV (= 391 μg L^{-1}), and the solid line the median values of POC estimates. The median values of POC estimates (M) are indicated in each panel.

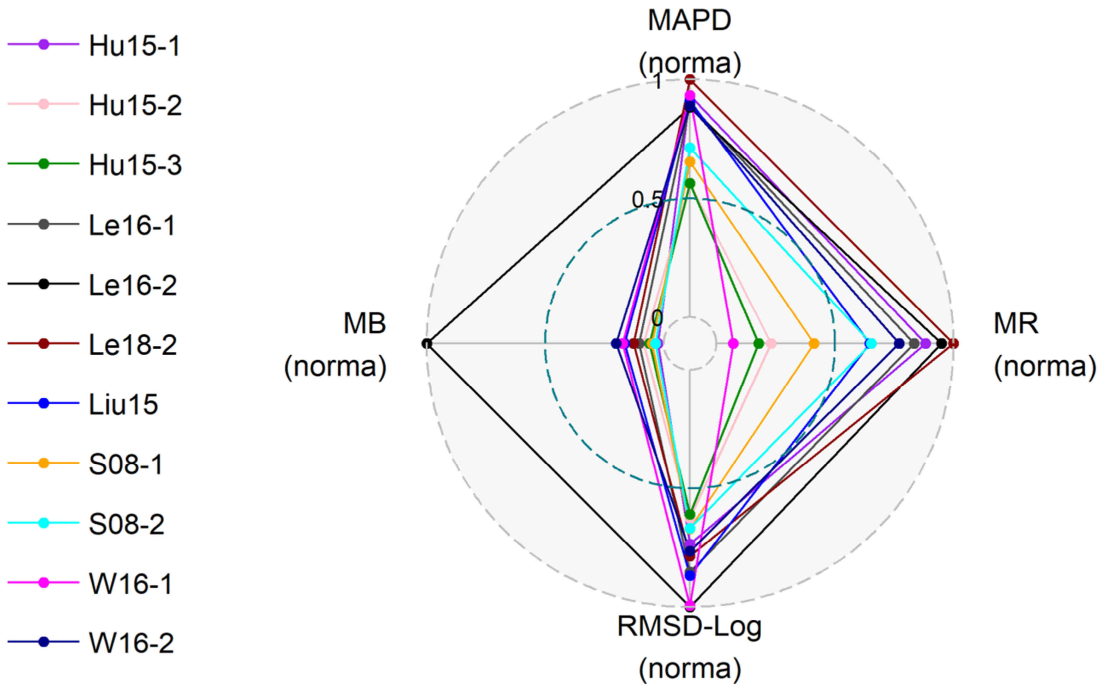

Figure 2.13. Comparison of the statistical performance of the eleven algorithms. The algorithms were tested using hyperspectral and multispectral data. The number of data changes according the considered algorithm (Table 5).

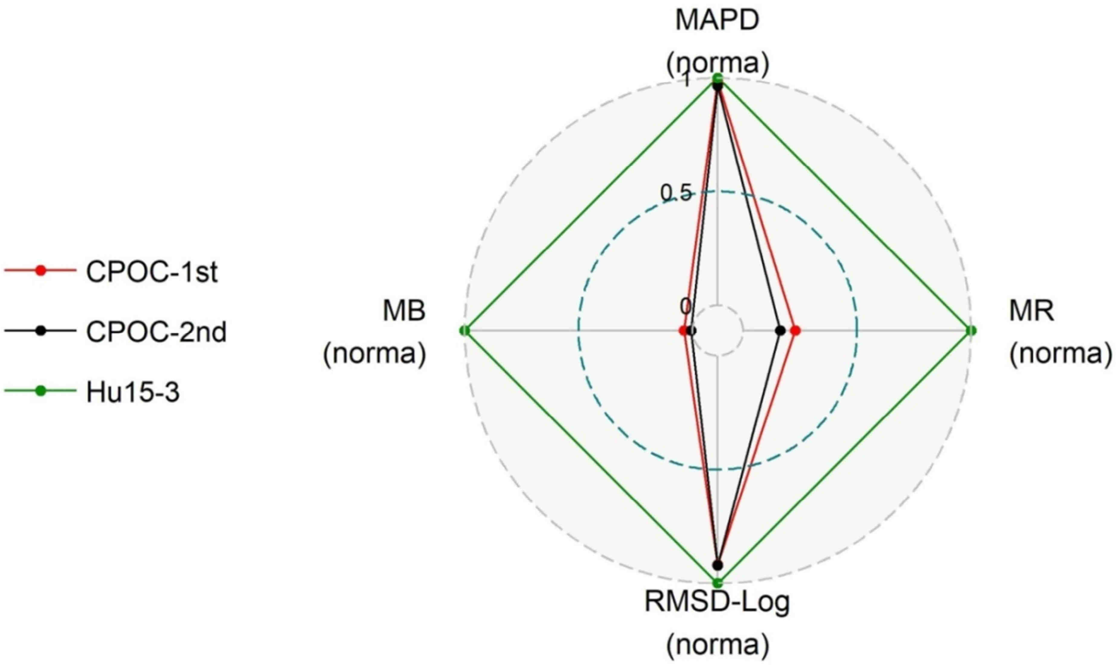

Figure 2.14. Statistical performance of the new developed algorithms named CPOC (Coastal POC) as compared to the Hu15-3 algorithm. The normalized MAPD, MR, MB, and $\mathrm{RMSD}_{\mathrm{log}}$ were calculated on DSV. The black line and red line present statistics obtained with the CPOC-1st and CPOC-2nd algorithm, respectively.

2.3.3. Performance of the new algorithms

The radar plot in Figure 2.14 and Table 2.5 illustrate that the CPOC-1^{st} and CPOC-2^{nd} algorithms improve the overall performance as compared to Hu15-3 algorithm. The second-order polynomial relationship shows the best performance with a smaller MAPD and smaller MB than the Type II linear regression. The MAPD is 37.48%, the $RMSD_{log}$ is 0.25, MB is = 0.54, MR is equal to 1.02, and the regression slope is around 0.78. Most of the POC values in waters identified as mineral-dominated are overestimated, whereas the POC values in organic-dominated waters are underestimated (Figure 2.15). We tried to develop a specific second-order polynomial regression according to the type of waters to adjust the POC concentration from Equation 2.28 according to the POC/SPM ratio with SPM concentration from Han et al., 2016. Results are not shown as it does not improve the accuracy of the estimates. As no specific regional pattern has been noticed on the validation results (not shown), the performance of the algorithm is more related to the chemical nature of the bulk suspended particulate matter, as opposed to any regional aspects. The shape of the POC distribution of model-derived and in situ data are quite similar (Figures 15b and 16b). Nevertheless, the maximum of occurrence is slightly shifted towards higher POC values. This results in the median calculated for modeled data being a bit higher (425 µg L^{-1} instead of 391 µg L^{-1}), whereas the mean values are equal (=569 µg L^{-1}).

The matchup analysis was conducted by applying CPOC-2nd on the satellite $R_{rs}(\lambda)$ measurements gathered in the match-up dataset described in section 2.2. The matchup analysis shows that the CPOC-2nd algorithm, developed only on $R_{rs}(\lambda)$ and POC in situ data, is able to estimate satisfactorily the surface POC concentration from satellite observation over coastal waters. The histograms (Figure 2.17) show a good agreement between the in situ and estimated maximum values (around 100 µg L^{-1}), as well as between the in situ and estimated median values (102.5 and 108.4 µg $L^{-1)}$, respectively. The MAPD, $RMSD_{log}$, MR, and MB values are 34.16%, 0.24, 0.92, and –25.93 µg L^{-1}, respectively (Loisel et al. 2018; Seegers et al. 2018). Note that overestimations and underestimations of POC values are only observed for two of the eight sampling stations (Banyuls-sur-Mer and Marseille). These differences can be due to uncertainties on in situ POC measurements as well as satellite remote-sensing reflectance (partly due to atmospheric corrections uncertainties). Concerning this latter aspect, we verified the retrieval accuracy of R_{rs} based on an extensive matchup exercise of 760 coincident data points collected from the AERONET-OC sites (Ocean Color component of the Aerosol Robotic Network). A bias of 3.4×10^{-3}, 1.5×10^{-3}, -1.9×10^{-4} between in situ AERONET and MERIS $R_{rs}(\lambda)$ at 490, 555 and 665 has been observed, respectively. Taking into account these bias values for the MERIS $R_{rs}(\lambda)$ values over the SOMLIT matchup dataset, we showed that this correction only slightly modifies the POC estimates. Inaccuracies can also be explained by the fact that the range of POC concentration used in this matchup exercise is lower than the range of POC concentration of DSD. For instance, the median POC value for the SOMLIT in situ dataset is 108.4 µg L^{-1}, while it reaches 366.4 for DSD. The fact that the statistical values are better for the match-up data set than for DSV may be partly explained by the fact that the SOMLIT POC data set used for the match-up exercise gathers less mineral dominated waters (38 %) for which a slight over-estimation by CPOC-2nd has been observed, against 50% for DSV.

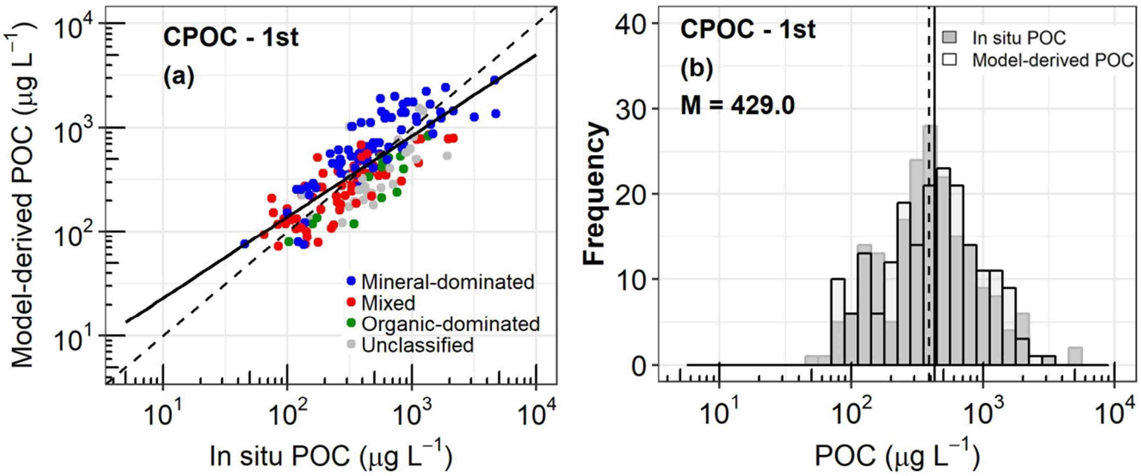

Figure 2.15. (a) Comparison of in situ and model-derived POC for the CPOC-1st algorithm. The dashed line is the 1:1 line, and the solid line is the type II linear regression. Green, red and blue dots correspond to organic-dominated, mixed and mineral-dominated waters; gray dots indicate the in-situ data points without information of SPM that cannot be classified according to the POC/SPM ratio. (b) The frequency distribution of in situ (grey) and POC measurements derived from the CPOC-1st algorithm (black contour). The dashed lines represent the median of in situ POC measurement of DSV (= 391 µg L^{-1}), and the solid line the median value of model-derived POC value of DSV.

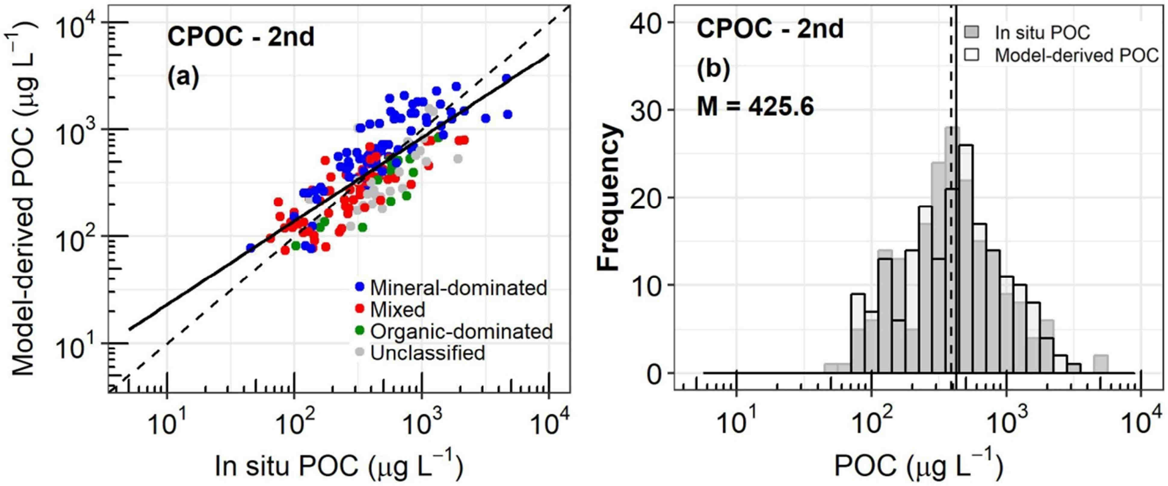

Figure 2.16. (a) Comparison of in situ and model-derived POC for the CPOC-2nd algorithm. The dashed line is the 1:1 line, and the solid line is the type II linear regression. Green, red and blue dots correspond to organic-dominated, mixed and mineral-dominated waters; gray dots indicate the in-situ data points without information of SPM that cannot be classified according to the POC/SPM ratio. (b) The frequency distribution of in situ (grey) and POC measurements derived from the CPOC-2nd algorithm (black contour). The dashed lines represent the median of in situ POC measurement of DSV (= 391 μg L^{-1}), and the solid line the median value of model-derived POC value of DSV.

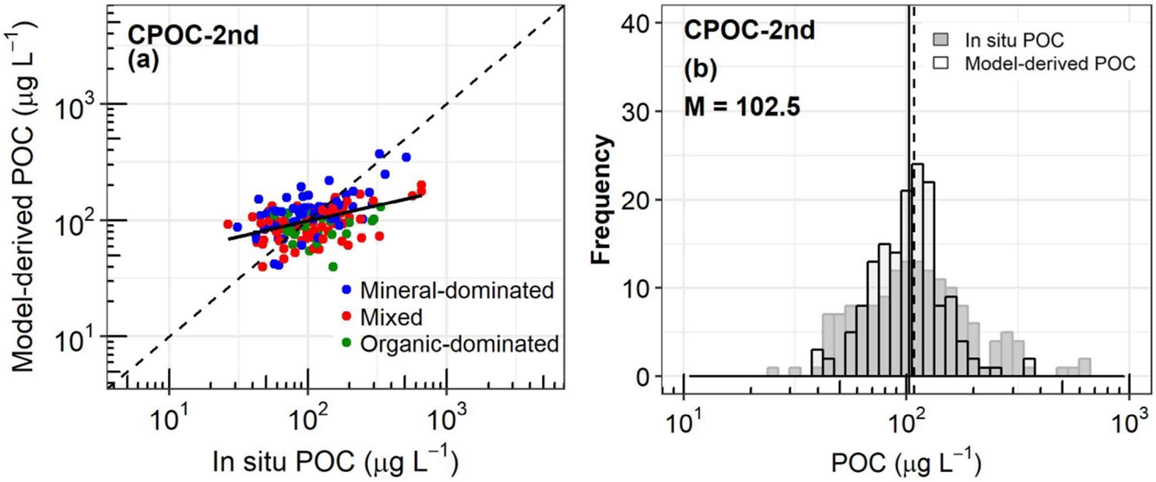

Figure 2.17. (a) Comparison of in situ and model-derived POC concentrations using the matchup dataset. The dashed line displays the 1:1 line and the solid one the linear type II regression. Green, red and blue dots correspond to organic-dominated, mixed and mineral-dominated waters, respectively. (b) Frequency distribution of in situ (grey) and POC measurements derived from the CPOC-2nd algorithm (black contour). The dashed lines represent the median of in situ POC measurement (= 108.4 μg L^{-1}), and the solid line the median value of model-derived POC value.

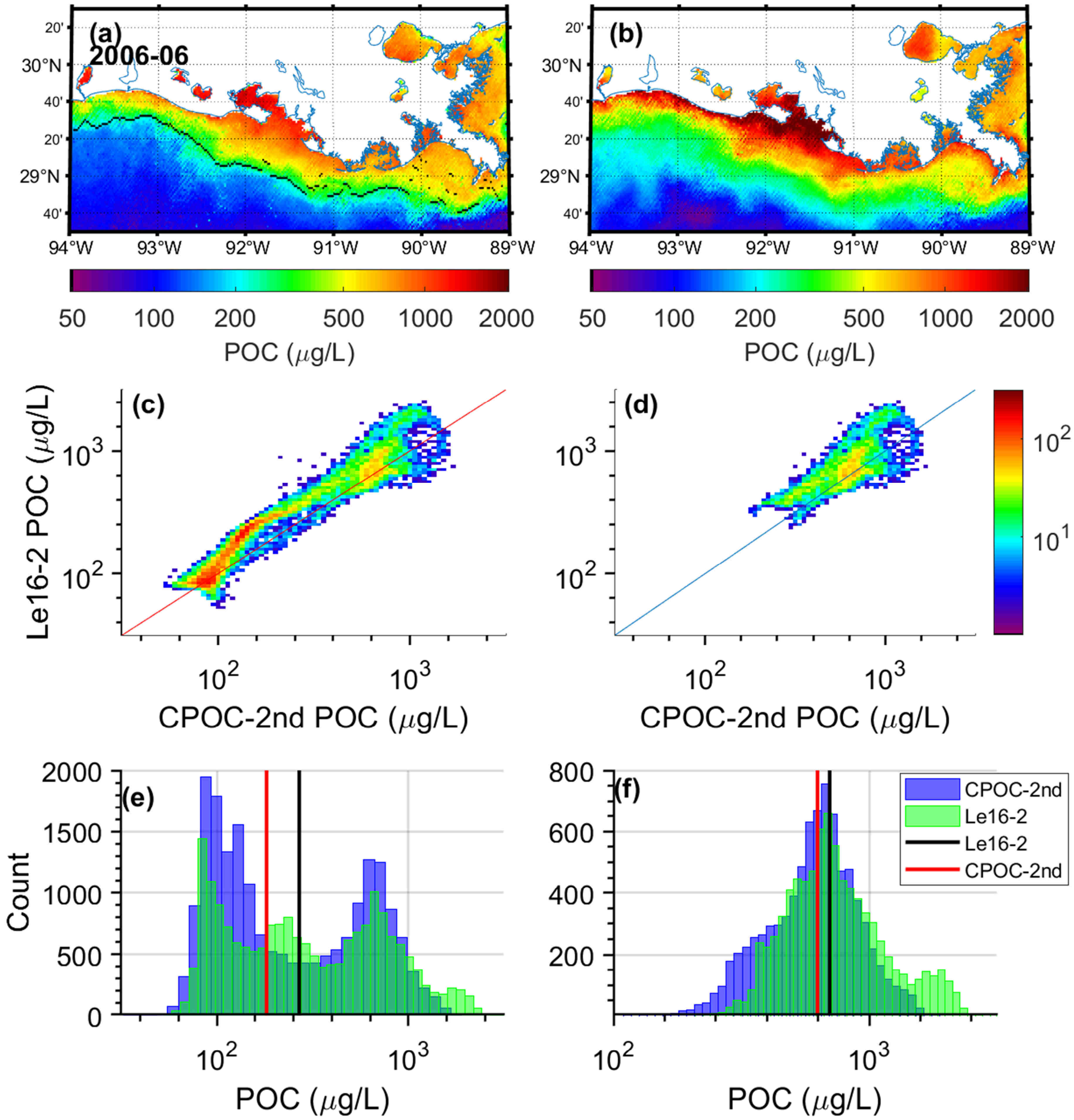

Figure 2.18. Near-surface POC concentration model-derived from MERIS, Louisiana Continental Shelf, June 2006 (a) using CPOC-2nd (b) Le16-2 algorithms. The black line in the upper left panel delimits pixels, close to the coast, with $R_{rs}(665) > 0.0012$ (Robinson et al. 2003) and offshore pixels with $R_{rs}(665) < 0.0012$ (c-d). Density plots of POC as derived with the CPOC-2nd and Le16-2 algorithms for (c) all the pixels of the scene (d) only for pixels with $R_{rs}(665) > 0.0012$. Distribution of POC estimates with CPOC-2nd and Le16-2 algorithm for (e) all pixels of the scene (f) only for pixels with $R_{rs}(665) > 0.0012$. The black and red lines represent the median of POC estimates using the Le16-2 and CPOC-2nd algorithms, respectively.

2.4. Concluding remarks

A variety of POC inversion algorithms based on different approaches were evaluated from an extensive dataset composed of coincident measurements of POC and $R_{rs}(\lambda)$, which were sampled in highly contrasting bio-optical coastal environments. While these existing algorithms perform relatively well over POC ranges for which they were developed, they present some lack of accuracy over a broad range of POC concentrations. With the objective of improving POC estimates at the global scale for coastal waters, a new empirical relationship was proposed based on a second-order polynomial regression using the maximum band ratio. The new algorithm (CPOC) shows relevant capacity to estimate POC concentrations on the in-situ validation dataset (MAPD = 37.48%, $RMSD_{log}$ = 0.25, MB = 0.54 μg L^{-1}, and MR = 1.02). Robust results were found when the algorithm was tested on the matchup dataset as illustrated by the consistency in the median values computed for the modeled POC (102.5 μg L^{-1}) and the in situ POC datasets (108.4 μg L^{-1}). While the use of a spectral band ratio to retrieve POC reduces the impact of atmospheric corrections, the latter continues to have an impact as the accuracy of R_{rs} retrieval is spectrally dependent (Jamet et al. 2011). The new algorithm was applied to MERIS data in the Louisiana Continental Shelf in June 2006. The observed spatial and temporal (not shown) patterns were in good agreement with the patterns observed by Le et al. who developed an algorithm specifically for this region in 2006. The algorithm developed in this study performs consistently across the three types of water (mineral-dominated, mixed, and organic-dominated). However, the POC concentration in mineral-dominated waters tends to be overestimated, whereas POC concentration in organic-dominated waters tends to be underestimated. Second-order polynomial regressions specific to the type of waters to adjust the POC concentration according to the POC/SPM ratio were evaluated, but such formulations did not improve the estimates. From these results, several key points of development are highlighted as as necessary to the development of greater knowledge pertaining to the composition of the particulate pool.

The use of POC/SPM ratio as a proxy for particulate composition according to the criteria of (Woźniak et al. 2010) should be re-examined. The criteria established by (Woźniak et al. 2010) to define the type of waters were fixed regarding the spectral shape of the absorption coefficient and the particle size distribution (PSD). This exercise was based on measurements sampled from optically contrasted conditions but in a restricted area (Imperial Beach, San Diego, Tijuana River watershed). It will be interesting to re-examine these criteria on a larger number of observations performed in different coastal regions to ensure their possible generalization at a global scale. However, in many cases, PSD is not available from the optical measurements and measurements of the particulate absorption spectra using benchtop spectrophotometers are not systematically performed. In this framework, the ratio of the particulate backscattering to scattering coefficient (b_{bp}/b_p), measured by commercial optical backscattering sensors, such as WetLabs Eco-VSF and ECO-BB, could be a valuable parameter. Indeed, previous studies (Duforêt-Gaurier et al. 2018; Loisel et al. 2007; Twardowski et al. 2001) have shown that b_{bp}/b_p could be an indicator of the amount of organic material relative to mineral particles. It would be interesting to re-conduct these studies on coincident POC, $R_{rs}(\lambda)$, SPM, and b_{bp}/b_p in situ measurements to define some criteria at the global scale and to better characterize which kind of particles dominate in a defined water mass.

Appendix

Table S.1. Statistics obtained on the 144 hyperspectral data of DSV with hyperspectral R_{rs} only. Multispectral data coming from CASES (Bélanger et al. 2008), Biosope (Leblanc et al. 2018) and Coastlooc (Babin et al. 2003b; Babin et al. 2003c) were removed.

Algorithms	N	MAPD	MB	$RMSD_{log}$	RMSD	MR	R^2	Slope	Intercept	Negative Value
Hu15-1	144	55.44	-50.55	0.31	651.0	1.41	0.37	0.28	1.98	0
Hu15-2	144	41.01	-142.6	0.29	666.9	1.14	0.41	0.31	1.82	0
Hu15-3	144	41.77	-101.3	0.28	677.6	1.11	0.41	0.44	1.48	0
Le16-1	144	62.68	126.8	0.4	1084	1.51	0.14	0.33	1.87	0
Le16-2	144	60.89	1237	0.44	4715	1.59	0.42	0.9	0.46	0
Le18-1	144	2818	1801776	1.87	15865153	29.19	0.03	0.68	2.26	0
Le18-2	144	53.89	50.53	0.32	674.9	1.44	0.37	0.43	1.63	0
Liu15	134	62.71	202.8	0.38	749.4	1.4	0.28	0.62	1.1	10
CPOC-2nd	144	44.62	22.60	0.27	561.7	1.18	0.55	0.77	0.64	0
S08-1	144	42.82	-139.5	0.3	665.5	1.16	0.37	0.31	1.83	0
S08-2	144	49.59	17.34	0.3	675.4	1.4	0.41	0.42	1.64	0
W16-1	144	64.08	228.8	0.43	859.7	1.18	0.45	1.06	-0.15	0
W16-2	144	61.32	252.4	0.34	719.9	1.51	0.53	0.9	0.39	0

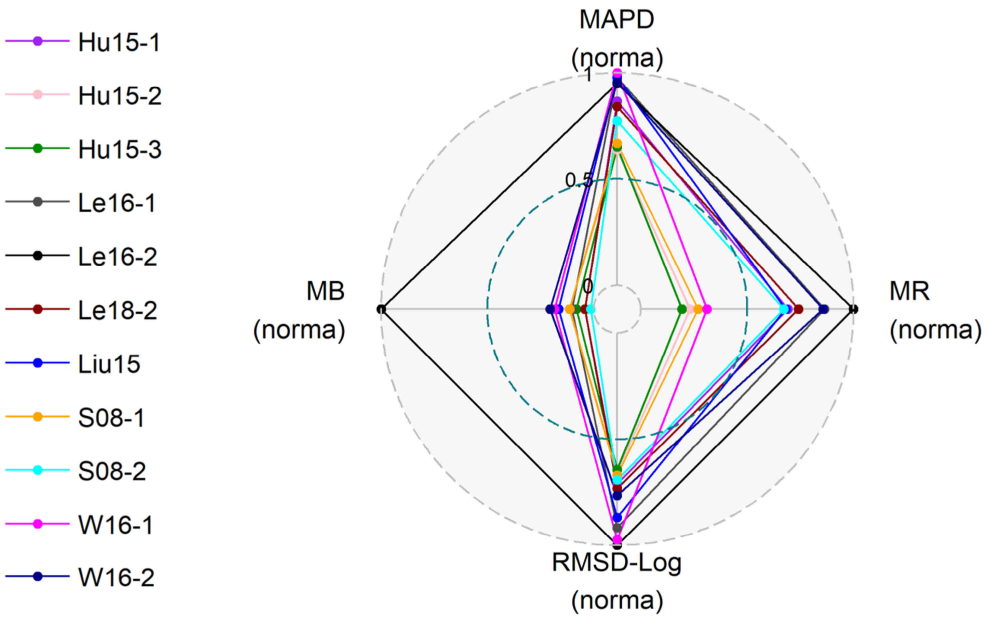

Figure S.1. Comparison of the statistical performance of the eleven algorithms. The algorithms were tested using hyperspectral data only. The number of data (N=144) is the same for the 11 algorithms (Table 2.5).

Chapter 3: Optical classification of coastal water

3.1. Introduction

In recent years, various approaches aiming to define water optical water types have been documented for applications on both open and coastal waters. These optical classification methods have been developed not only to provide a better understanding of water optical diversity and of the related in-water constituents variability but also to potentially improve accuracy of ocean color algorithms (Baker and Smith 1982; Garcia et al. 2006; Han et al. 2016; Le et al. 2011; Lubac and Loisel 2007; Mélin and Vantrepotte 2015; Monolisha et al. 2018; Moore et al. 2009; Shen et al. 2015; Tranvik et al. 2009; Vantrepotte et al. 2012; Ye et al. 2016).

Different methodologies have been developed to classify ocean color radiometric data (i.e. R_{rs} spectra) collected from in situ or spatial measurements. For instance, fuzzy logic classification was used by (Moore et al. 2001) to classify open ocean waters into 6 classes. The authors developed fuzzy scheme to apply on SeaWIFS imagery in order to select and blend class specific algorithm. Later, Lubac and Loisel (2007) applied unsupervised classification (hierarchical cluster analysis) to partition in situ measurement of normalized remote-sensing reflectance collected in the English Channel and North Sea waters into 5 optical classes. Interestingly, the latter authors have further demonstrated that the classes they defined can be associated with a specific bio-optical environment: *Phaeocystis* bloom situation, mineral and detritus dominant, non-living particles and 2 mixed classes. The original aspect of their approach is that they used normalized R_{rs} spectra, in order to focus on the shape of the R_{rs} spectra and thus on the optical quality of the waters, removing the first order variability in the R_{rs} spectra related to the change of the concentration of biogeochemical parameters (e.g. variation in the turbidity level). Based on a broader in situ data set encompassing contrasted coastal water masses (Vietnam, English Channel, and French Guiana) and using globally the same approach on normalized R_{rs}, Vantrepotte et al. (2012), classified coastal water into 4 classes: mineral origin, 2 mixed optical situations, one phytoplankton dominated class. Few years later, (Mélin and

Vantrepotte 2015) showed from a SeaWiFS training data set that the coastal waters ocean color diversity can be gathered into 16 radiometric classes. Recently, (Monolisha et al. 2018) identified eight coastal optical classes in the northern Indian Ocean using Fuzzy C Mean algorithm on normalized R_{rs} which were derived from OC-CCI products (merged data from SeaWIFS, MODIS Aqua and MERIS). These 8 classes presented similarities with those documented by (Mélin and Vantrepotte 2015).

The first goal of this study is: first, to define optical water types based on an extended data set of in situ R_{rs} spectra and second, to better understand the bio-optical meaning of each optical class identified from their radiometric signatures. For that purpose, an unsupervised classification approach was used to partition in situ hyperspectral R_{rs} spectra collected in various coastal waters into separated clusters. The second goal is to apply optical classification to satellite data in contrasted coastal waters (MERIS data) in order to assess the potential applicability of new defined classes for depicting the optical diversity of coastal environments.

3.2. Data and method

3.2.1. In situ measurements

In situ measurements used in this study include radiometric (R_{rs}), optical $\left(a_{\phi}(443), a_{NAP}(443), a_{CDOM}(443) \text{and } b_{bp}(665)\right)$ and biogeochemical parameters (POC, SPM and Chla). Note that $\left(a_{\phi}(443), a_{NAP}(443), a_{CDOM}(443)\right)$ are the absorption coefficient (m^{-1}) of phytoplankton, non-algal particles, and colored dissolved organic matter at 443 nm, respectively, whereas $b_{bp}(665)$ is the backscattering coefficient of particles at 665 nm. The whole dataset consists of 391 measurements of hyperspectral R_{rs} (N_{Rrs}) associated with biogeochemical (POC, SPM and Chla) and IOP parameters (a_{CDOM}, b_{bp}). It should be noted that for some of the 285 R_{rs} measurements, coincident bio-parameters and IOP are missing thus $N_{Rrs} > N_{IOP} > N_{bio\text{-}parameters}$.

Sampling areas

In situ measurements were collected from 8 cruises from 2011 to 2015 (see Figure 3.1 and Table 3.1). The dataset covers different coastal areas (Mekong estuary - the East sea of Vietnam, coastal zone of French Guiana and Gironde Estuary - the Bay of Biscay-France, English Channel and the south part of the North Sea), with different bio-optical environments, as already described in Chapter 2.

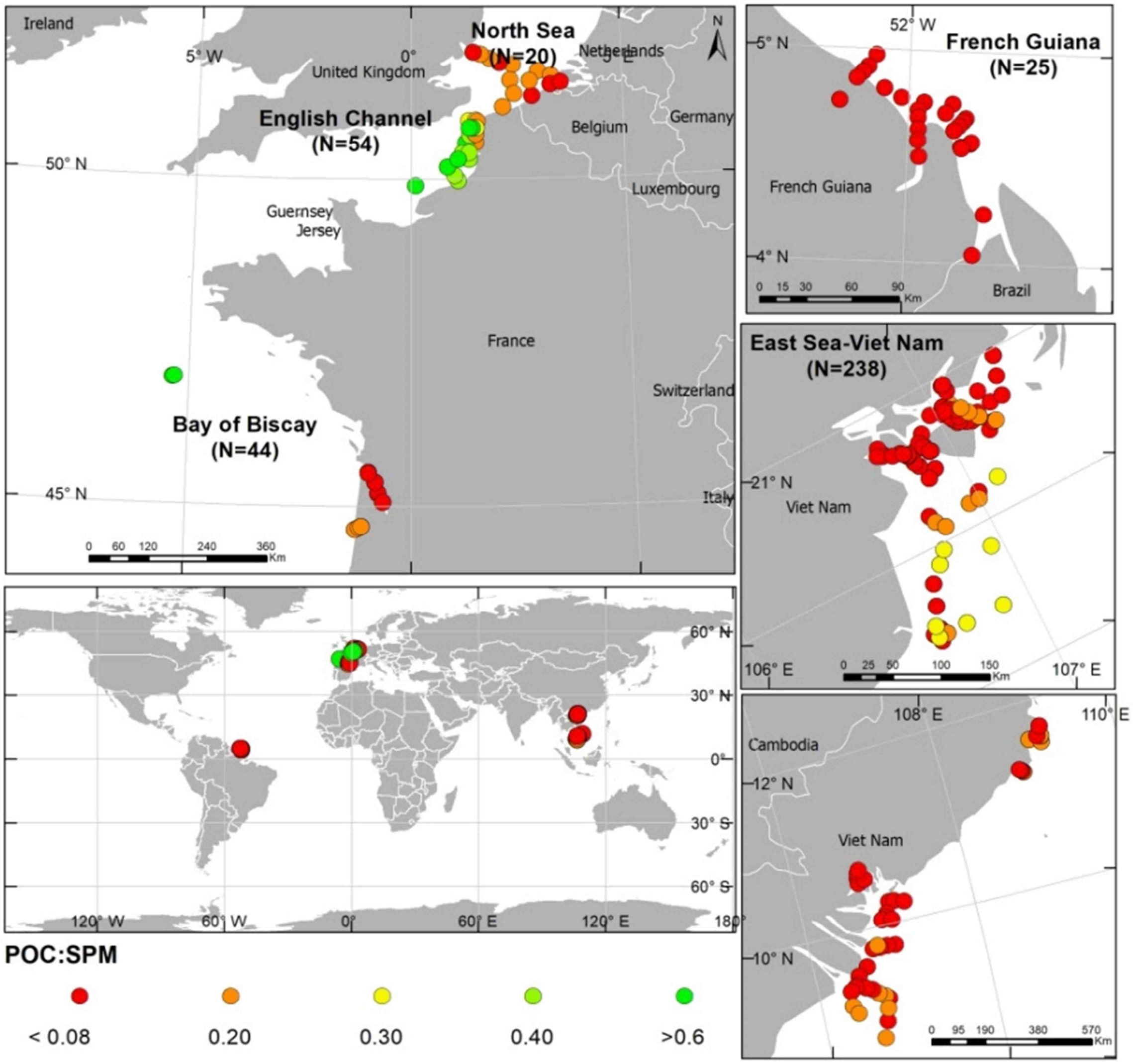

Figure 3.1. Geographical distribution of the 391 in situ coincident measurements of POC and Rrs listed in Table 3.1; (a) European coastal water, (b) coastal zone of French Guyana, (c-d) Tonkin bay and Mekong estuary, the East sea of Vietnam. The color scale presents values of POC and SPM ratio.

Remote sensing reflectance

TriOS radiometers were used to measure upwelling radiance, $L_u(0^-,\lambda)$ at 1-3 cm below sea surface and above water down-welling irradiance $E_d(0^+,\lambda)$. After instrument self-shading effect correction (Leathers et al. 2004), the remote sensing reflectance, Rrs(λ), is calculated as:

$$R_{rs}(\lambda) = \frac{1-\rho}{n^2} L_u \tag{3.1}$$

where ρ~0.025 is the Fresnel reflectance of the air sea interface, and n~1.34 is the refractive index of seawater. $(1 - \rho)/n^2 \sim 0.543$ is the upward radiance transmittance of the sea surface for normal incidence from below.

A detail description of the measurement method in East sea of Vietnam and French Guiana are documented in (Loisel et al. 2017; Vantrepotte et al. 2012), and a dataset collected in Bay of Briscay, France is referred (Novoa et al. 2017) (Table 3.1).

The dataset in English Channel was acquired by using three TRiOS radiometers to measure the above surface downward irradiance, $E_d(0^+,\lambda)$, the in water irradiance profile, $E_d(z,\lambda)$ and the nadir upward radiance profile, $L_u(z,\lambda)$. L_u was computed from $L_u(z,\lambda)$ with the attenuation coefficient for upward radiance, $K_{Lu}(z_0,\lambda)$ at 5m depth while $R_{rs}(\lambda)$ were then computed using the equation 3.1 (Lubac and Loisel 2007). Remote-sensing reflectance in the Southern North Sea and in the Bay of Biscay France were computed from the upwelling radiance $L_w(0^+)$, and the down-welling irradiance $E_d(0^+)$ measured just above the water surface (Nechad et al. 2010).

Biogeochemical parameters

Water samples were collected just below the sea surface using Niskin bottles, simultaneously to the radiometric measurements. The biogeochemical parameters (Chla, SPM and POC) concentrations were measured from the particulate matter collected on Whatmann GF/F glass fiber filters and analyzed following standard methodologies described in (Loisel et al. 2007). SPM includes all organic and mineral material which size is approximately higher than 0.5–0.7 μm. POC which corresponds to autotrophic organisms, heterotrophic bacteria, and detritus with a diameter between 0.4 and 200 mm, a pre-filtration being usually performed. POC concentration was measured by the CHN method according to the JGOFS protocol (Knap et al., 1996). The concentration of Chla was determined by spectrophotometry according to the protocol defined by Lorenzen (1967).

Table 3.1. Information of the in situ data used in this study: number of Rrs data (N).

Region	Year	N	References
Bay of Biscay-France	2012	41	(Novoa et al. 2017)
East sea of Viet Nam	2011	105	(Loisel et al. 2014; Loisel et al. 2017)
	2012	10	
	2013	35	
	2014	68	
	2015	15	
English Channel	2010	2	(Neukermans et al. 2012)
	2004	61	(Lubac and Loisel 2007)
French Guiana	2012	32	(Vantrepotte et al. 2015; Vantrepotte et al. 2012)
North Sea	2010	16	(Nechad et al. 2010)
Total		**385**	

The mean and standard deviation values of Chla, POC, and SPM were 4.60±4.98 μgL^{-1}, 726.53± 987.65 μgL^{-1}, and 40.69x10^3 ± 98.98x103 μgL^{-1}, respectively. Chla [0.12; 33.37] μgL^{-1}, POC [45.36; 7888] μgL^{-1}, and SPM [218; 844.67 x10^3] μgL^{-1} ranges cover 3, 3, and 4 orders of magnitude respectively (Figure 3.2). The highest concentrations of POC and SPM were observed in Gironde estuary, France, which samples also show the highest reflectance recorded in our data set. High SPM values were also recorded in French Guiana and Mekong estuary, and can be related to coastal or bottom erosion processes and regional river particles discharge.

POC, SPM and Chla were then converted to the same unit ($\mu g\ L^{-1}$) before computing the POC/SPM and POC/Chla ratios, which were used to better characterize the bulk particulate matter. For instance, the POC/SPM ratio can be used as a good proxy of the relative fraction of organic matter composing the suspended particulate matter assemblage, while the POC/Chla ratio provides the relative proportion of both living and nonliving material relative to autotrophic organisms (this ratio is also sensitive to variation in the intracellular photosynthetic pigment concentration during photo-acclimation effects). These ratios, which have recently been used to characterize the bio-optical environment of the suspended particulate matter in coastal and open ocean waters (Behrenfeld and Boss 2003; Koestner et al. 2018; Loisel and Morel 1998; Neukermans et al. 2016; Tran et al. 2019; Woźniak et al. 2011), will be considered in this study to identify the particulate environment associated with each cluster defined from the marine reflectance spectra.

Optical parameters

The particulate backscattering coefficient (b_{bp}, m^{-1}) was estimated using the WET Labs ECO-BB or the ECOBB-9 instruments as described in (Neukermans et al. 2012). The absorption coefficient by colored dissolved organic matter (a_{CDOM}, m^{-1}) was measured (every nanometer from 250 to 850 nm) following the NASA protocol (Mitchell et al. 2000). The details of method are documented in (Vantrepotte et al. 2007).

CDOM absorption coefficient at 443 nm, varies from 5.1×10^{-3} to 2.58 m^{-1} (average = 0.227 m^{-1}, Stdv = 0.285 m^{-1}) high values were observed in French Guiana (2.58 m^{-1}) were the highest value of ratio $a_{CDOM}(443)/(a_{CDOM}(443) + a_p(443))$ (0.8) was also observed. The particulate backscattering coefficient, $b_{bp}(650)$ ranged from 1.8×10^{-3} to 0.387 m^{-1} (average 0.0561 m^{-1}, Stdv = 0.0634 m^{-1}).

Because of the lack of in situ measurement of phytoplankton absorption (a_{Φ}) and non-algal particulate matter absorption coefficient (a_{NAP}), the latter variables have been both estimated at 443 nm from Chla and SPM, respectively. Phytoplankton absorption coefficient was retrieved from the Chla concentration using the relationship by (Bricaud et al. 1998) which was verified for coastal waters by (Babin et al. 2003c). Non-algal particulate matter absorption coefficient ($a_{NAP}(443)$) was estimated from SPM concentration using the empirical relationship developed by (Babin et al. 2003c). The particulate absorption coefficient ($a_p(443)$) was then estimated as the sum of $a_{\Phi}(443)$ and $a_{NAP}(443)$.

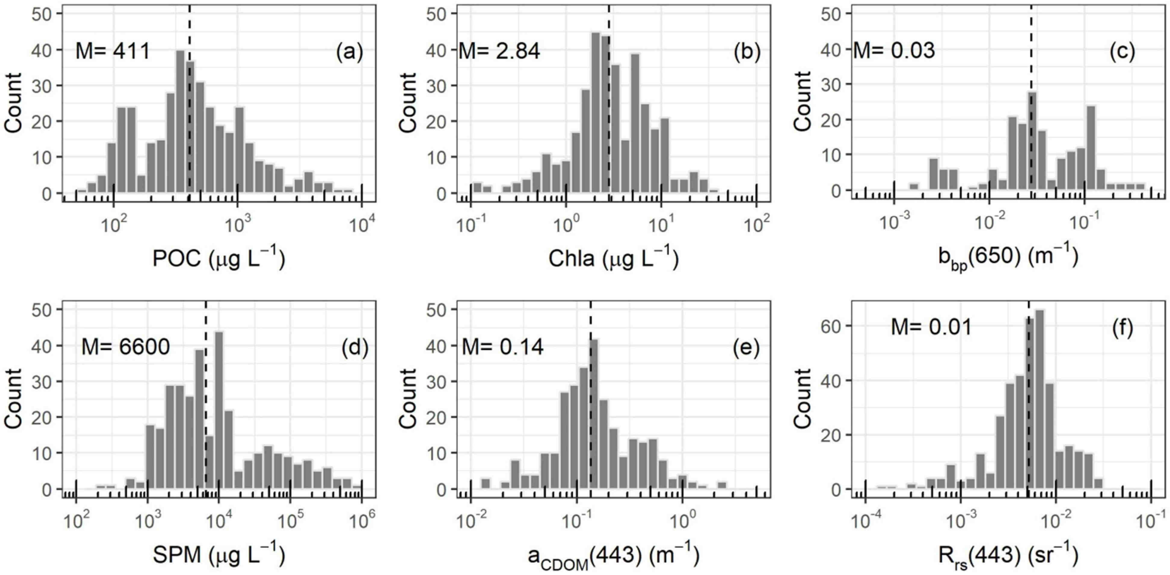

Figure 3.2. Frequency distribution histograms of selected biogeochemical (POC, Chla, SPM), radiometric ($R_{rs}(443)$) and bio-optical ($a_{CDOM}(443)$, $b_{bp}(650)$) variables composing the in situ dataset considered for the classification. M stands for median and dash lines present the median.

3.2.2. Satellite reflectance data

Daily MERIS Level 1 images were processed to Level 2 R_{rs} data based on Polymer atmospheric correction algorithm (Steinmetz et al. 2011), which was adapted for coastal waters (Loisel 2017). Coastal water pixels were extracted from Level 2 using criteria of depth (not deeper than 4000 m) and distance to the coast (lower than 200 km). Monthly products have been then processed from the daily data based on arithmetic mean.

3.2.3. Classification of in situ Rrs spectra

The procedure of classification is based on following steps: (1) data normalization; (2) unsupervised classification (3) cluster homogeneity test:

(1) Hyperspectral R_{rs} in the visible part of the spectrum (from 400 to 700 nm) were normalized to remove the reflectance first order variability. This normalization was performed as in Lubac and Loisel (2007), by dividing each R_{rs} spectrum by its integrated value (i. e. the surface below the spectrum) following the formula:

$$R_{nrs}(\lambda) = R_{rs}(\lambda)/\int_{\lambda_{700}}^{\lambda_{400}} R_{rs}(\lambda)d\lambda \tag{3.2}$$

where R_{nrs} (in units of nm^{-1}) indicates the normalized spectrum obtained by integration between $\lambda = 400$ nm and $\lambda=700$ nm. The R_{rs} normalization allows a better analysis of the variability in the shape of R_{rs} spectra related to changes in the bio-optical environment (and not only on the change in the absolute concentration of the optically active water constituents).

(2) The normalized spectrum, R_{nrs} was then performed with unsupervised classification in order to partition the data into optical groups. The method of Ward (1963) was applied since it has been shown in previous works (Vantrepotte et al. 2012) to be less sensitive to noise and outliers than other methods. This method quantifies the Euclidian distance between different clusters, which is described as:

$$D_{xy} = \left(\frac{n_A n_B}{n_A+n_B}\right) d_{AB} \tag{3.3}$$

$$d_{AB} = \sum (g_A - g_B)^2 \tag{3.4}$$

where d_{AB} is the squared Euclidian distance between class A and B; n_i is the number of sample and g_i corresponds to mean vector of cluster i (i indicating class A or B).

(3) The homogeneity of the derived clusters was checked by using the "Silhouette width" (Rousseeuw 1987) which measures how well each individual normalized reflectance spectrum was clustered:

$$sil_j = \frac{(b_j - a_j)}{max(a_j, b_j)} \tag{3.5}$$

where sil_j ranges ($-1<sil_j<1$), a_j is the average distance from point j to all other points in cluster i and b_j is the minimum average distance from point j to all points in another cluster.

In practice, spectra with $sil_j<0$ (i.e. wrongly classed) have been excluded from the analysis. Some pre-tests were performed with other unsupervised clustering methods (e.g. such as K-mean, Fuzzy). It did not change drastically the average characteristics of the classes derived (not shown) illustrating the strong heterogeneity in the spectra composing development data set.

3.2.4. Satellite $R_{rs}(\lambda)$ labeling

Labeling is a procedure to "label" or associate each satellite remote sensing reflectance spectrum with the different optical classes identified from the in situ data set. This method utilizes Euclidean distance to assign satellite R_{rs} to reference classes. This approach is similar to Minimum Distance method which has been applied on remote-sensing classification (Jensen 2005; Jensen and Lulla 1987; Manolakis et al. 2016; Sohn and Rebello 2002).

Minimum Distance algorithm calculates the Euclidean distance d(x,y) between spectral signatures of each pixels and reference spectral signatures, according to the following equation:

$$d(x,y) = \sqrt{\sum_{i=1}^{n}(x_i - y_i)^2} \tag{3.6}$$

with: x = $\log_{10}(R_{rs})$, spectral signature vector of an pixel; y is spectral signature vector of a reference class and n is number of wavelength.

Therefore, the distance is calculated for every pixel in the image, assigning the class of the spectral signature that is closer

$$x \in C_k \Leftrightarrow d(x,y_k) < d(x,y_j) \forall k \neq j$$

with C_k refer to a class k, y_k and y_j is spectral of class k and class j.

3.3. Results and discussion

3.3.1. In situ R_{rs} classification

The biogeochemical variability directly affects the water optical properties thus impacting the shape and intensity of the remote-sensing reflectance spectra. Figure 3.3 illustrates the variability in the raw reflectance data found in the data set used for defining the different optical water types through the classification procedure.

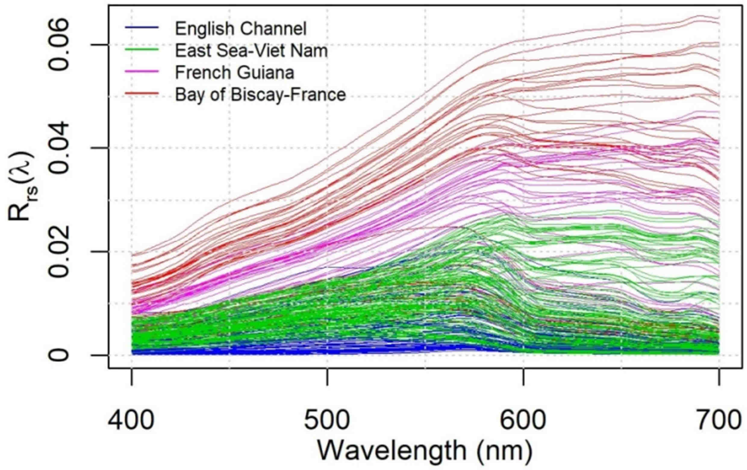

Figure 3.3. Hyperspectral $R_{rs}(\lambda)$ spectra (N = 385) in the different coastal regions considered in the optical clustering exercise.

The classification analysis performed on this training dataset including initially 391 in situ spectra provided 6 distinct optical classes. Note that after the Silhouette width selection, 6 spectra only were removed from the analysis (leading to a final number of data of 385, Figure 3.3, 3.4), the latter being too far from the mean characteristics of the class to which they have been assigned after the cluster analysis (sil<0). Each class can be associated with a specific spectral shape and biogeochemical environment (Table 3.2) as detailed below:

Class 1 (N=77) spectra present strong reflectance in red region with wide plateau from 570 to 700 nm and a slope from the blue to green (Figure 3.5a). Class 1 samples show the highest average values of POC, SPM concentration (1953 μg L^{-1}, CV: 122.6% and 156.92 10^3 μg L^{-1} CV: 98.2%, respectively), while a low concentration of Chla (4.44 μg L^{-1}, CV: 117%) is found for the corresponding samples (Table 3.2, Figure 3.6c).

The very low POC/SPM ratio (0.016) found for the Class 1 samples tend to indicate samples with particulate matter dominated by mineral particles (Doxaran et al. 2015; Doxaran et al. 2012a; Woźniak et al. 2016; Woźniak et al. 2010). Further, the high value for the ratio POC to Chl*a* (1060) as well as the low $a_{\Phi}(443)/a_p(443)$ (0.04) found for the Class 1 samples also suggest that the organic particles for these waters are mainly dominated by detrital material. The average values of $b_{bp}(650)$ and $b_{bp}(650)$ /SPM were of 0.298 m^{-1} and 8.39 x 10^{-3} (m^2/g), being the maximal values for these parameters among the different classes. Finally, Class 1 samples also displayed the highest average value for $a_{CDOM}(443)(0.87\ m^{-1})$ although the lowest value of $a_{CDOM}(443)/(a_{CDOM}(443)+a_p(443))$ ratio (0.231) was found for the corresponding samples.

The Class 1 spectra therefore correspond to mineral particles dominated waters. The high absorption of CDOM and non-algal particles explains the low R_{rs} values in the blue domain for the corresponding spectra while the high R_{rs} values in the red domain can be related to high back scattering related to the overall high turbidity of the Class 1 waters when compared to the other classes.

Class 2 (N=67): The $R_{rs}(\lambda)$ spectra for this class show a strong peak around 570 nm and a second peak at 683 nm, which reflect chlorophyll fluorescence pattern (Figure 3.5b). The second peak was related to data points sampled in offshore Boulogne Sur Mer in April and May when phytoplankton bloom occurred. The seasonal impact of such spring bloom (especially of P. Globosa) on the optical properties at regional scale has been already reported in previous works (Loisel et al. 2007; Lubac and Loisel 2007; Vantrepotte et al. 2012).

Concentration of POC, SPM and $b_{bp}(650)$ are very high (second highest after class 1). In comparison with the other classes, this class was also characterized by the highest average Chl*a* concentration (10.08 $\mu g\ L^{-1}$) and the lowest mean ratio of POC to Chl*a* (95.84), which indicate that the particulate organic material is dominated by autotrophic organisms. This phytoplankton bloom situation was also underlined by the occurrence of the maximal $b_{bp}(650)/SPM$ ratio ($8.39 \times 10^{-3}\ m^2/g$) for the corresponding samples. In addition Class 2 samples were also showing very high $a_{CDOM}(443)$ average values.

In summary, this class represents waters co-dominated by phytoplankton and CDOM.

Class 3 (N=58): Class 3 and 4 present quite similar spectral shape patterns being associated with relatively mixed situations. The average $R_{rs}(\lambda)$ spectrum for Class 3 is characterized by a strong peak around 570 nm (Figure 3.5c). Average POC, SPM and Chl*a* for this class were of 527.27 µg L^{-1}, 8.31 10^3 µg L^{-1} and 7.37 µg L^{-1}, respectively (Table 3.2). Average of POC/SPM (0.09) and $b_{bp}(650)$/SPM (5.996 x 10^{-3} m^2/g) are relatively low for these samples.

Class 4 (N=102): While Class 3 spectra showed a steep increasing gradient from the blue to the green reaching a peak at 580 nm, Class 4 samples present a smoother blue to green slope (Figure 3.5d) and a smaller peak at 580 nm. A second peak at 680 nm is in addition found for marking the signature of a moderate chlorophyll fluorescence pattern. This fluorescence peak associated Class 4 samples is however less pronounced than the Class 2 samples.

Class 5 (N=50): Spectral pattern showed a wide plateau from 500 to 570 nm, while a decrease in the R_{rs} is then found towards the red part of spectrum (Figure 3.5e) as also reflected by the high $R_{rs}(555)/R_{rs}(665)$ values found for these samples (Figure 3.6). Class 5 presented very low average values of POC, SPM, Chl*a* and $a_{CDOM}(443)$. POC/SPM was found relatively low (0.08) denoting the relatively important contribution of mineral particulate matter. A high ratio of $a_{CDOM}(443)/(a_{CDOM}(443)+a_p(443))$ was also found for these waters (Table 3.2).

Class 6 (N=32) The R_{rs} (λ) spectra for the Class 6 show high reflectance in blue part of the spectrum and a strong peak around 490 nm, while reflectance data are decreasing gradually from this peak to 555 nm and then drastically falling around 600 nm remaining low throughout the red part of the spectrum (Figure 3.5f). Class 6 samples present the lowest average values of POC (159.25 µg L^{-1}), SPM (1.19 10^3 µg L^{-1}), Chl*a* (0.53 µg L^{-1}), $a_{CDOM}(443)$ (0.08 m^{-1}) and $b_{bp}(665)$ (0.003 m^{-1}). Conversely, POC/SPM and $a_{CDOM}(443)/(a_{CDOM}(443)+a_p(443))$ ratios are the highest (0.15, 0.52, respectively) for the corresponding samples (Table 3.2).

In summary, from Class 1 to Class 6 the whole examined biogeochemical parameters (POC, SPM and Chla) sharply decrease, as well as the $b_{bp}(650)$ (i.e. proxy of SPM) and $a_{CDOM}(443)$ values. One of the greatest decreases is for instance observed for SPM which average concentration change by a factor of 150 from Class 1 to Class 6. Along the same line a remarkable decrease in the bbp(650) average values is also found (by a factor of 99 between class 1 and class 6). This latter pattern clearly shows that the classes, even after normalization, are still affected by the turbidity and absorption levels (whatever the origin of this turbidity). In contrast, $a_\phi(443)/a_p(443)$, $a_{CDOM}(443)/(a_{CDOM}(443)+a_p(443))$ and POC/SPM increased from Class 1 to Class 6 emphasizing that these classes are also well organized in terms of phytoplankton vs. NAP, dissolved vs particulate material and organic vs mineral particles relative contributions. The latter biogeochemical gradients are translated in a clear gradient of the ratio $R_{rs}(555)/R_{rs}(665)$ which also gradually decrease from Class 1 to Class 6 samples.

Class 1 represented very turbid waters (high POC, SPM, $b_{bp}(650)$) which particulate assemblage is dominated by mineral particles (low POC/SPM). The latter pattern together with the high a_{CDOM} for this class suggests the strong impact of material from terrestrial origin as also underlined by the location of the corresponding stations in Figure 3.4. Class 2 corresponds to coastal phytoplankton bloom events as underlined by the very high value of Chla (average 10.08, maximum 33.37 $\mu g\ L^{-1}$) and the relative high values also found for SPM, POC and CDOM. Classes 3 and 4 present rather mixed situation with no clear dominant components although the Class 4 show a clearer chlorophyll fluorescence pattern. Class 5 and 6 are associated with clearer water masses, Class 5 showing a greater proportion of mineral particles contrasting with the Class 6 samples that are more likely associated with water masses where organic material is predominating. As shown in the Figure 3.4, Class 6 samples were found relatively far from the coast and river mouth.

When comparing the classes obtained from our analyses to those obtained by Vantrepotte et al., (2012) on almost the same areas (except the Gironde data) but using a much restricted data set, we can observe a good agreement for the Classes 1, 3 and 5 with the classes 1, 2, 3 obtained in this previous work. Our new partition of optical water types allow to gain precision in the bloom conditions which where depicted by one class only in this previous work (Class 4 in Vantrepotte et al., 2012) while our classification shows at least two classes with a well-defined Chl*a* fluorescence peak (Classes 2 and 4). Finally, the class 6 here describing clearest water with R_{rs} spectra peaking in the blue were lacking in the previous work by Vantrepotte et al., (2012).

Mélin and Vantrepotte (2015) defined 16 classes from a classification applied to SeaWiFS satellite data among which 9 classes were defined as representative of the "Case 2" waters with the two last showing two situations of R_{rs} spectra peaking in the blue spectral domain. The 6 Classes obtained here in situ are overlapping most of the classes defined by the previous authors who also found additional intermediary situations with those depicted from our in situ data set.

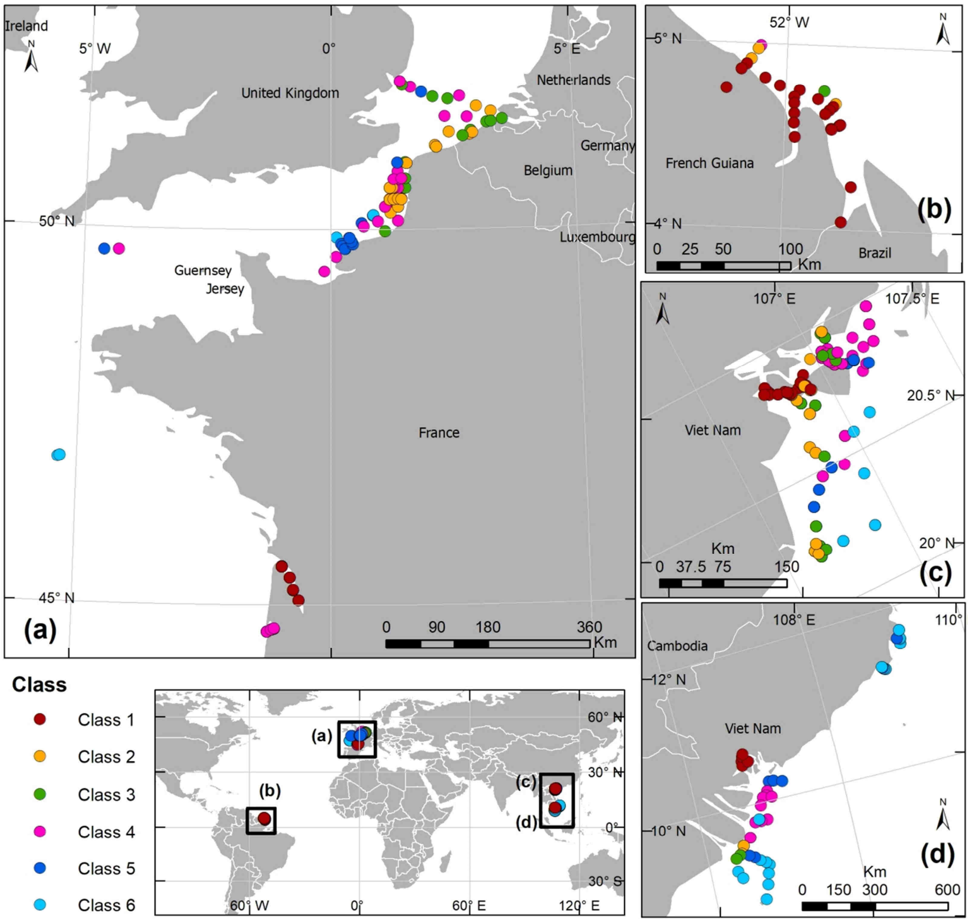

Figure 3.4. Spatial distribution of the in situ measurements in (a) European coastal water, (b)coastal zone of French Guiana, (c-d) Tonkin bay and Mekong estuary, the East sea of Viet Nam. Colors correspond to the 6 optical classes which were identified from the Ward classification.

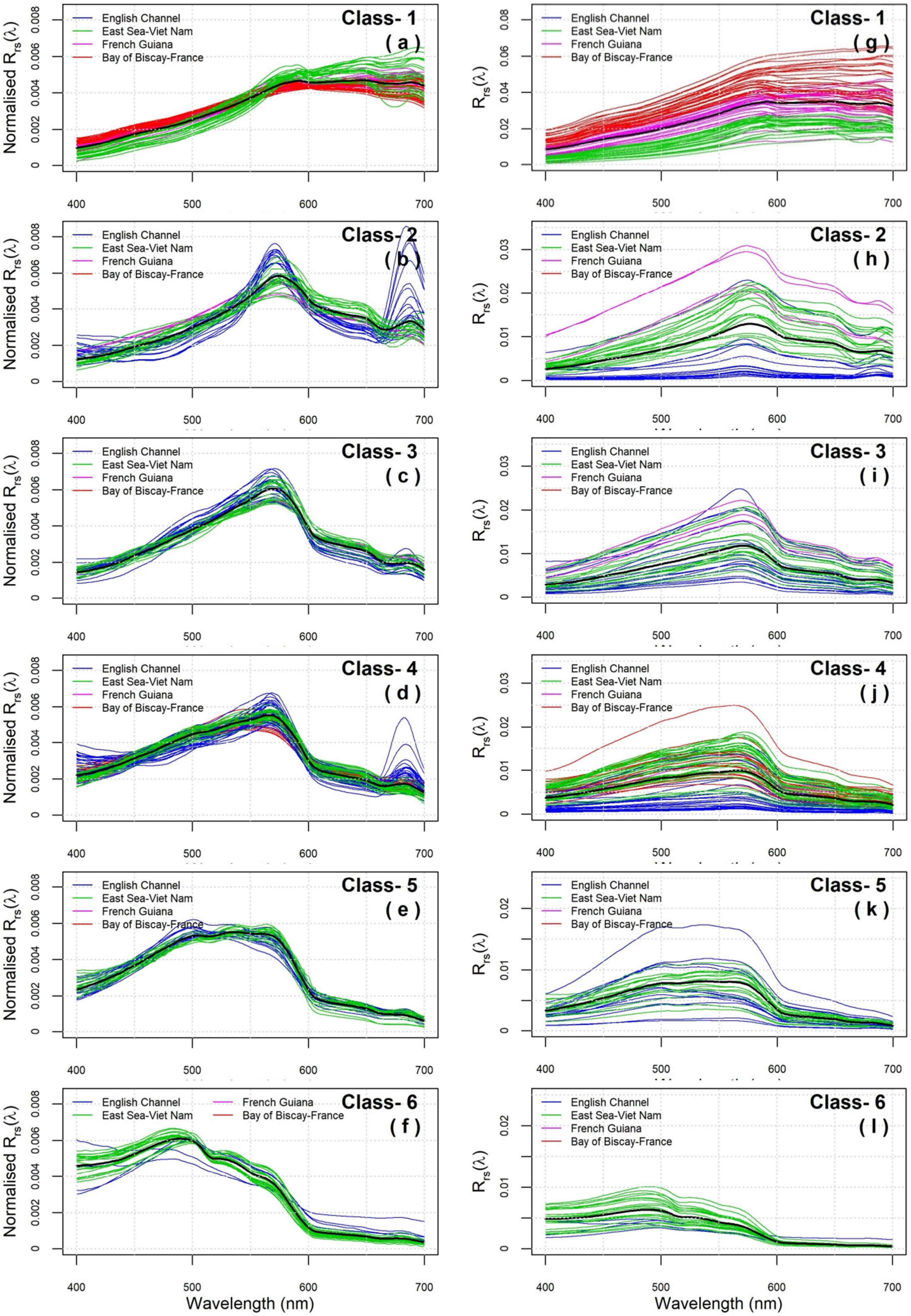

Figure 3.5. Left panel: Normalized reflectance spectra associated with the 6 optical classes defined from our in situ data set (a–e). Right panel: (f–j) show the raw reflectance spectra associated with 6 classes. The different colors for the spectra show the geographical regions where in situ data were collected.

Table 3.2. Statistical parameters (Avg: average; Med: median; Stdv: standard deviation; minimum and maximum) of POC, SPM, Chla, $a_{CDOM}(443)$,$b_{bp}(650)$, POC/SPM, POC/Chla, Chla/SPM, $a_{\phi}(443)/a_{p}(443)$, $a_{CDOM}(443)/(a_p(443)+a_{CDOM}(443))$ and $b_{bp}(650)$/SPM for each class.

Class	Parameters	N	Avg	Med	Min	Max	CV (%)	Stdv
1	SPM (mg L^{-1})	76	156.92	90.21	23.93	844.67	98.2	159.80
	POC/SPM (g/g)	76	0.016	0.014	0.001	0.037	247.2	0.006
	POC/Chla (g/g)	53	1060	246.63	39.50	8324	58.6	1809
	POC (μg L^{-1})	77	1953	1287	391.73	7888	122.6	1594
	Chla/SPM (g/g)	52	0.073	0.048	0.001	0.704	67.0	0.109
	Chla (μg L^{-1})	53	4.44	3.70	0.12	20.99	117.7	3.77
	$b_{bp}(650)$/SPM x10^{-3} (m^2/g)	6	8.393	8.151	3.458	13.684	251.5	3.337
	$b_{bp}(650)$ (m^{-1})	6	0.298	0.320	0.187	0.387	392.5	0.076
	$a_{\phi}(443)/a_{p}(443)$	52	0.040	0.040	0.002	0.207	105.7	0.038
	$a_{CDOM}(443)/(a_{CDOM}(443)+a_p(443))$	40	0.231	0.210	0.050	0.758	155.2	0.149
	$a_{CDOM}(443)$ (m^{-1})	41	0.876	0.544	0.302	7.844	72.3	1.212
2	SPM (mg L^{-1})	52	12.12	11.33	3.44	26.44	260.6	4.65
	POC/SPM (g/g)	52	0.066	0.043	0.018	0.232	120.5	0.055
	POC/Chla (g/g)	67	95.84	76.35	36.10	356.02	167.1	57.35
	POC (μg L^{-1})	67	735.59	550.30	312.11	2262	171.0	430.12
	Chla/SPM (g/g)	52	0.815	0.475	0.129	2.876	108.1	0.754
	Chla (μg L^{-1})	67	10.08	6.93	2.16	33.37	129.8	7.77
	$b_{bp}(650)$/SPM x10^{-3} (m^2/g)	47	8.397	8.777	2.774	14.513	332.5	2.525
	$b_{bp}(650)$ (m^{-1})	50	0.100	0.118	0.017	0.259	212.5	0.047
	$a_{\phi}(443)/a_{p}(443)$	52	0.267	0.235	0.090	0.548	220.0	0.121
	$a_{CDOM}(443)/(a_{CDOM}(443)+a_p(443))$	40	0.278	0.255	0.089	0.566	252.1	0.110
	$a_{CDOM}(443)$ (m^{-1})	54	0.207	0.160	0.054	0.921	131.8	0.157
3	SPM (mg L^{-1})	54	8.31	6.88	1.67	32.65	150.6	5.52
	POC/SPM (g/g)	54	0.090	0.058	0.014	0.391	103.9	0.087
	POC/Chla (g/g)	55	120.78	98.53	23.59	673.77	116.9	103.32
	POC (μg L^{-1})	57	527.27	410.05	132.11	1819	149.3	353.07
	Chla/SPM (g/g)	53	0.985	0.709	0.082	4.032	115.1	0.856
	Chla (μg L^{-1})	55	5.37	5.40	1.30	11.94	209.7	2.56
	$b_{bp}(650)$/SPM x10^{-3} (m^2/g)	38	5.994	5.052	1.714	11.304	244.0	2.456
	$b_{bp}(650)$ (m^{-1})	39	0.052	0.052	0.009	0.123	152.9	0.034
	$a_{\phi}(443)/a_{p}(443)$	53	0.333	0.291	0.063	0.690	217.4	0.153
	$a_{CDOM}(443)/(a_{CDOM}(443)+a_p(443))$	40	0.331	0.290	0.061	0.658	227.6	0.145

	$a_{CDOM}(443)$ (m^{-1})	42	0.201	0.153	0.015	0.687	134.8	0.149
4	SPM (mg L^{-1})	82	4.90	3.88	1.09	31.01	113.9	4.31
	POC/SPM (g/g)	82	0.103	0.047	0.011	0.468	89.1	0.115
	POC/Chla (g/g)	101	127.52	115.91	42.33	532.76	161.2	79.12
	POC (μg L^{-1})	102	339.05	288.97	107.09	794.48	170.9	198.38
	Chla/SPM (g/g)	82	0.855	0.580	0.042	4.660	94.6	0.903
	Chla (μg L^{-1})	101	3.17	2.33	0.97	11.52	137.5	2.30
	$b_{bp}(650)$/SPM x10^{-3} (m^2/g)	46	7.177	7.446	0.641	11.795	329.6	2.178
	$b_{bp}(650)$ (m^{-1})	49	0.030	0.030	0.012	0.055	311.2	0.010
	$a_{\phi}(443)/\,a_p(443)$	82	0.351	0.340	0.043	0.726	223.8	0.157
	$a_{CDOM}(443)/(a_{CDOM}(443)+a_p(443))$	40	0.364	0.360	0.029	0.692	257.0	0.142
	$a_{CDOM}(443)$ (m^{-1})	78	0.133	0.114	0.005	0.640	141.9	0.094
5	SPM (mg L^{-1})	39	2.84	2.40	0.80	7.50	186.2	1.52
	POC/SPM (g/g)	39	0.081	0.047	0.018	0.435	94.0	0.086
	POC/Chla (g/g)	48	131.43	92.04	28.05	686.10	110.8	118.63
	POC (μg L^{-1})	50	205.77	138.05	59.58	541.90	170.2	120.94
	Chla/SPM (g/g)	37	0.800	0.790	0.075	2.441	178.3	0.449
	Chla (μg L^{-1})	48	2.03	1.67	0.33	9.85	139.0	1.46
	$b_{bp}(650)$/SPM x10^{-3} (m^2/g)	31	6.367	7.592	0.455	12.200	187.3	3.399
	$b_{bp}(650)$ (m^{-1})	31	0.015	0.016	0.002	0.026	212.5	0.007
	$a_{\phi}(443)/\,a_p(443)$	37	0.407	0.444	0.101	0.674	341.7	0.119
	$a_{CDOM}(443)/(a_{CDOM}(443)+a_p(443))$	40	0.393	0.418	0.108	0.707	241.8	0.163
	$a_{CDOM}(443)$ (m^{-1})	42	0.106	0.100	0.014	0.334	162.3	0.065
6	SPM (mg L^{-1})	30	1.19	1.17	0.22	3.10	195.4	0.61
	POC/SPM (g/g)	30	0.150	0.112	0.032	0.505	136.8	0.110
	POC/Chla (g/g)	32	319.43	269.87	130.77	644.61	205.9	155.11
	POC (μg L^{-1})	32	159.25	119.23	45.37	462.67	154.1	103.32
	Chla/SPM (g/g)	30	0.541	0.440	0.156	2.569	113.0	0.479
	Chla (μg L^{-1})	32	0.53	0.57	0.13	1.17	213.2	0.25
	$b_{bp}(650)$/SPM x10^{-3}(m^2/g)	18	3.627	2.799	0.814	8.116	176.1	2.059
	$b_{bp}(650)$ (m^{-1})	18	0.003	0.003	0.002	0.004	403.6	0.001
	$a_{\phi}(443)/\,a_p(443)$	30	0.411	0.399	0.238	0.794	330.7	0.124
	$a_{CDOM}(443)/(a_{CDOM}(443)+a_p(443))$	40	0.524	0.531	0.204	0.810	269.9	0.194
	$a_{CDOM}(443)$ (m^{-1})	30	0.081	0.074	0.014	0.212	160.6	0.051

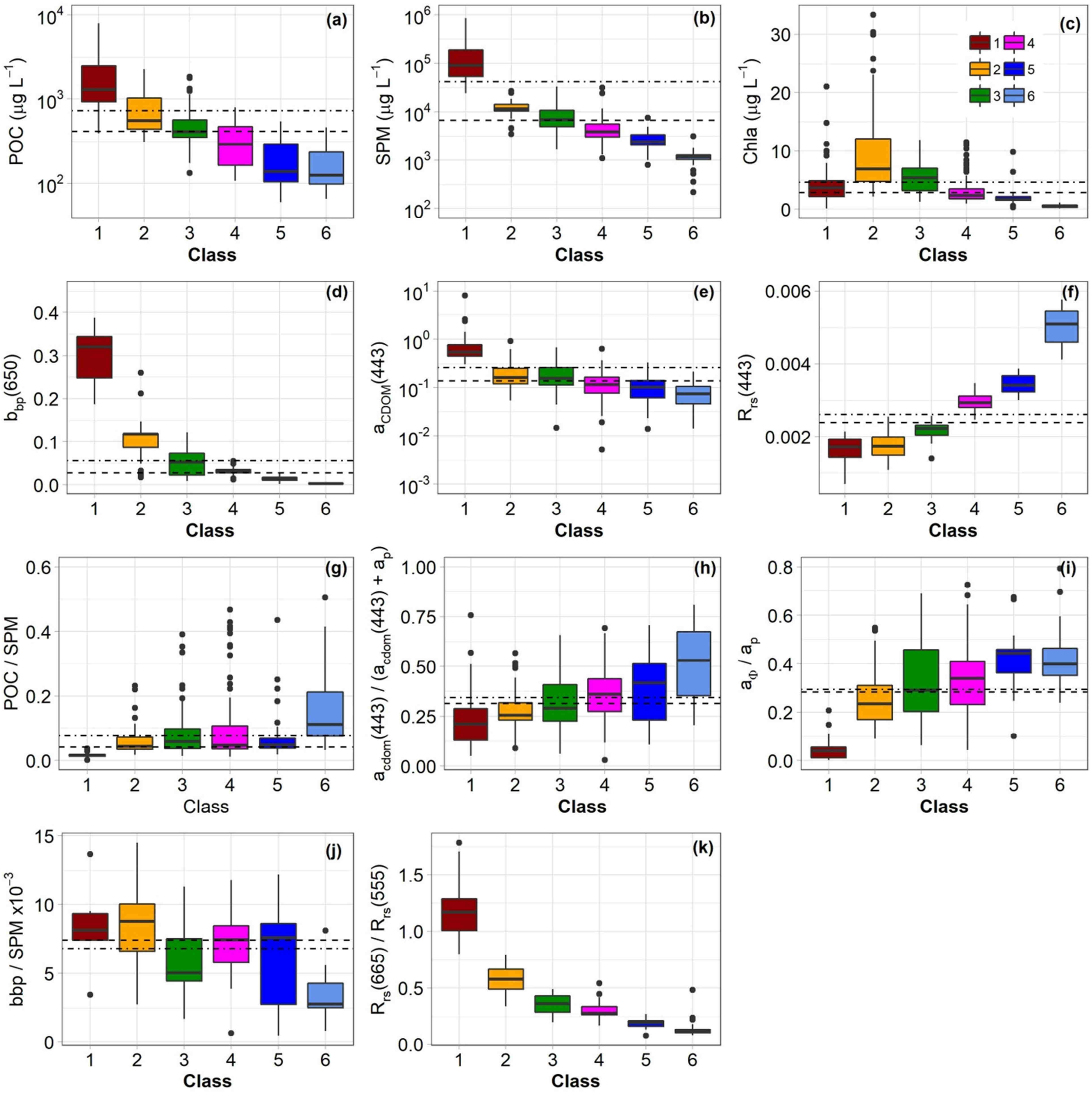

Figure 3.6. Boxplots of (a) POC, (b) SPM, (c) Chl*a*, (d) bbp(670), (e) a_{CDOM}(443), (f) R_{rs}(443), (g) POC/SPM, (h) $a_{CDOM}(443)/(a_{CDOM}(443)+a_p(443))$, (i) $a_{\phi}(443)/\ a_p(443)$, (j) b_{bp}(650)/SPM and (k) $R_{rs}(665)/R_{rs}(555)$ for the six classes obtained from the optical classification. Boxes extend from the 25th to the 75th percentile with the dash line and dot-dash lines present the median and mean of whole data respectively. Observations further than 1.5 times the length of the box away from the box are considered outliers and indicated by black dot.

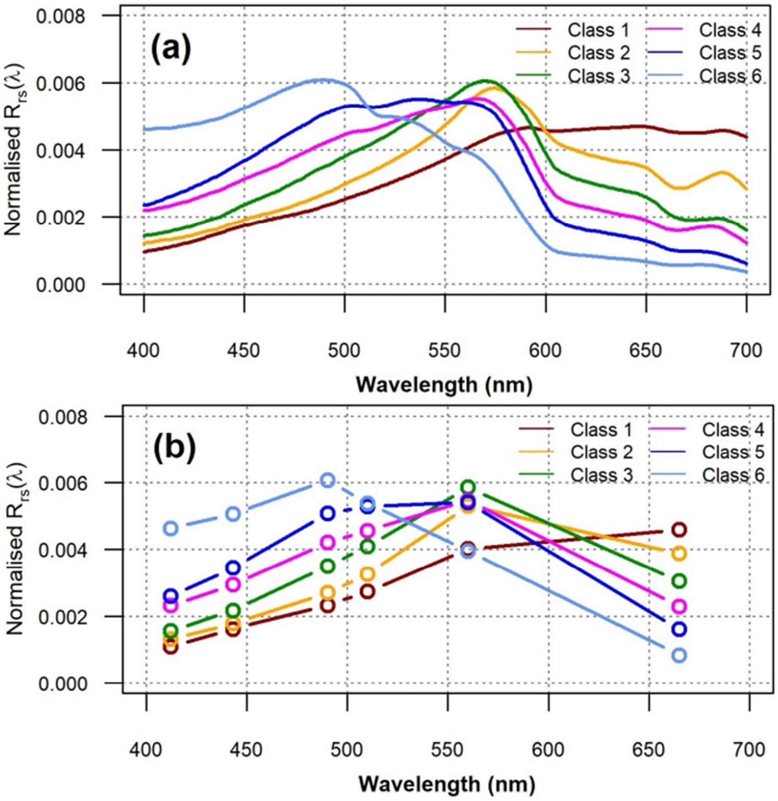

Figure 3.7. (a) Average normalized reflectance spectra of 6 classes derived for the Ward's hierarchical classification; normalized reflectance were degraded to simulate MERIS bands, the circles present the central wavelengths of MERIS (412, 443, 450, 510, 560, 620 and 665 nm) raw R_{rs} (b)

3.3.2. Satellite image application

In the context of satellite application, the monthly average images of MERIS level 3 were used in order to assess the distribution of the optical classes defined from our in situ data set over various coastal sites. Figure 3.7a shows the average hyperspectral R_{rs} of 6 classes previously defined while the Figure 3.7b shows the corresponding average spectra degraded to multispectral MERIS bands. Note that the labeling of satellite pixels from in situ defined optical classes might have to take into account the possible spectral variation in the precision of the satellite R_{rs} data assessed after applying atmospheric correction (D'Alimonte et al. 2003; Vantrepotte et al. 2012). The retrieval accuracy of R_{rs} based has been checked based on a matchup exercise of 778 coincident data points collected from the AERONET-OC sites. A bias of 4.7×10^{-3}, 4.2×10^{-3}, 3.4×10^{-3}, 1.5×10^{-3}, -1.9×10^{-4} between in situ AERONET and MERIS $R_{rs}(\lambda)$ at 412, 443, 490, 560 and 665 nm has been observed, respectively and used to correct the MERIS data at each individual bands before performing the pixels labeling. Considering this correction, the seven visible wavelengths of MERIS were then considered in the labeling procedure (R_{rs} 412, 443, 490, 510, 560, 620, 665 nm).

The Figure 3.8 presents the distribution of the classes for different coastal regions including areas where in situ data used for the classes definition were gathered (English Channel, North Sea, Vietnam, French Guiana) but also other coastal contrasted coastal regions (Amazon river mouth, Louisiana continental Shelf). A general good agreement is found between the in situ class average spectra and those extracted from the pixels classified for the corresponding classes on the MERIS images confirming the relevant labeling of the satellite data.

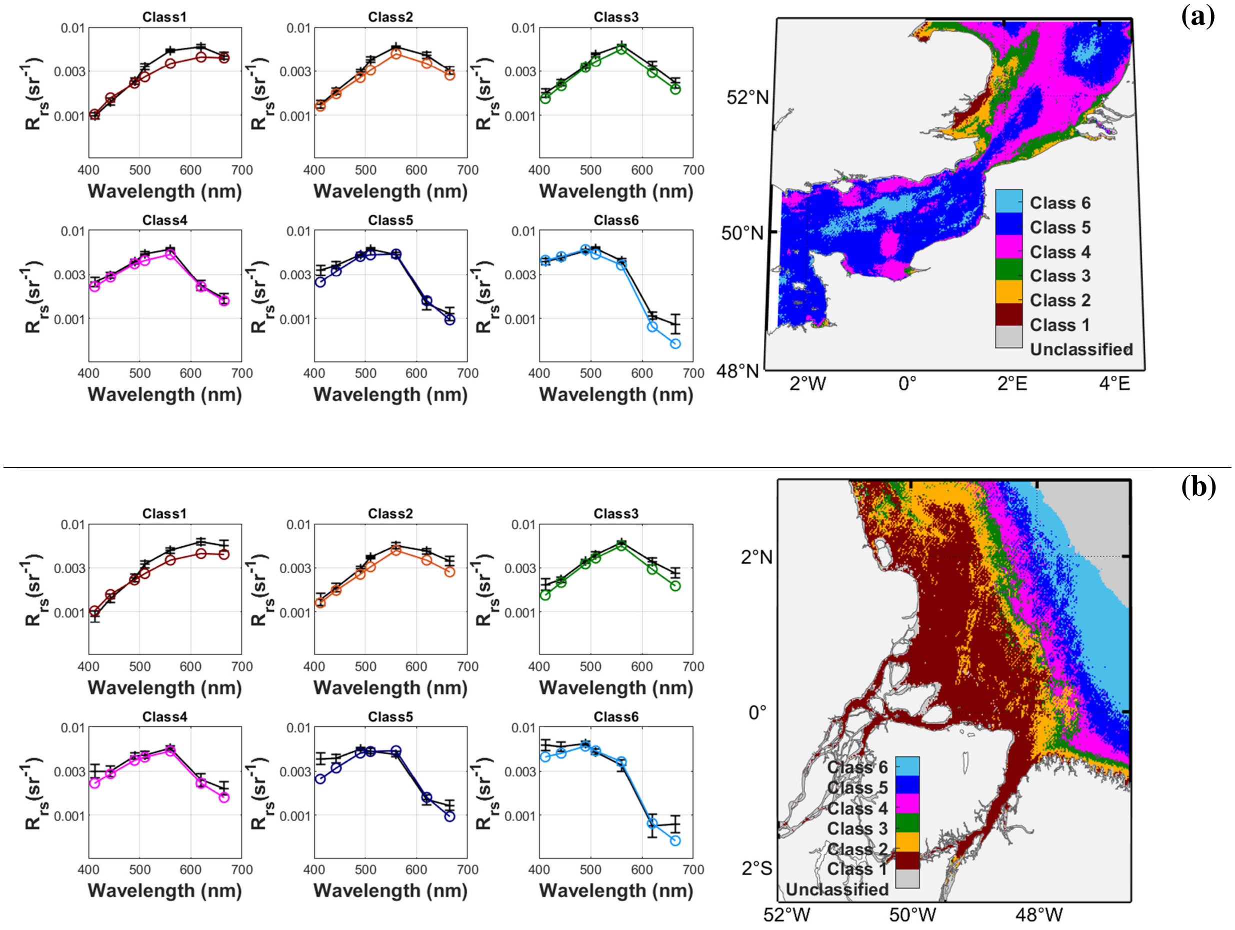

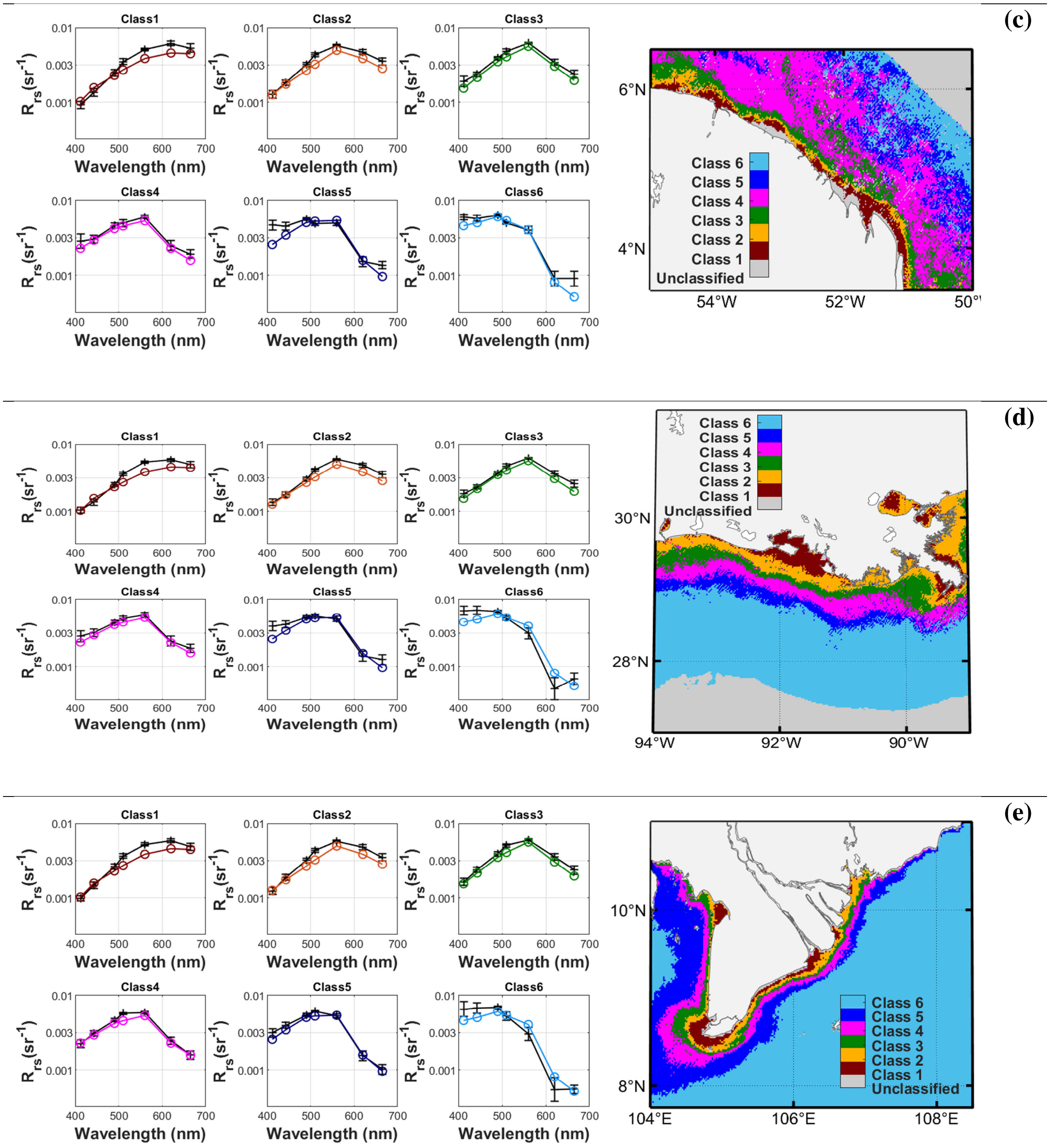

Figure 3.8. Example of classification product derived from average monthly MERIS (May 2010) in the coastal water of (a) the English Channel,(b) Amazon estuary, (c) French Guiana, (d) Louisiana Continental Shelf, (e) Mekong Estuary. Black lines with error bars illustrate the mean value of satellite reflectance, R_{rs} in each group associated with the standard deviation at each wavelength. Color lines with circles presents the mean lines of 6 reference classes obtained from in situ data (class 1 to 6: dark red, orange, dark green, magenta and light blue respectively, gray color is unclassified waters)

Note that a good correspondence between the reference spectra defined in situ and those corresponding to the labeled satellite pixels remain valid for coastal areas not considered within the training in situ data set, further emphasizing that the 6 classes defined here are able to cover a large part of the optical variability found in coastal waters. It is worth to notice that Mélin and Vantrepotte (2015) reported that on average 5.2 classes are sufficient enough for describing 90% of the optical variability of coastal waters, which is in agreement with our current results.

A common distribution pattern was observed for the different classes in the different coastal regions investigated with a clear coastal to offshore gradient from Class 1 to Class 6. This again underlines that although classes definition were based on normalized reflectance spectra, variation in the R_{rs} spectral shape are still depicting variations for instance in term of turbidity as already pointed out in previous studies (Mélin and Vantrepotte 2015). Class 1 pixels are globally located in river influenced turbid waters in the different regions related to terrestrial influenced waters (including the estuarine waters of the main rivers in the different areas) while class 6 data are associated with clear waters environments. Beside this general pattern, optical water types spatial distribution also show some patchy features (e.g. Class 1 in the Louisiana Shelf , Figure 3.8d, Class 6 in the North Sea, Figure 3.8a) that might reveal the impact of local physical (e.g. resuspension) or biological (patchy phytoplankton blooms) processes.

Class 4 is contrasting with that for the Class 5 which coverage is maximal in July probably marking the presence of offshore water masses during post bloom conditions (nutrient depleted waters associated with low phytoplankton loads, Vantrepotte et al., 2007).

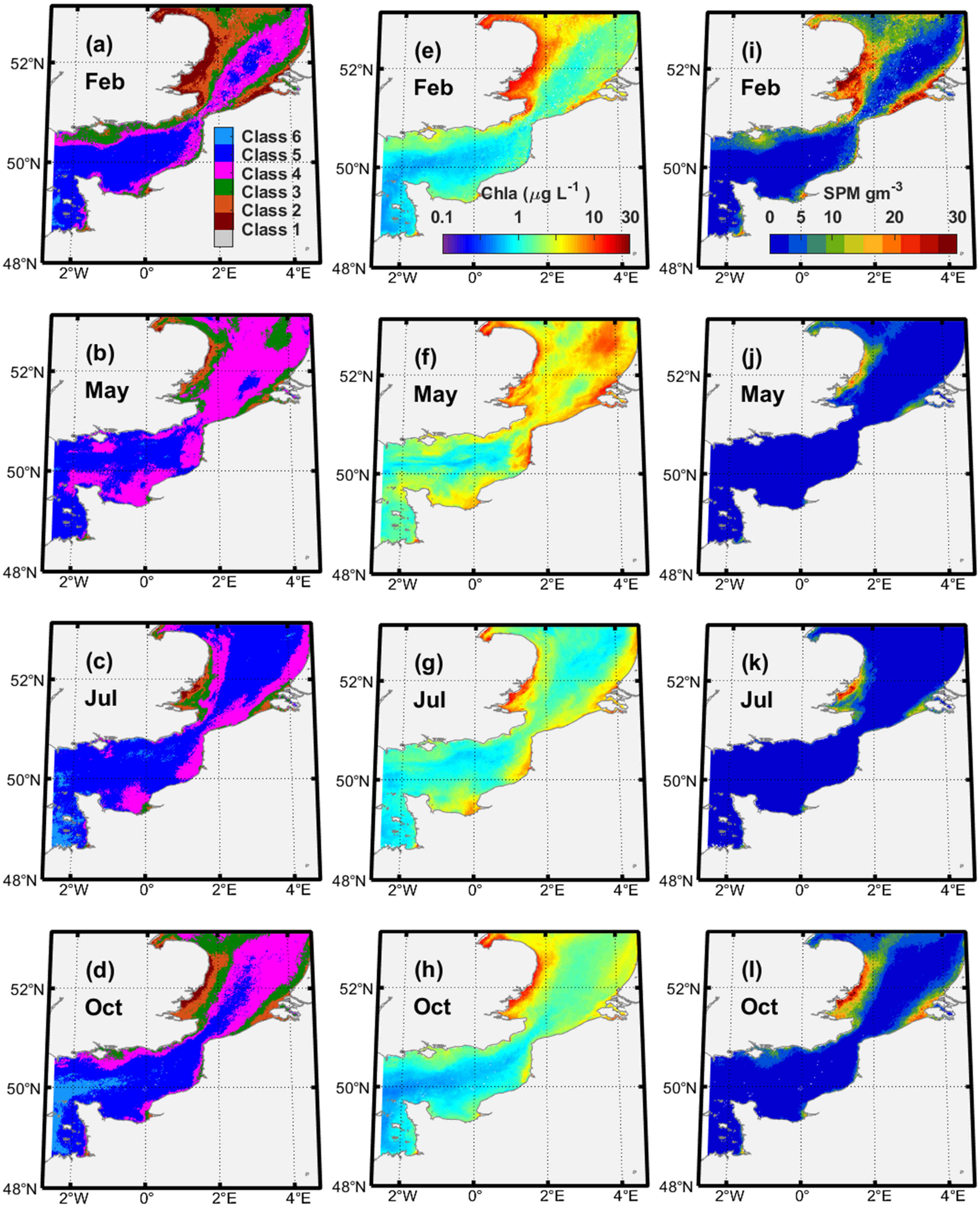

Figure 3.9. MERIS classes distribution for 4 selected months: January, April, July, October (a, b, c, d) were obtained from in 2004 data over the English Channel-Southern North Sea area. Corresponding MERIS derived Chlorophyll-a concentration from OC4-Chla algorithm of (Hu et al. 2012) (e, f, g, h) and derived SPM concentration from (Han et al. 2016) (m, n, o, p).

.

3.4. Conclusions

Based on cluster analysis performed on an extended in situ data set covering different coastal ecosystems (English Channel-Southern North Sea, Gironde, Vietnam, French Guiana) 6 optical water types depicting the optical diversity of coastal waters from the very turbid (Class 1) to the clear water environments (Class 6) were defined. The latter 6 classes provide a more detailed description of the coastal water optical diversity than the 4 ones obtained from a restricted data set by Vantrepotte et al. (2012) with an additional class corresponding to the clear water environment (Class 6) and a more precise description of the phytoplankton bloom conditions (Class 2 and Class 4 in shallow and offshore water environments, respectively).

Although classes were defined from normalized R_{rs} spectra, they showed a remarkable organization from Class 1 to Class 6 with a decreasing gradient in SPM, POC, b_{bp} and CDOM and an increasing gradient in the ratios $a_{\phi}(443)/a_{p}(443)$, $a_{CDOM}/(a_{CDOM} + a_{p})$ and POC/SPM. This clear definition of the bio-optical biogeochemical environments associated with the 6 optical classes defined in this work, which can be associated at a first order with a dilution gradient from the turbid to the clear water environments, are in that respect more clear than the results obtained from 4 classes in Vantrepotte et al. (2012).

The labeling of MERIS monthly data from the 6 classes defined in situ showed that they are able to cover a wide part of the optical variability of coastal waters including over areas not considered within the in situ training data set. The examination of the MERIS classes distribution further illustrates the interest of the optical classes for providing synthetic information on the temporal dynamics of coastal water optical (and thus biogeochemical) quality related for instance to seasonal variation in the river plume extension (including the potential presence of offshore patches showing coastal-river influenced like patches as for instance observed offshore the Thames river).

A first perspective would be to more deeply investigate the spatio-temporal dynamics of the different classes identified for investigating the usefulness of classes based approaches for monitoring small scale physical-biological processes (e.g. river plume dispersion, re-suspension, bloom extension) from the daily data or investigate the potential of optical water types for providing a synthetic information on the long term (seasonal, inter-annual) variation in coastal water masses quality.

A second perspective would be to define is the corresponding optical classes can provide a relevant frame for deriving class-based inversion algorithms taking into account the optical variability of coastal environment within the algorithm development procedure. The illustration proposed for SPM inversion in Vantrepotte et al., (2012) from a 4 classes partition should be performed from the optical typology proposed here on a variety of ocean color products now available from ocean color remote sensing observation over coastal environments.

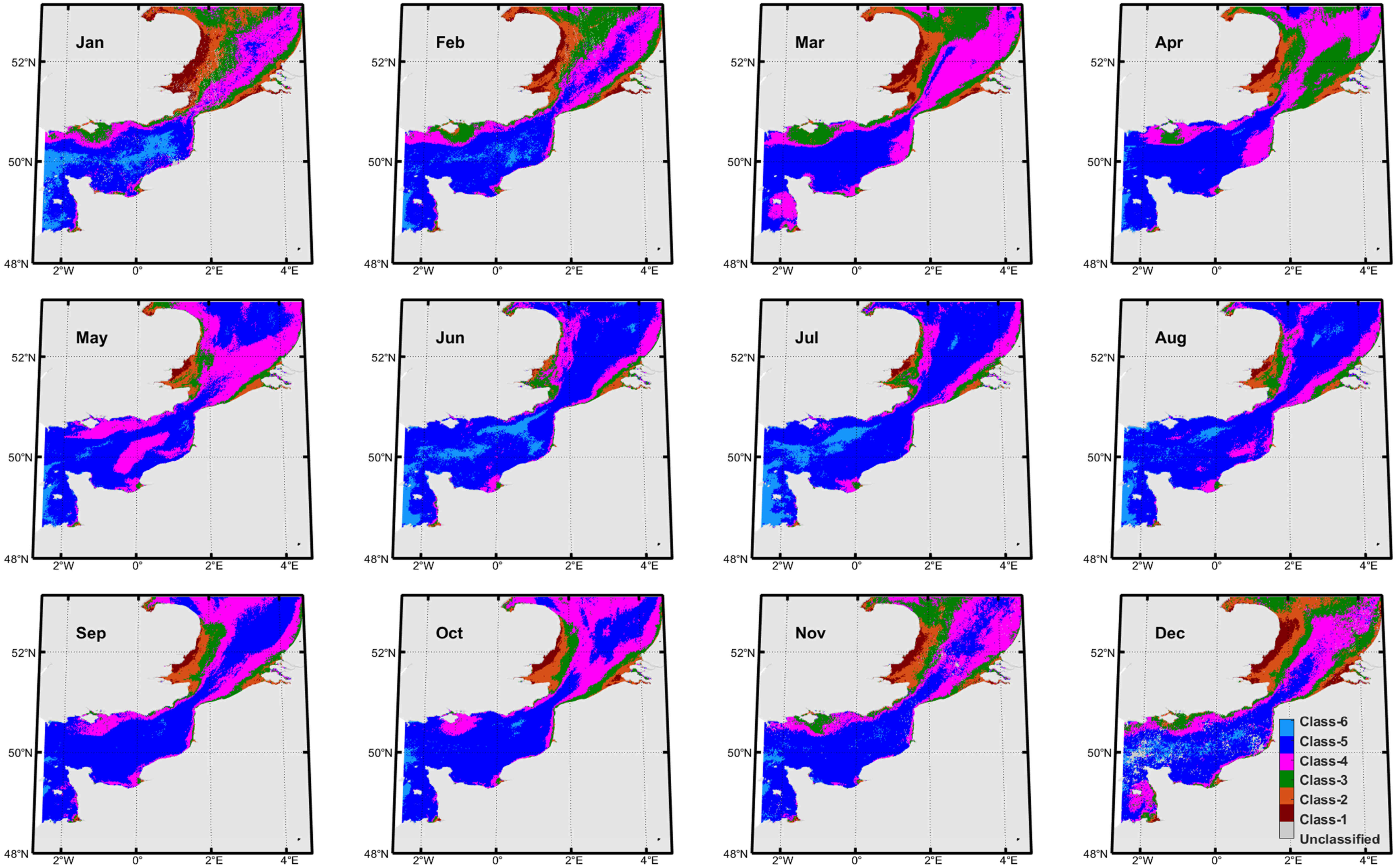

Figure 3.10. Classes derived from average monthly MERIS in the coastal water of the English Channel for the year 2011.

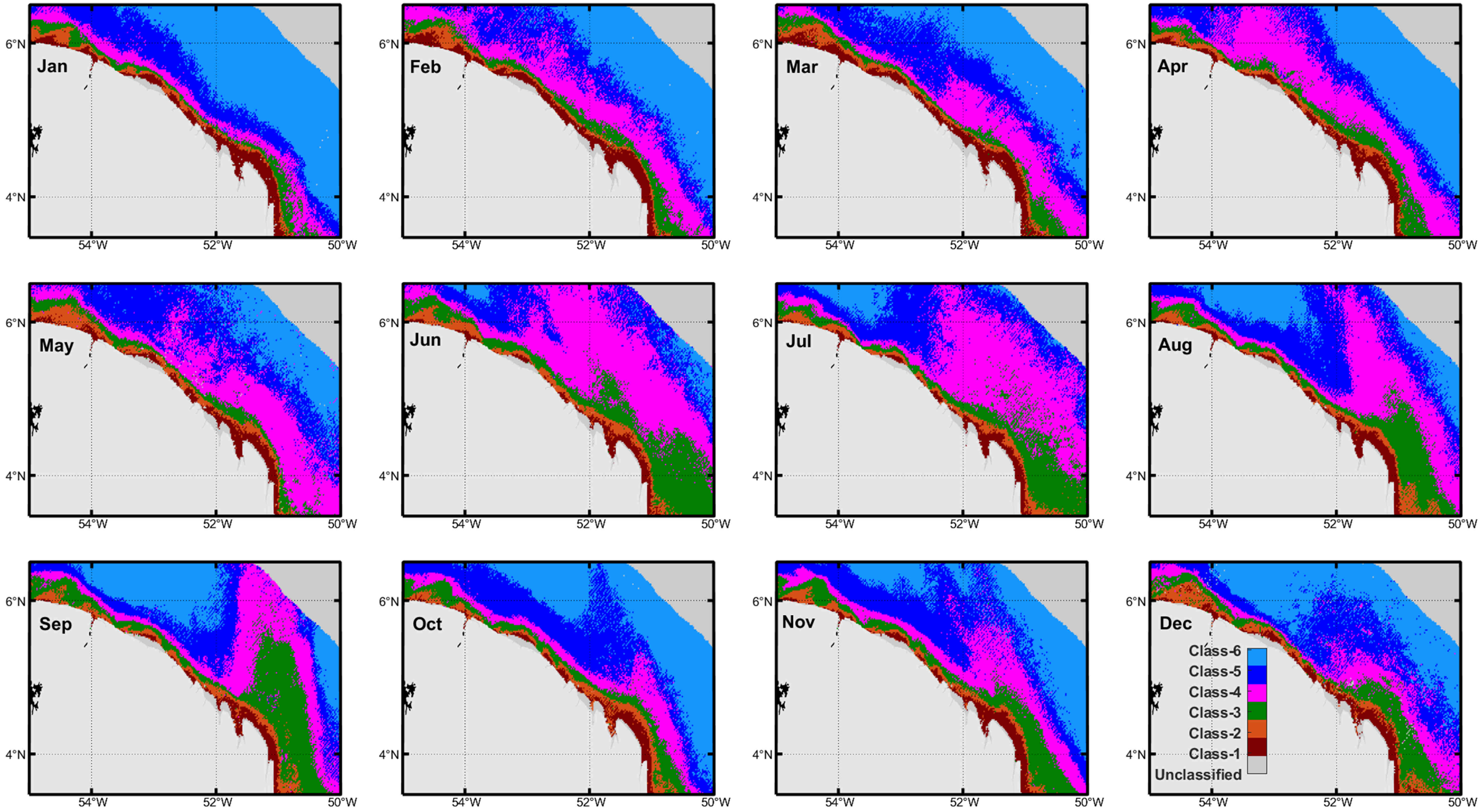

Figure 3.11. Classes derived from average monthly MERIS in the coastal water of the French Guiana for the year 2011.

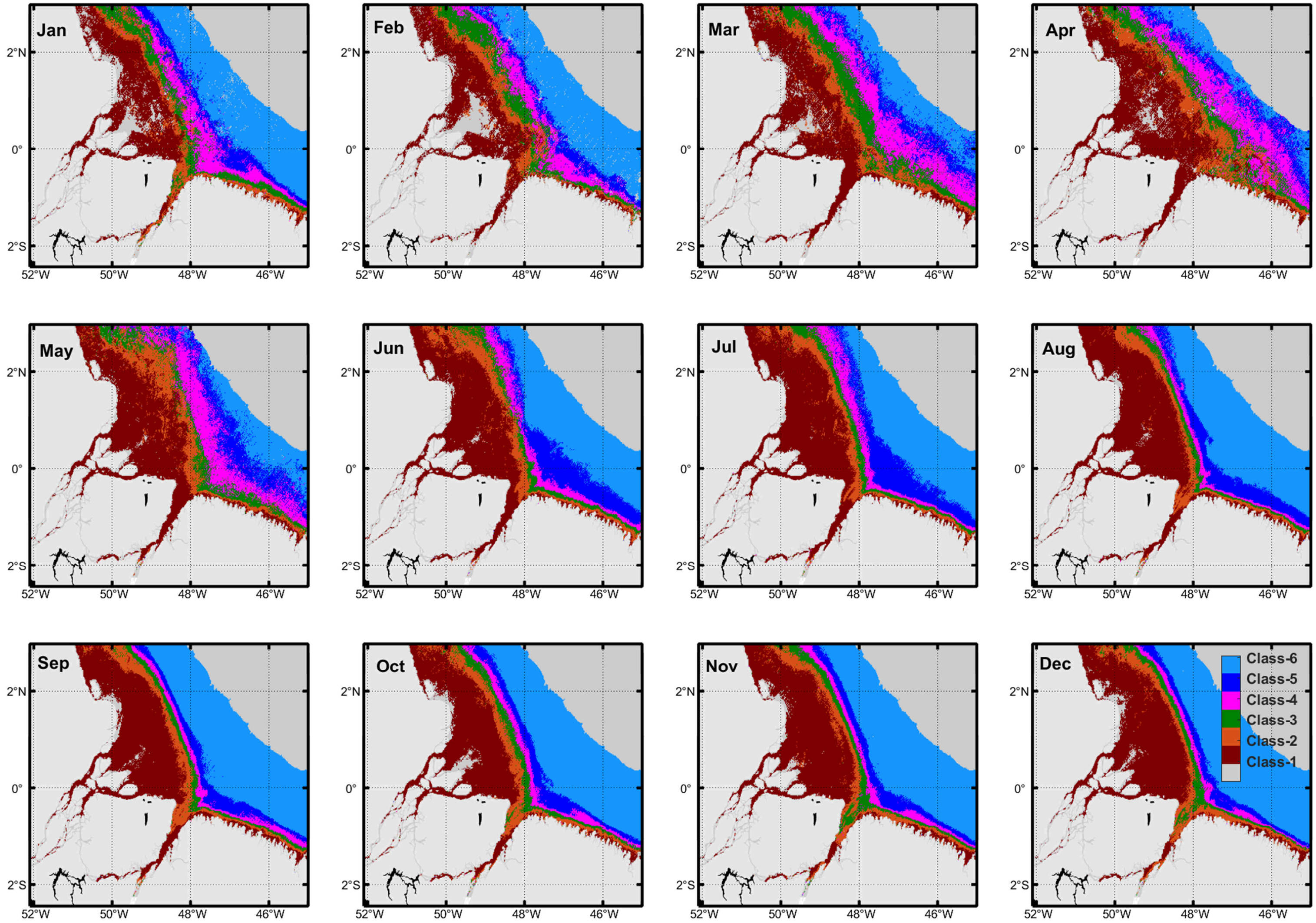

Figure 3.12. Classes derived from average monthly MERIS in the coastal water of the Amazon estuary for the year 2011.

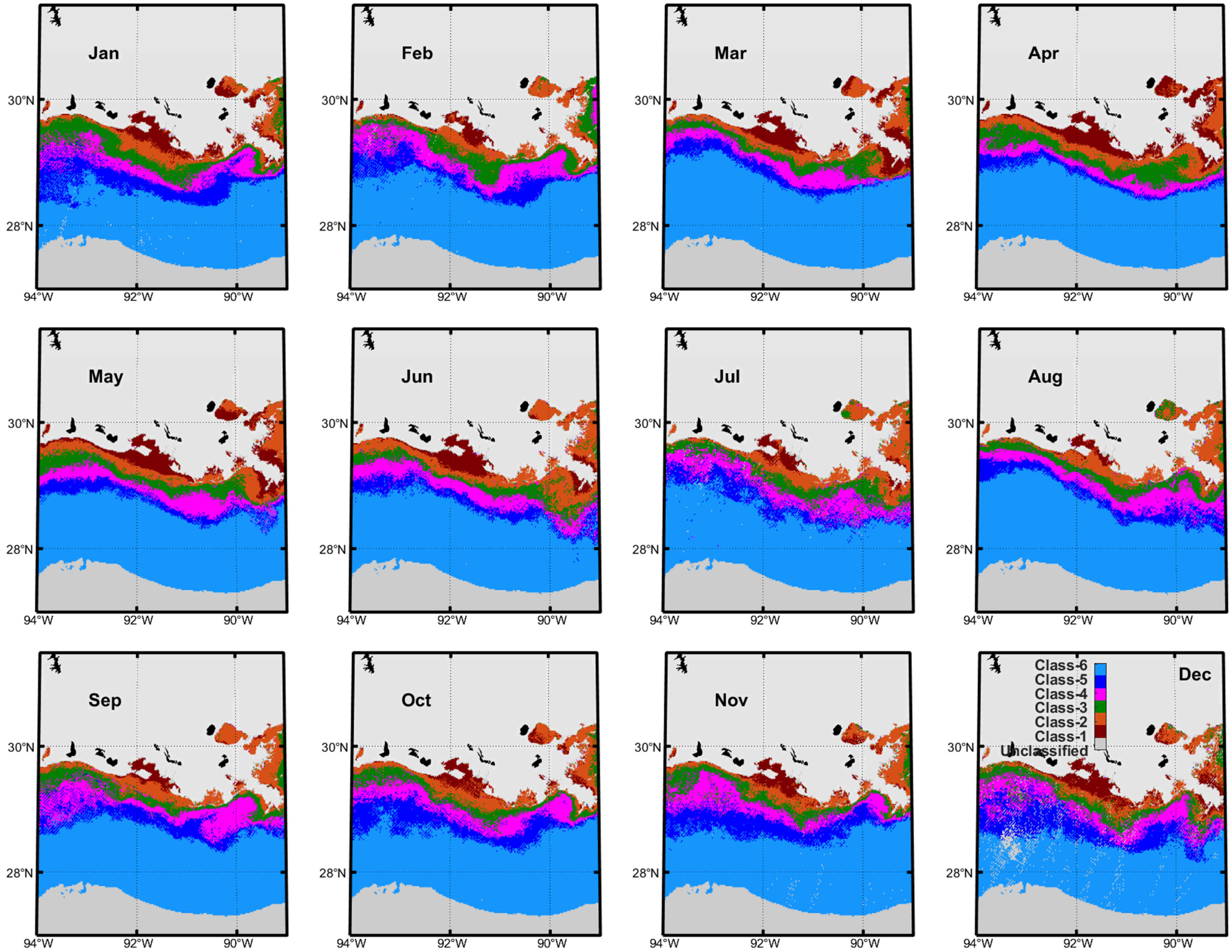

Figure 3.13. Classes derived from average monthly MERIS in the coastal water of the Louisiana Continental Shelf for the year 2011.

Chapter 4: Optical partitioning of contrasted coastal waters

4.1. Introduction

Many researches try to improve our understanding of the dynamics of the coastal ecosystems and their associated biogeochemical cycles. A better knowledge of the coastal environment is primordial as coastal waters are the location of strong coupling between aquatic and terrestrial systems and are under the pressure of large natural and anthropogenic forcing. The spatio-temporal distribution of biological, biogeochemical and physical parameters in coastal waters is of a fundamental importance for a variety of applications dedicated to coastal management, which often contains economical interest. Amongst the large set of biogeochemical parameters sampled in coastal waters, the concentration of the suspended particulate matter (SPM) is a key parameter to understand the sediment transport, downstream sedimentation, and coastal geo-morphological processes. As well, the particulate organic carbon (POC), which is a major of carbon in the ocean, provides information about micro-organisms and their associated detritus. Information on the SPM and POC variability represents crucial inputs for the initiation and validation of sediment transport models (Douillet et al. 2001; Fettweis 2007; Toth et al. 2015) and biogeochemical models (Aumont et al. 2015). Besides, the dimensionless ratio, POC to SPM, is used in many studies (Coynel et al. 2005; Doxaran et al. 2015; Doxaran et al. 2012a, b) to describe the seasonal variability in the particulate matter pool composition and origin, which is often relate to variation in the regional environmental forcing (e.g. water discharge, phytoplankton bloom dynamics).

In marine optics, in situ measurements of optical parameters are performed to obtain complementary information about the biogeochemical characteristics of water mass. Indeed, optical sensors as backscattering sensors and flow through attenuation meters are potential tools for characterizing stocks and dynamics of biogeochemical significant constituents of water. For example, the knowledge of the backscattering (b_{bp}), scattering (b_p), and attenuation (c_p) coefficients of particles allows obtaining information about the variability of the physical nature (i.e., refractive index) of the bulk particulate matter in oceanic and coastal environments. As a matter of fact, from in situ measurements sampled in the English Channel, (Loisel et al. 2007) showed that low b_{bp}/b_p values are observed for a particle population dominated by low refractive index material such as phytoplankton, whereas high b_{bp}/b_p values are generally observed in presence of relatively high concentration of inorganic particles as minerals. In the red part of the spectrum, the attenuation coefficient can be consider as a good proxy for b_p (Loisel et al. 2007; Loisel and Morel 1998) and b_{bp}/c_p can be used instead of b_{bp}/b_p. Information on the composition of the particle assemblage can also be obtained from the POC to SPM ratio (Babin et al. 2003b; Emmerton et al. 2008; Koestner et al. 2018; Lubac and Loisel 2007; Neukermans et al. 2016; Reynolds and Stramski 2019; Reynolds et al. 2016; Stramski et al. 2007; Stramski et al. 2008; Woźniak 2014; Woźniak et al. 2016; Woźniak et al. 2011; Woźniak et al. 2010). From in situ data in the near-shore marine environment at Imperial Beach, California, Woźniak et al. 2010 set threshold values on POC to SPM ratio to identify changes in the particulate assemblage from the dominance of mineral particles (POC/SPM<0.06) to the dominance of organic particles (POC/SPM>0.25) and accounting for waters composed of mixed particles (0.25<POC/SPM<0.6). (Neukermans et al. 2016; Reynolds et al. 2016) followed the approach of Woźniak et al. 2010 to partition their dataset into these three broad compositional classes. These authors explained that "*these categories represent arbitrary divisions along a continuum of particle mixtures, but provide a useful means of initially classifying particle assemblages and but they helped them to interpret their associated optical measurements*".

Due to the high variability of the physical and biogeochemical processes occurring in coastal waters, traditional approaches as oceanographic cruises and in situ time series, although essential, are very time-consuming, expensive and sometimes uncertain to yield meaningful results on the studied phenomena. For few years now, ocean-color remote sensing is a powerful tool to monitor the spatio-temporal distribution of biogeochemical and physical parameters. A large set of biogeochemical parameters including SPM (Han et al. 2016) and POC (Gardner et al. 2006; Loisel et al. 2002; Mishonov et al. 2003; Pabi and Arrigo 2006; Son et al. 2009; Stramska 2009; Stramski et al. 2008; Stramski et al. 1999; Tran et al. 2019) are retrieved from space-born measurements of the remote-sensing reflectance (R_{rs}). A completely new data set covering the global coastal waters was processed in the frame of the GlobCoast project funded by the French Research National Agency (Vantrepotte 2016). For MERIS period (2002-2012), SPM, concentration of chlorophyll, dissolved organic carbon (DOC), and b_{bp}, are available at global scale at 1 km resolution. Very recently, the POC concentration has been derived using the algorithm developed specifically for global coastal waters by (Tran et al. 2019).

The present chapter aims to study the nature of the particle assemblage from MERIS data over the global coastal waters with a focus on the English Channel and Black Sea, known for their high variability in particle assemblages and dynamics. SPM and POC concentrations will be derived using the recently developed algorithms of (Han et al. 2016) and (Tran et al. 2019), respectively. Before using the POC to SPM ratio to identify the compositional classes, we will re-examine the threshold values using an extensive in situ data set covering a wider range of optical and biogeochemical variability than the previous dataset used by Woźniak et al. (2010). The relevance of the new thresholds will be discussed as a function of the b_{bp}/c_p ratio in the res (650 nm). The remote-sensed estimates of POC/SPM ratio will be tested against in situ measurements before any applications on MERIS data.

4.2. Data & Methods

4.2.1. In Situ data

The in situ dataset includes concentration of biogeochemical parameters (POC and SPM), and inherent optical properties (IOP) (b_{bp} and c_p at 650 nm). Measurements were collected by different sources (Table 4.1) between 2004 and 2014 in various geographic regions (Figure 4.2): European coastal waters (Lubac and Loisel 2007; Lubac et al. 2008; Neukermans et al. 2012), French Guiana (Vantrepotte et al. 2012), Eastern Viet Nam Sea (Loisel et al. 2014; Loisel et al. 2017). The field measurement protocols and the data processing are described in details in related papers listed in Table 4.1. The whole dataset (named DSW, DataSet Whole) includes 353 coincident POC, SPM, c_p, and b_{bp} measurements. As much contrasted coastal waters were sampled, POC, SPM, c_p, b_{bp} parameters present a large variability (Table 4.1 and Figure 4.3). The POC/SPM ratio ranges between 0.01 and 0.87 and b_{bp}/c_p spans from 0.006 to 0.0519 m^{-1}. In comparison, Woźniak et al. 2010 collected 44 samples in Imperial Beach near-shore (California) with 0.023<POC/SPM<0.42. DSW is used in section 4.3.2 to re-examine the threshold values applied to POC/SPM ratio, used to discriminate the type of the water mass (mineral-dominated, mixed or organic-dominated). From DSW, a subset is extracted to test the performance of the algorithms of Han et al. (2016) and Tran et al., (2019) in retrieving the POC to SPM ratio from R_{rs}. In practice, we selected data (POC, SPM, $c_p(650)$, $b_{bp}(650)$) with coincident R_{rs} measurements, and checked that selected data were not used previously by Tran et al. (2019) to develop the POC algorithm. The subset is named DSV (DataSet Validation) and is composed of 169 in situ measurements.

4.2.2. Satellite data

Daily images MEdium Resolution Imaging Spectrometer (MERIS) level 1 with full resolution (MERIS-FR) from 01/04/2002 to 30/04/2012 were collected from the ESA archive system. Level 1 images were then processed following 2 steps. The first step was done by using Polymer algorithm (Steinmetz et al. 2011) which was validated for coastal waters (Loisel 2017) to derive remote sensing reflectance, R_{rs} at a 1x1 km resolution. A second step was then apply in order to mask the R_{rs} maps in order to keep only pixels presenting a distance to the coast lower than 200 km and with a bottom depth not deeper than 4000 m (Loisel et al. 2017). The POC and SPM concentrations were derived using the algorithms developed by Tran et al. (2019) and Han et al. (2016), respectively. These algorithms are detailed in section 4.2.3.

Monthly average of MERIS level 3 R_{rs} from 2002 to 2012 were processed to retrieve POC and SPM which then were used to estimate POC to SPM ratio. For each pixel, the monthly POC to SPM ratio is used to sort the pixel according to its water type (mineral-dominated, mixed or organic-dominated). The occurrence of each water class (%) is computed for the period 2002-2012 for each pixel (Figure 4.1).

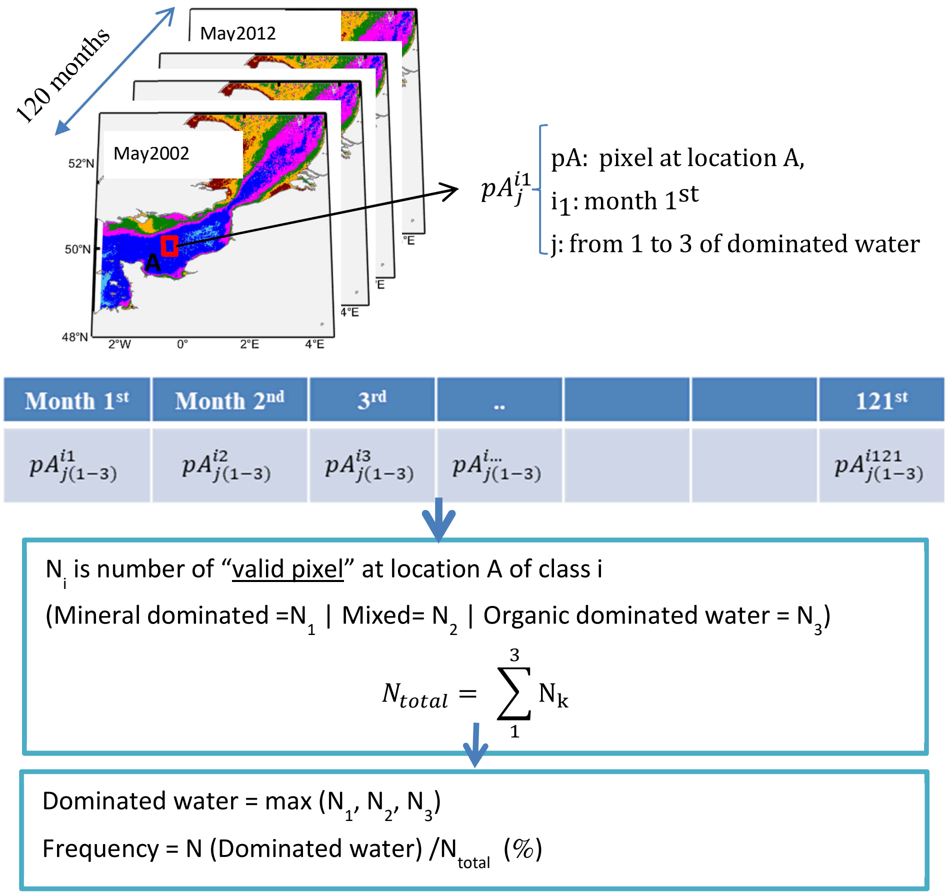

Figure 4.1. Flow chart of the procedure using for computing the frequency and dominance of the class associated with each pixel of dominant class over the time period of 2002 – 2012.

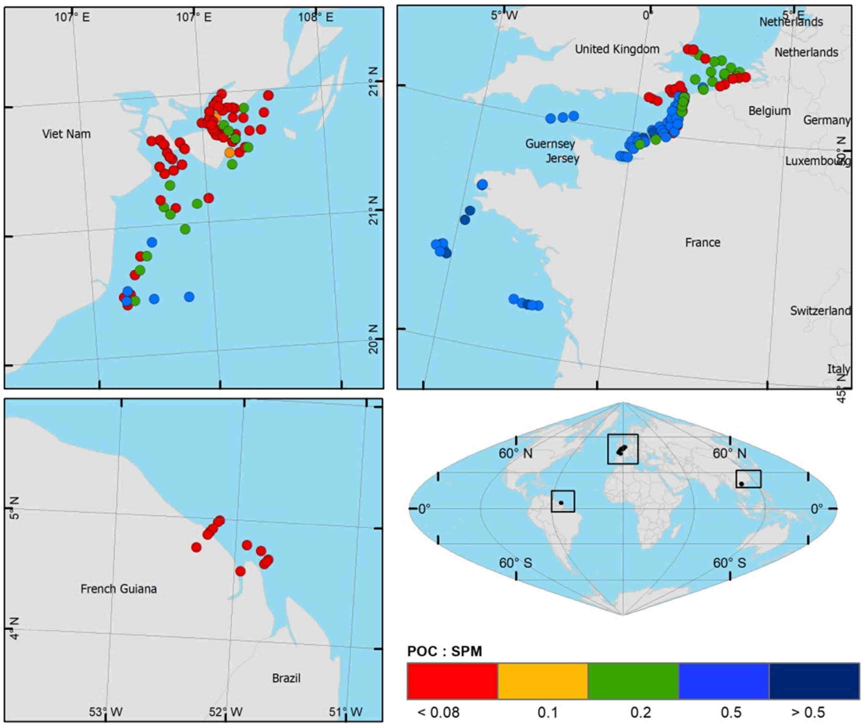

Figure 4.2. Geographical distribution of in situ coincident POC, SPM, b_{bp} and c_p measurements listed in Table 4.1. The color scale corresponds to the ratio of POC to SPM concentration.

4.2.3 SPM and POC algorithms

POC algorithm - Tran et al. (2019) developed an empirical algorithm to derive POC in coastal waters. POC concentration is obtained from (Equation 4.1) using the maximum of red-to-green or red-to-blue band ratio (Equation 4.2).

$$POC = 10^{0.025X^2+0.945X+2.873} \tag{4.1}$$

with:

$$X = log_{10}\left[maximum\left(\frac{R_{rs}(665)}{R_{rs}(490)},\frac{R_{rs}(665)}{R_{rs}(510)},\frac{R_{rs}(665)}{R_{rs}(555)}\right)\right] \tag{4.2}$$

SPM algorithm - The algorithm developed by Han et al. 2016 is based on two standard semi-analytical equations calibrated for low-to-medium SPM conditions (SAA-L: SPM < 100 gm^{-3}) (Equation 4.3) and highly turbid waters (SSA-H: SPM ≥ 100 gm-3) (Equation 4.4):

<u>SAA-L</u>

$$SPM_L = A_L^{\rho}\rho_w(\lambda_0)/\left(1-\rho_{w(670)}/C_L^{\rho}\right),$$

where: $A_L^{\rho} = 391.082 \wedge C_L^{\rho} = 0.5000.$ (4.3)

SAA-H

$$SPM_H = A_H^{\rho}\rho_w(\lambda_0)/\left(1-\rho_{w(670)}/C_H^{\rho}\right),$$
where $A_H^{\rho} = 1444.853 \wedge C_H^{\rho} = 0.3539.$ (4.4)

A mixing law was also developed for intermediate environments (Equation 4.5). The smoothing method adopted consists in defining a weighting function of the low-medium and high SPM algorithms. In practice, two weights, and for low (W_L) and high (W_H) SPM conditions, are given by Equation 4.6 and Equation 4.7, respectively.

$$SPM = \frac{W_L SPM_L + W_H SPM_H}{W_L + W_h} \tag{4.5}$$

$$W_L = \begin{cases} 1 If R_{rs}(\lambda_0) \leq 0.03 sr^{-1} \\ 0 If R_{rs}(\lambda_0) \geq 0.04 sr^{-1} \\ log_{10}(0.04) - log_{10}[R_{rs}(\lambda_0)] \end{cases} \tag{4.6}$$

$$W_H = \begin{cases} 0 If R_{rs}(\lambda_0) \leq 0.03 sr^{-1} \\ 1 If R_{rs}(\lambda_0) \geq 0.04 sr^{-1} \\ log_{10}[R_{rs}(\lambda_0)] - log_{10}(0.04) \end{cases} \tag{4.7}$$

where: $\rho_w(\lambda_0)$ is the water-leaving reflectance $\rho_w(\lambda_0) = \Pi R_{rs}(\lambda_0)$;

For MERIS sensor: $R_{rs}(\lambda_0 = 670)$, $A_L = 396.005$; $B_L = 0.5$; $A_H = 1208.481$; $B_H = 0.3375$.

4.2.4. Statistical Indicators of Model Performance

To assess the performance of POC and SPM algorithms presented in section 2.3 to retrieve the POC to SPM ratio, we used the graphical comparison of model predictions and in situ observations as well as quantitative statistical metrics of differences between the corresponding predictions of model and in situ measurements. These indicators include the Root-Mean-Square-Deviation for log-transformed data ($RMSD_{log}$) (Equation 3.10); the Root-Mean-Square Deviation for un-transformed data (RMSD) (Equation 4.11); the median absolute percent difference (MAPD) (Equation 4.12); the mean bias (MB) (Equation 4.13) and the median ratio (MR) (Equation 4.14).

$$RMSD_{log} = \left(\sum_{i=1}^{N} \left(log\left(POC/SPM_i^{mod}\right) - log\left(POC/SPM_i^{obs}\right)\right)^2 \Big/ N\right)^{\frac{1}{2}} \tag{4.10}$$

$$RMSD = \left(\sum_{i=1}^{N} \left(POC/SPM_i^{mod} - POC/SPM_i^{obs}\right)^2 \Big/ N\right)^{\frac{1}{2}} \tag{4.11}$$

$$MAPD = median\left(\left|\frac{POC/SPM_i^{mod} - POC/SPM_i^{obs}}{POC/SPM_i^{obs}}\right|\right) \times 100 \tag{4.12}$$

$$MB = \frac{1}{N}\sum_{i=1}^{N} \left(POC/SPM_i^{mod} - POC/SPM_i^{obs}\right) \tag{4.13}$$

$$MR = median\left(\frac{POC/SPM_i^{mod}}{POC/SPM_i^{obs}}\right) \tag{4.14}$$

where POC/SPM_i^{obs} and POC/SPM_i^{mod} are the in situ and model - derived POC/SPM.

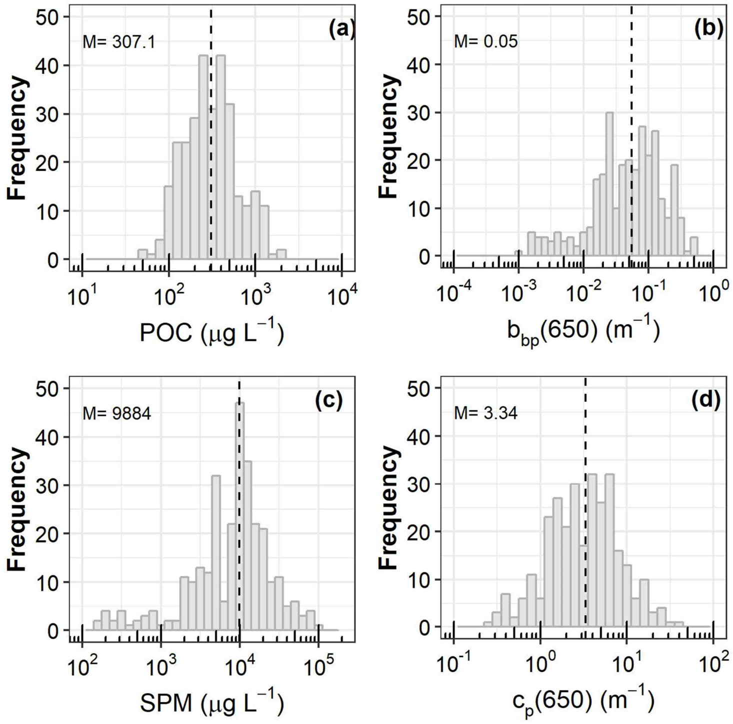

Figure 4.3. Frequency distribution of (a) POC, (b) $b_{bp}(650)$, (c) SPM concentration and (d) $c_p(650)$. Dashed lines stand for the median values (M) of each parameter. The number of data (DSW) is equal to 300 for each parameter.

Table 4.1. Information on the in situ data used in this study: number of data (N), mean, [minimum (Min), maximum (Max)], and standard deviation (StdDev) values of POC and SPM concentrations (µg L^{-1}), $c_p(650)$ and $b_{bp}(650)$ (m^{-1}).

Region	**Year**	**N**	**POC**	**SPM (x 10^3)**	**POC/SPM**	**$b_{bp}(650)$**	**$c_p(650)$**	**$b_{bp}(650)/c_p(650)$**	**Reference**
North Sea	2010	28	497.3 [105.04-2159.35] (481.5)	8.935 [0.8-19.47] (5.71)	0.077 [0.01-0.18] (0.058)	0.092 [0.0068-0.2642] (0.076)	3.83 [0.72-8.89] (2.09)	0.022 [0.006-0.0519] (0.0139)	(Neukermans et al. 2012)
English Channel	2004	53	735.5 [264.9-1781] (320.9)	2.65 [0.65-11.1] (2.23)	0.345 [0.10-0.59] (0.11)	0.018 [0.0031-0.0806] (0.017)	2.02 [0.4948-14.0005] (1.96)	0.011 [0.0002-0.0419] (0.0077)	(Lubac et al. 2008) (Lubac and Loisel 2007)
	2012	21	492.1 [49.85-1519] (410.7)	48.00 [17.77-118.7] (26.06)	0.012 [0.001-0.045] (0.011)	0.041 [0.0069-0.0911] (0.025)	1.71 [0.31-3.99] (0.96)	0.025 [0.0089-0.0446] (0.0112)	https://campagnes.flotteoceanographique.fr/campagnes/12480030/
Bay of Biscay-France	2010	21	145.4 [54.81-303.8] (66.43)	0.41 [0.16-0.81] (0.21)	0.397 [0.179-0.867] (0.169)	0.0029 [0.001-0.0079] (0.0016)	0.52 [0.26-0.84] (0.18)	0.005 [0.0025-0.01] (0.0014)	(Novoa et al. 2017)
French Guiana	2012	16	563.7 [215.9-1061] (247.1)	20.58 [4.26-54.12] (16.11)	0.048 [0.01-0.234] (0.053)	0.145 [0.02-0.3481] (0.113)	11.25 [1.98-36.63] (9.90)	0.012 [0.0013-0.0261] (0.005)	(Vantrepotte et al. 2015; Vantrepotte et al. 2012)
East sea of Viet Nam	2011	137	307.9 [94.14-1202] (213.8)	11.53 [2.02-76.8] (10.49)	0.034 [0.007-0.082] (0.017)	0.102 [0.0067-0.3294] (0.084)	5.52 [1.13-16.57] (4.09)	0.017 [0.0059-0.022] (0.0032)	(Loisel et al. 2014; Loisel et al. 2017)
	2012	33	486.4 [166-1248] (301.6)	10.12 [4.22-27.19] (4.58)	0.048 [0.019-0.132] (0.023)	0.066 [0.0209-0.1731] (0.032)	3.98 [1.42-7.66] (1.62)	0.016 [0.0118-0.0226] (0.0019)	(Loisel et al. 2014; Loisel et al. 2017)
	2013	17	358.8 [199-562] (119.7)	13.28 [4.67-32.65] (8.06)	0.034 [0.011-0.071] (0.017)	0.036 [0.0093-0.0668] (0.018)	2.6367 [1.05-4.68] (1.16)	0.013 [0.0089-0.0177] (0.0019)	(Loisel et al. 2014; Loisel et al. 2017)
	2014	27	704.8 [234.2-1971] (436.1)	11.51 [1.05-65.83] (15.70)	0.129 [0.018-0.251] (0.07)	0.119 [0.0023-0.5101] (0.182)	6.513 [0.86-29.89] (8.88)	0.012 [0.0026-0.0251] (0.0067)	(Loisel et al. 2014; Loisel et al. 2017)
Overall		353	449.5 [49.85-2159] (343.7)	11.86 [0.16-118.7] (14.88)	0.114 [0.001-0.867] (0.146)	0.076 [0.001-0.5101] (0.089)	4.3721 [0.26-36.63] (4.77)	0.015 [0.0002-0.0519] (0.0078)	

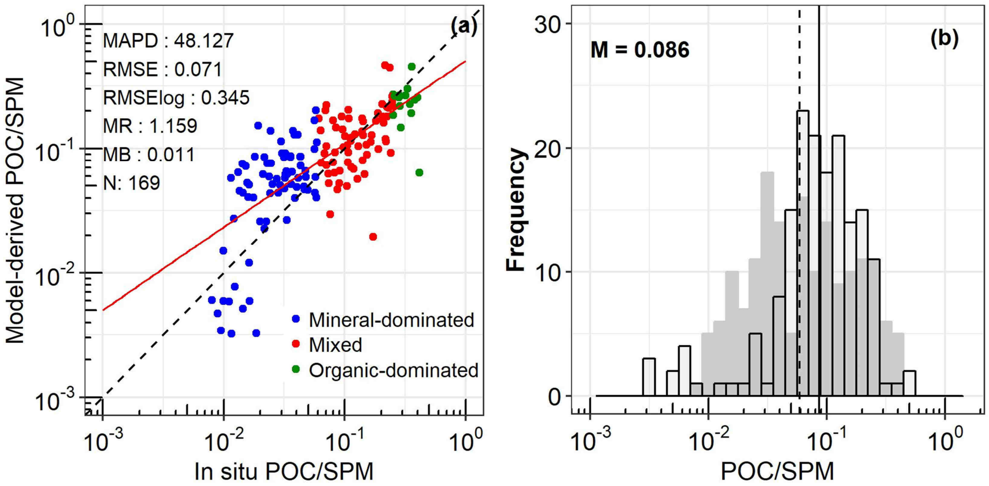

Figure 4.4. (a) Comparison of in situ and model-derived POC/SPM. The dashed line is the 1:1 line, and the solid line is the type II linear regression (log-transformed data). Green, red and blue dots correspond to organic-dominated, mixed and mineral-dominated waters (Woźniak et al. 2010). (b) Frequency distribution of in situ (grey) and model-derived (black contour) POC/SPM. The dashed and solid lines represent the median of in situ (M =0.059) and model-derived (M=0.086) POC/SPM, respectively.

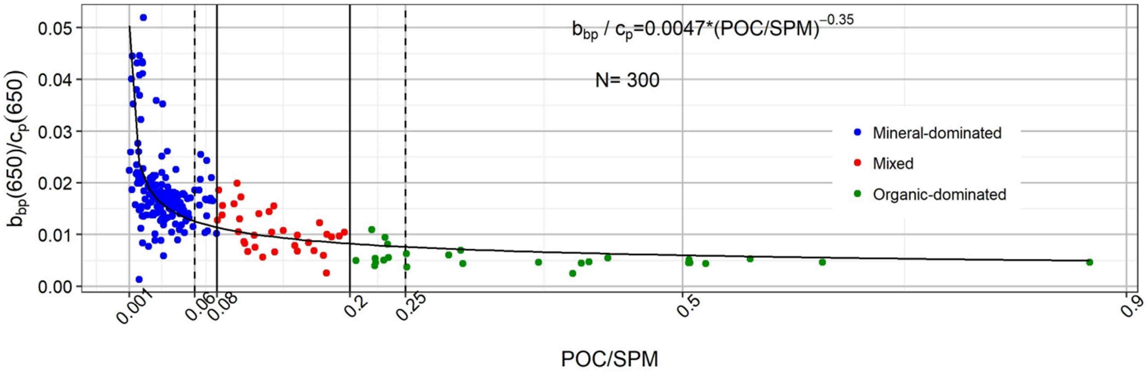

Figure 4.5. Relationships between POC/SPM ratio and b_{bp}(650)/cp(650) ratio for DSW (N=353). The black line stands for the power regression. The vertical dashed lines represent the thresholds delimiting the 3 water types (mineral-dominated POC/SPM<0.06, organic-dominated POC/SPM>0.25, and mixed 0.06≤POC/SPM≤0.25) according to Woźniak et al. (2010). The vertical solid line shows the new thresholds defined here (mineral-dominated POC/SPM<0.08, organic-dominated if POC/SPM > 0.2, and mixed 0.08≤POC/SPM≤0.2).

4.3. Results and discussion

4.3.1 Performance of the algorithms used to retrieve the POC/SPM from R_{rs}

The algorithms of Han et al. (2016) and Tran et al. (2019) were used to retrieve from in situ R_{rs} (DSV dataset) the SPM and POC concentrations, respectively. Figure 4.4a shows model-derived POC/SPM against in situ values. Figure 4.4b compares the histograms of the frequency distribution of in situ and model-derived POC/SPM. The slope of the type II regression (log-transformed data) is 0.69 with a coefficient of determination $R^2=0.5$. The POC/SPM ratio is overestimated or underestimated for mineral-dominated waters (Figure 4.4, blue dots). The overestimation may be due to POC estimates as an overestimation was observed by Tran et al. (2019) on their POC estimates for mineral-dominated waters (blue dots in Figure 2.15 and 2.16 in Chapter 2). The $RMSD_{log} = 0.35$ is higher than the $RMSD_{log}$ (= 0.25) observed on model-derived POC but has rather the same order of magnitude as $RMSD_{log}$ (=0.31) observed on SPM estimates (Han et al., 2016).

POC to SPM ratio is subject to two sources of errors as two bio-optical algorithms are used, instead of a single algorithm when only POC or SPM concentrations are derived. It may explain why the uncertainties on POC/SPM are higher than uncertainties on POC or SPM concentrations.

4.3.2. Partitioning the particle assemblage from POC to SPM ratio: a re-examination

The Figure 4.5 displays the dimensionless optical ratio b_{bp}/c_p at 650 nm against POC to SPM ratio. As expected $b_{bp}(650)/c_p(650)$ decreases when POC/SPM increases as low $b_{bp}(650)/c_p(650)$ are observed for a particle population dominated by low refractive index material such as phytoplankton (Boss et al. 2004; Duforêt-Gaurier et al. 2018; Loisel et al. 2007; Twardowski et al. 2001). In contrast, $b_{bp}(650)/c_p(650)$ increases when the relative proportion of inorganic particles increases as compared to the proportion of the total particulate matter, that's to say when the POC to SPM ratio decreases.

Figure 4.5 displays a rapid decrease of the regression line for a narrow range corresponding to small POC/SPM values (POC/SPM<0.08). This rapid decrease is globally related to high $b_{bp}(650)/c_p(650)$ values (most of the data are above 0.01). Conversely, an asymptote is reached at high POC/SPM values and concerns data points with the lowest $b_{bp}(650)/c_p(650)$ ratio (below 0.01). The in situ measurements located along the rapid decrease (blue dots in Figure 4.5) are associated with mineral-dominated waters, whereas the data points located along the asymptote (green dots) are associated with organic-dominated waters. The cut-off values for mineral-dominated waters is fixed to 0.08, instead of 0.06 for Woźniak et al. (2010) to include all data points with high $b_{bp}(650)/c_p(650)$ values above 0.01 and also above 0.02. The cut-off value for organic-dominated waters, here set to 0.2 is rather similar to the value previously obtained by Woźniak et al. (2010.)

4.3.3 Satellite application

The POC and SPM algorithms were applied to MERIS monthly R_{rs} over the 2002-2012 time periods. Figure 4.6 displays for each coastal pixel the water class having the maximum of occurrence over the period. The overall corresponding frequency (in %) is further indicated by the color scale. As expected, we observe a color gradient from mineral-dominated waters close to near-shores to organic-dominated waters far from the coast with a transition zone corresponding to mixed waters. Deltas with huge discharge volume as Amazon River Delta or Mekong Delta are characterized by a very high occurrence of mineral-dominated waters (70-90%). The Figure 4.7 shows the coefficient of variations (CV) of the POC/SPM over the 10 years. The range of CV is quite large as we observed values lower than 30% and values greater than 70%. While the complete analysis of results presented in Figure 4.6 and 4.7 as a whole does not fall under the scope of this PhD, we chose to focus on two specific areas: the Eastern English Channel and the Southern North Sea, and the Black Sea, for which the biogeochemical processes and physical forcing are well-documented.

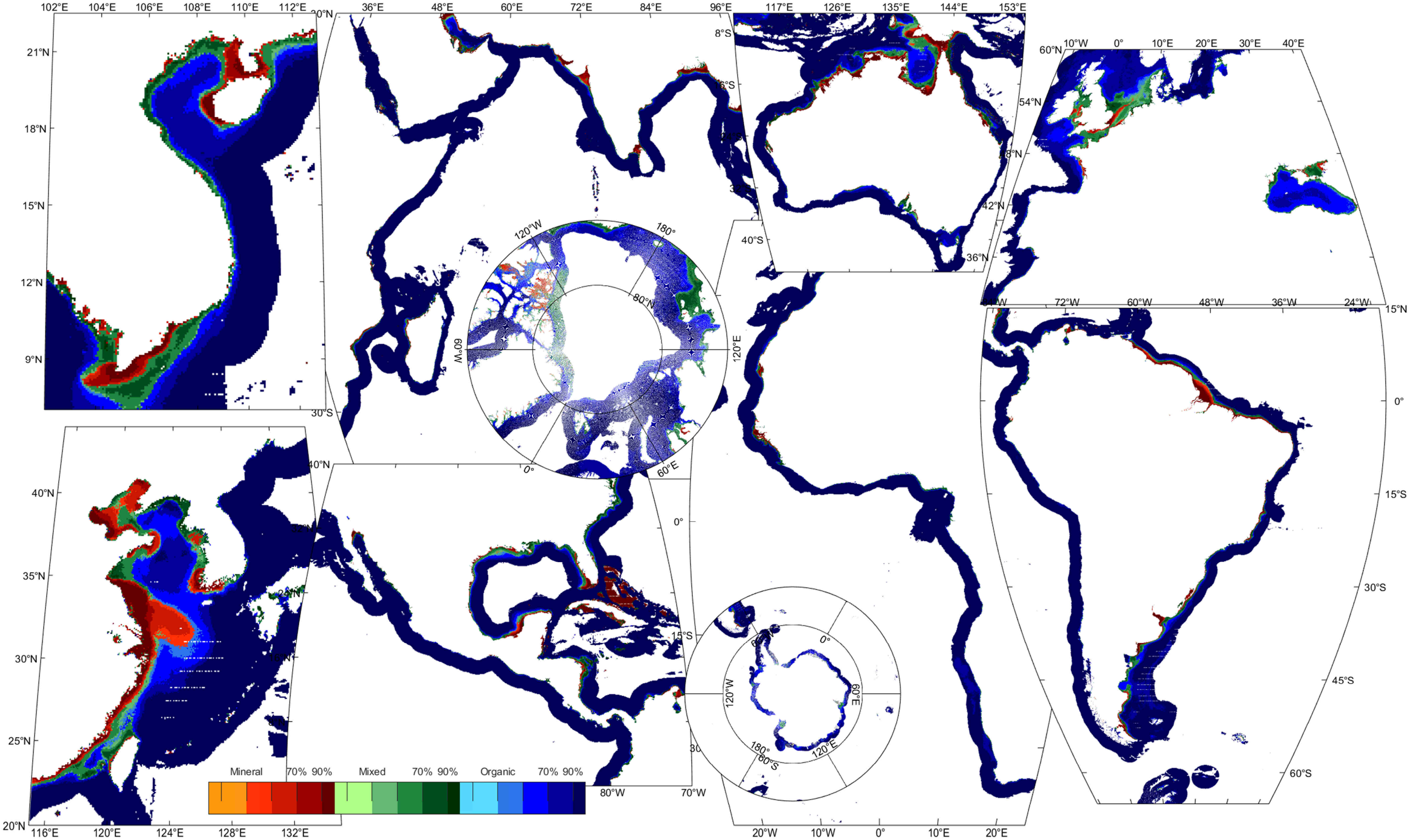

Figure 4.6. Dominant (mineral/mixed/organic) class distribution over the MERIS time period 2002-2012. The frequency (%) related to the class showing the dominant occurrence is indicated by the color scale.

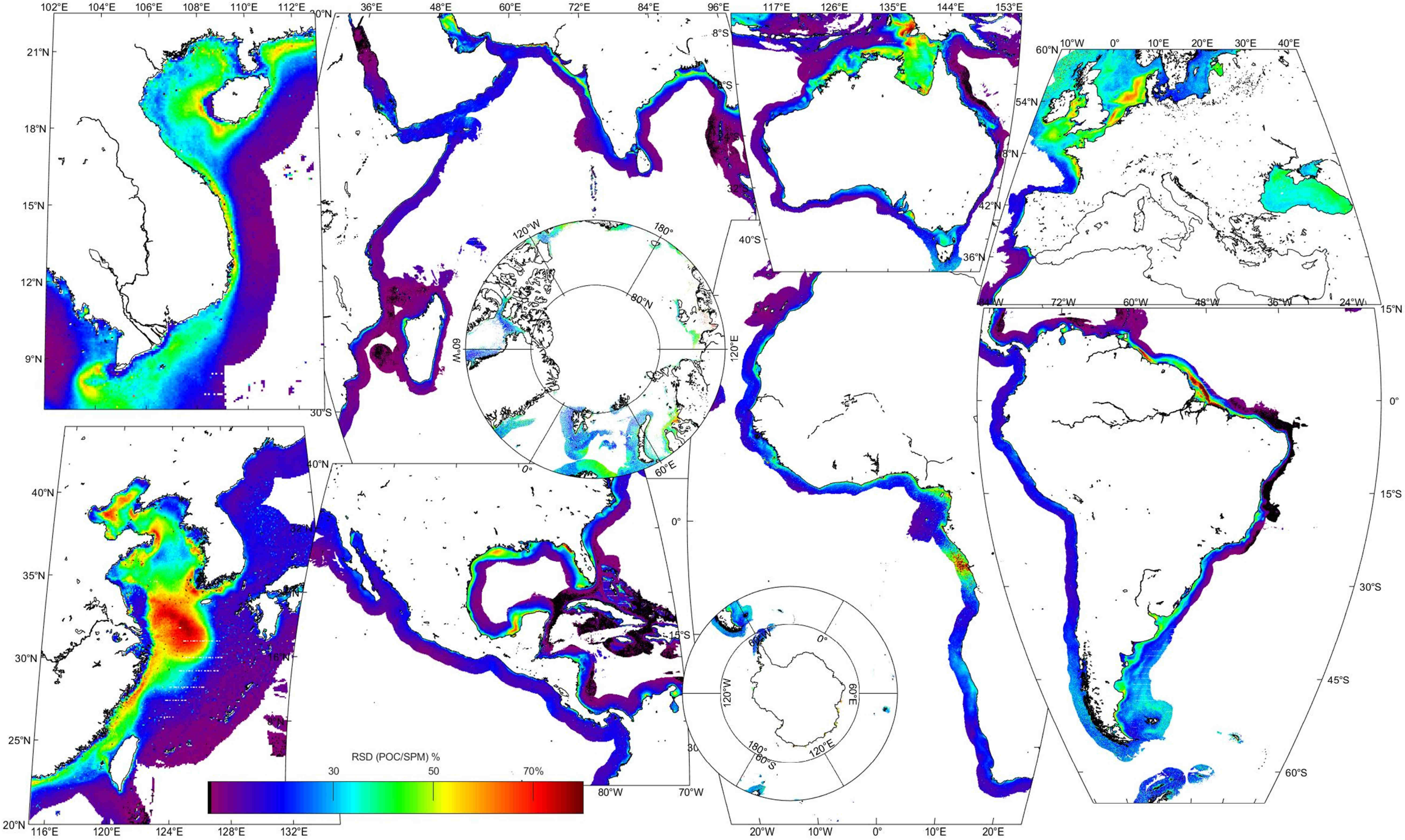

Figure 4.7. The relative standard deviation, RSD (also known as coefficient of variation, CV) of POC/SPM over the MERIS time period (2002–2012).

4.3.3.1. Regional variability

4.3.3.1.1. Eastern English Channel and Southern North Sea

Figure 4.8 illustrates the monthly representativeness of the POC/SPM derived water types over the 2002-2012 periods in the Eastern English Channel and Southern North Sea. This region is characterized by a strong spring phytoplankton bloom, strong hydrodynamic processes (as strong tidal currents), shallow waters and numerous freshwater inputs, illustrated by the numerous rivers along the coast from the Bay of the Seine up to the Cape Gris-Nez (Strait of Dover) or in the Thames estuary. The 12 panels display for each pixel the water class having the maximum of occurrence (%) for each month. Globally, the particulate matter pool of English Channel and North Sea are characterized by mineral-dominated and mixed waters between mid-fall and winter (from October to February). In January, the southern North Sea is quasi-exclusively covered by mineral-dominated pixels with a high occurrence. This is consistent with results of (Vantrepotte et al. 2012) who observed that relative contribution of particulate matter assemblage with a strong proportion of mineral particles (Class 3 pixels in their paper) increases significantly during winter time period. The authors explained that "t*his feature is related to the fact that this optical class mostly marks the water masses impacted by the land–sea interactions processes leading to the presence of very high sediment loads when strong hydrodynamic regime occurs*". In March, organic-dominated pixels appear. During spring, the area covered by organic-dominated pixels increase to be maximum in the early summer. A lot of studies (Bonato et al. 2015; Breton 2000; Brunet et al. 1996; Gomez and Souissi 2007; Grattepanche et al. 2010; Grattepanche et al. 2011; Lefebvre et al. 2011; Loisel et al. 2007; Lubac and Loisel 2007; Schapira et al. 2008) documented the dynamics of the regional phytoplankton spring blooms and reported the dominance of *Phaeocystis globosa* and diatoms in terms of abundance and biomass from late winter to mid-late spring. Most of the time after the initial outburst of diatoms (April), *Phaeocystis globosa* co-occurred or followed the spring diatom peak in May. The highest POC values were observed during blooms of diatoms (from April to May) and during *Phaeocystis globosa blooms* (May), which causes very high POC to SPM ratio. We notice that the spring bloom starts earlier in the Southern North Sea compared with the Eastern English Channel. This was previously observed by *(Brunet et al. 1996).*

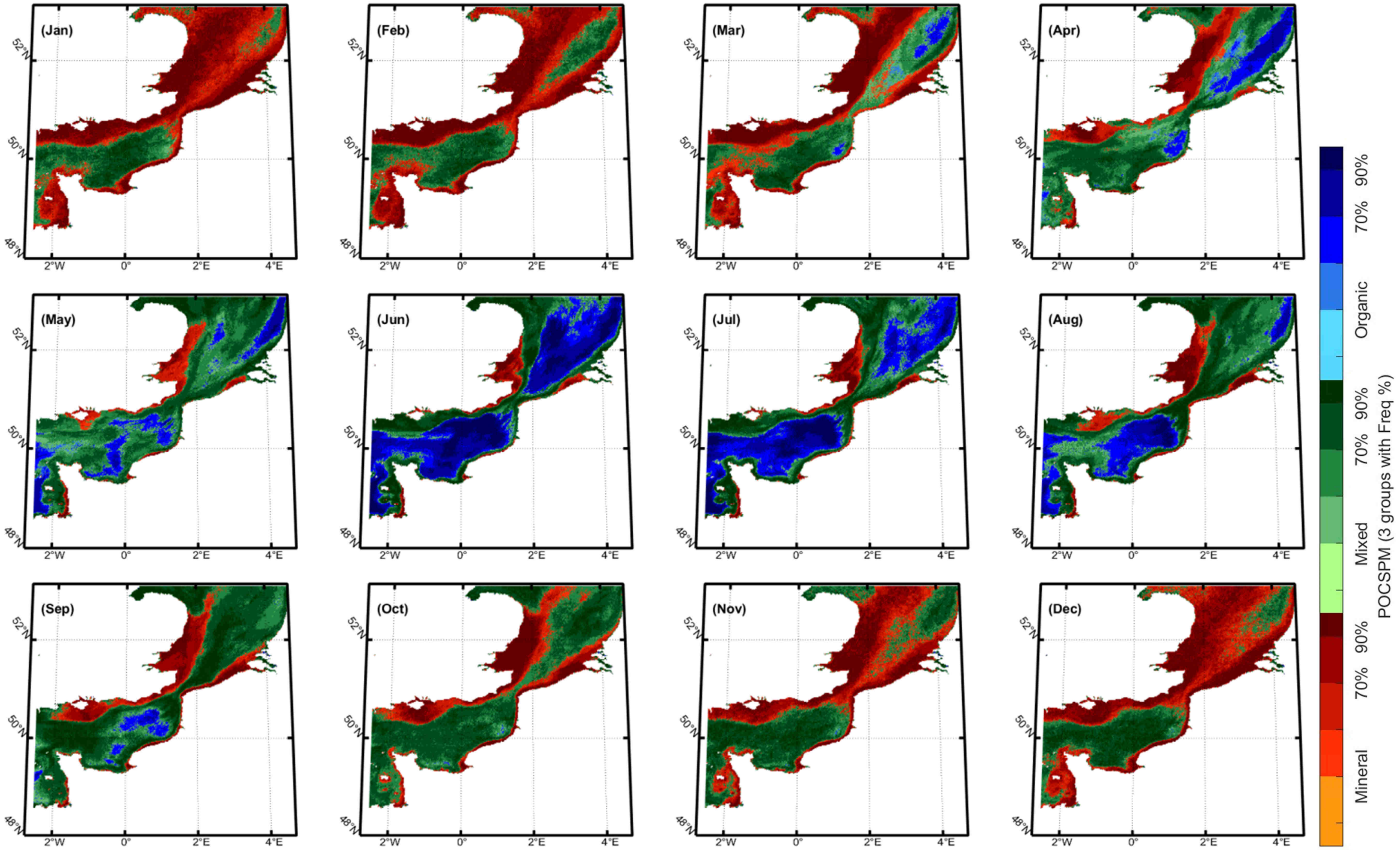

Figure 4.8. Water class having the maximum of occurrence over the MERIS period 2002-2012 in the Eastern English Channel and Southern North Sea. The maximum occurrence (%) for each month is indicated by the color scale.

4.3.3.1.2. Black sea

Figure 4.10 displays, for each pixel, the water class for which the maximum of occurrence (in %) occurs. The spatial distribution of the particulate pool classes, observed in Figure 4.10, can be described using four geographical areas, commonly used to partition the Black Sea. These four geographical regions were clearly identified on the basis of several Black Sea characteristics, like bathymetry, currents and riverine influence (Miladinova et al. 2016; Miladinova et al. 2017b). They are the inner part of the basin with depth deeper than 1500 m, the shelf slope 200-1500 m, the North Western Shelf and the coastal regions (Figure 4.9. from (Miladinova et al. 2017a), JRC technical report). The 4 regions will be named INP (INner Part), SHS (SHelf Slope), NWS (North Western Shelf) and CR (Coastal Regions) in the following. The area covered by mineral-dominated pixels is small-sized whatever the season. Small patches of mineral-dominated pixels are observed in coastal areas very close to the Danube Delta, in the Karkinit Bay and in Kerch Strait (Figure 4.11. The coastal regions and a portion of NWS are globally dominated by mixed waters. It can be explained by a mixing between inorganic particles from riverine mouths (Danube, Dniester, Dniep, Rioni and Coruhsuyu Figure 4.9) and organic particles from phytoplankton blooms. Indeed, previous studies reported that the NWS and the coastal areas of the Black Sea exhibit very elevated phytoplankton concentrations in the surface layers. For example, high chlorophyll concentration was observed in the Danube and Dniester nearby zones and close to the Kerch Strait (Miladinova et al. 2017a). High chlorophyll concentrations close to the shelf are explained by high nutrient river inputs. The inner part and shelf slope are most of the time organic-dominated waters, except in May and June, where the whole basin is quasi exclusively dominated by mixed waters. Basin wide blooms of coccolithophores blooms were reported in previous studies at that time of the year (Cokacar et al. 2001; Cokacar et al. 2003; Ogu□ and Ediger 2006). The biogenic $CaCO_3$ particles often encountered during coccolithophore blooms can explain the dominance of mixed waters. Previous studies showed that at this time, the water temperature is optimal not only for growth of coccolithophorids, but also for the process of its cell calcification (Stelmakh and Gorbunova 2018). Total duration of the summer coccolithophore bloom events as well as timing of their peak periods undergoes year-to-year variations. Late coccolithophore blooms are also observed in July. In July, shifts in phytoplankton species composition (diatoms or dinoflagellates) are observed. It may explain the bi-partitioning of Black Sea pixels, where organic-dominated waters represent areas with a larger abundance of diatoms or dinoflagellates, whereas mixed waters represents waters where coccolithophores remain. Besides, the Figure 4.10 shows that for January and February the spatial distribution of mixed pixels seems to follow the RIM current jet (Figure 4.12, (Korotenko 2018)).

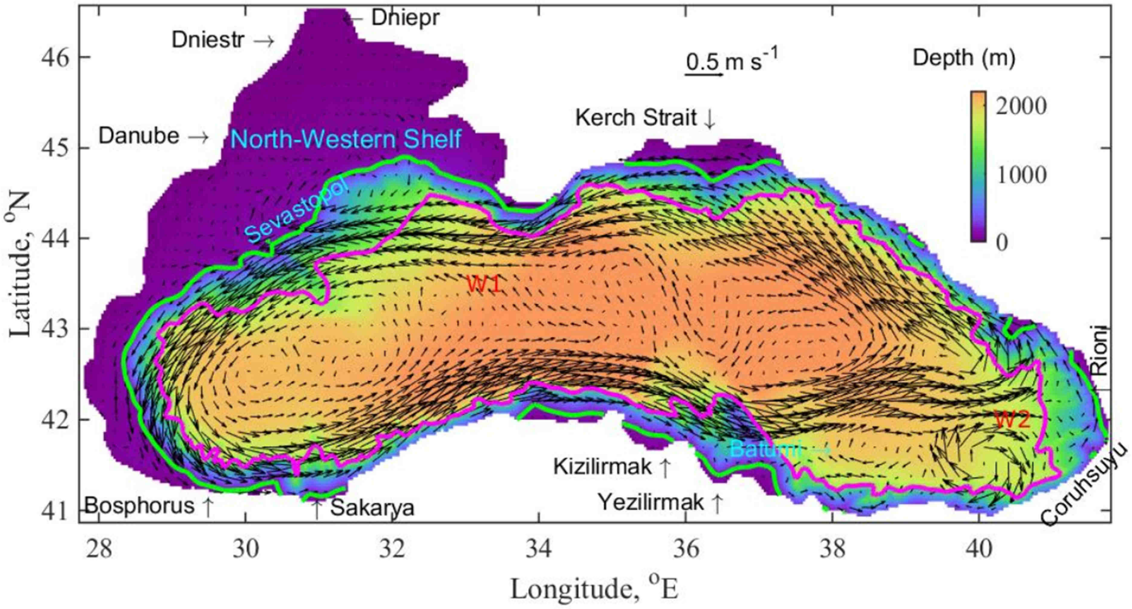

Figure 4.9. Extracted map from (Miladinova et al. 2017a), JRC technical report: bathymetry and location map of the Black Sea, main rivers and locations of Batumi and Sevastopol anticyclonic eddies. The 1500 m is drawn in magenta and the 200 m isobaths is given in green. Simulated climatological velocity vectors at 5 m depth in September, averaged over 1991-2015, are presented by black arrows.

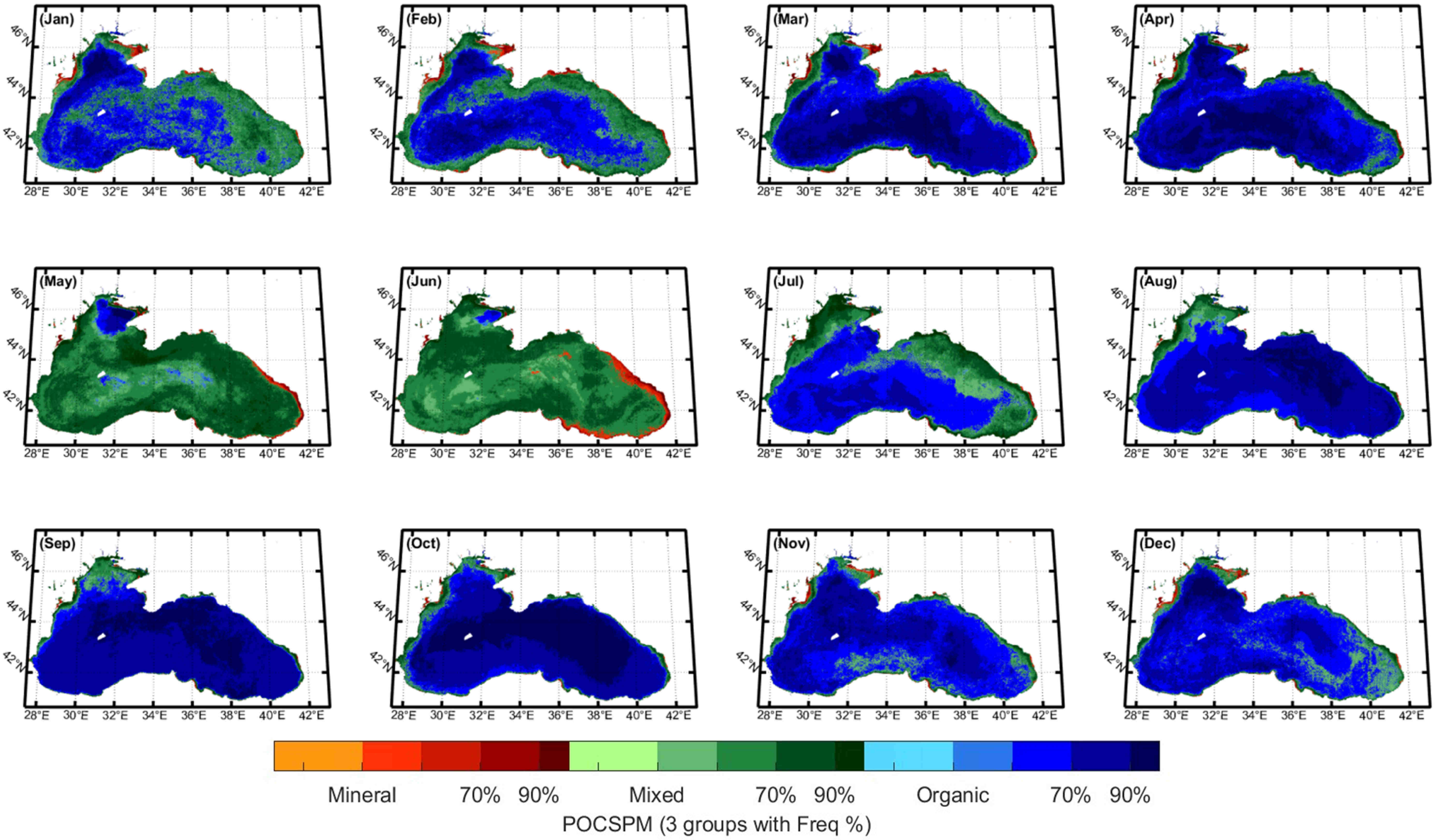

Figure 4.10. Water class having the maximum of occurrence over the MERIS period 2002-2012 in the Eastern English Channel and Southern North Sea. The maximum occurrence (%) for each month is indicated by the color scale.

Figure 4.11. Map of the Black Sea from Encyclopædia Britannica, inc..

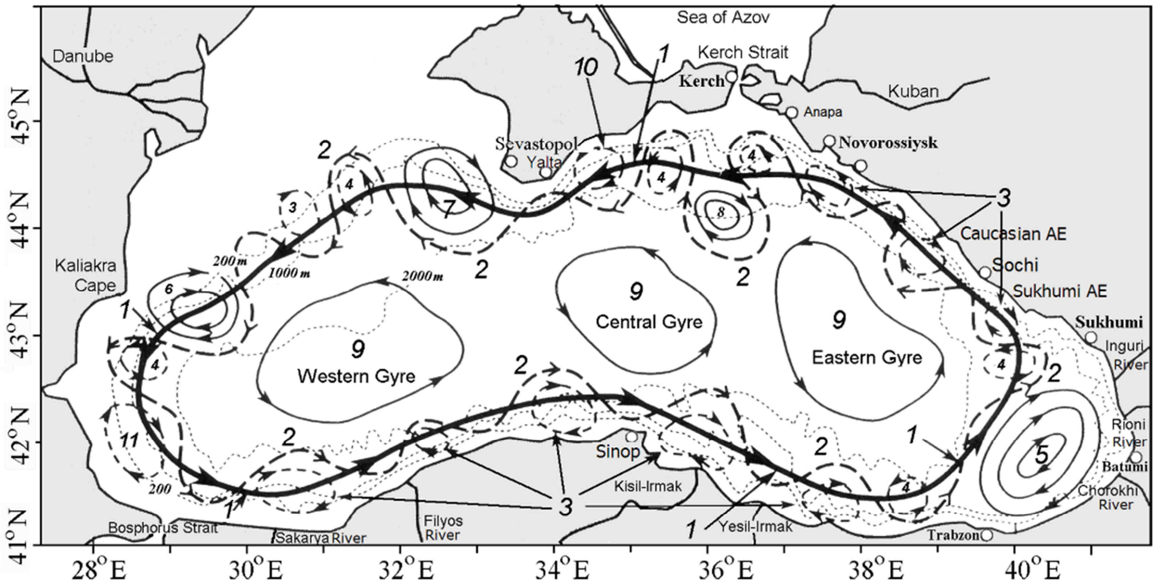

Figure 4.12. map from Schematic of the Black Sea circulation (modified from (Korotenko 2018)). 1-mean position of the Rim Current jet; 2-meanders; 3-near-shore anticyclonic eddies (NAEs); 4-cyclonic eddies (CEs); 5-Batumi anticyclonic eddy; 6-Kaliakra anticyclonic eddy; 7-Sevastopol anticyclonic eddy; 8-Kerch anticyclonic eddy; 9-quasi-stationary cyclonic gyres; and 10-Crimea anticyclonic eddy; and 11-Bosphorus anticyclonic eddy. DOI: 10.7717/peerj.5448/fig-2.

4.4. Conclusion and perspectives

Two recently developed bio-optical algorithms were used to derive POC and SPM concentrations and then POC to SPM ratio. A first application was to use the POC to SPM ratio to partition the particulate matter assemblages into basic groups as in Woźniak et al. (2010). The thresholds fixed by Woźniak et al. (2010) were re-examined from an extensive in situ data set covering a wider range of optical and biogeochemical variability than the dataset used previously by Woźniak et al. (2010). The remote-sensed estimates of POC/SPM ratio were derived from MERIS data over the period 2002-2012 for two areas: the Eastern English Channel and Southern North Sea and the Black Sea. The spatio-temporal dynamics of the 3 defined water types still remains highly relevant when facing the seasonal changes occurring in the water masses of the two studied regions as they are consistent with the general features previously documented in the literature. For a future study, it will be relevant to study how the variability in the particulate assemblage and in the biogeochemical parameters (Chla, POC and SPM) is influenced by hydrodynamic processes. The idea would be to use observations of physical properties that could help to identify different waster mass such as ocean currents and fresh water discharged from rivers, maybe combined with satellite estimates of sea surface temperature. It will be also interesting to study the spatio-temporal variability of the particulate assemblage using hydrodynamic models as for example Princeton Ocean Model in the Eastern English Channel (Sentchev and Korotenko 2007).

Global maps of POC to SPM ratio were generated (not shown) and the coefficient of variation was computed for the coastal waters over the globe. A next step will be to generate POC/SPM climatology over specific coastal areas and study the POC/SPM temporal variation schemes (irregular variability, seasonal variability, and long term trend) using for example the Census-X-11 time series decomposition method. The different spatio-temporal patterns could be analyzed with regard to regional oceanographic and hydrologic conditions of the considered areas. For example, an interesting perspective will be to characterize the origin of the processes controlling the seasonality of the observed parameter.

General conclusions and perspectives

This work contributes to the coastal studies of particular organic carbon and aims also at contributing to a better characterization of the optical quality of coastal water masses through water mass classification. The first objective was to estimate coastal POC concentration from satellite measurements in global coastal waters. The performance of 12 existing historical algorithms was examined. Through the inter-comparison exercise, the higher performance was observed for the blue-green band ratio algorithm of Hu et al. 2015 (Hu15-3). However, Hu15-3 tends to provide underestimated values for POC concentration higher than 1000 μg L^{-1}, corresponding to mineral-dominated waters and overestimated values for POC concentration lower than 1000 μg L^{-1}.

The new algorithm (CPOC) was then developed and validated from two independent extended in situ data sets (development and validation datasets) which were both sampled in different coastal areas and both cover various bio-optical conditions. The new algorithm is based on an empirical relationship between POC and a maximum band ratio (MBR) max ($R_{rs}(665)/R_{rs}(490)$, $R_{rs}(665)/R_{rs}(510)$, $R_{rs}(665)/R_{rs}(555)$). These wavelengths are available in most ocean colour sensors and the usage of band ratios allows to switch from a given band ratio to another, thereby avoiding, in some cases, a low and potentially noisy band ratio. Thus, in the context of satellite applications, it is expected that using MBR instead of a single band ratio allows the maximization of the model precision over the entire range of POC. In general, the new POC algorithm improves the performance over a wide range of POC concentrations and presents better accuracy ($RMSD_{log}$ of 0.25, MAPD of 37.48%, MB of 0.54 μg L^{-1} and MR of 1.02) in comparison with 12 historical algorithms.

Furthermore, the optical classification of coastal water, following the method presented in Vantrepotte et al., 2012, was re-examined based on an extended in situ data set covering various bio-optical and biogeochemical conditions. Six optical water classes were obtained. Class 1 and

6 represent the optical diversity of coastal waters from the very turbid (Class 1) to the clear water environments (Class 6). Class 2 and 4 describe the phytoplankton bloom conditions in shallow water (Class 2) and offshore water (Class 4). The two remaining classes (class 3 and 5) are related to optically mixed situations with a high proportion of particulate mineral material. Moreover, the applicability of 6 classes was demonstrated by applying the present classification on monthly MERIS data. The results showed that the 6 classes cover a wide part of the optical variability and provide not only synthetic information on the temporal dynamics of the optical quality of coastal water but also show the variation in the river plume extension. The previous study of Vantrepotte et al., 2012 demonstrated the potential to retrieve SPM from class-based inversion algorithms. It would be an interesting perspective to define if the corresponding optical classes can provide a relevant frame for deriving class-based inversion algorithms taking into account the optical variability of the coastal environment within the algorithm development procedure.

Another key contribution of this PhD work is that it offers a comprehensive approach to assess POC/SPM ratio as a proxy for water masses. The relationship between POC/SPM ratio and b_{bp}/c_p was investigated based on a large range of in situ POC/SPM data (0.001 – 0.87) which were collected in various geographic regions. The in situ dataset was classified into 3 groups: mineral-dominated (POC/SPM $<$ 0.08), organic-dominated (POC/SPM $>$ 0.2) and mixed water mass ($0.08 \leq$ POC/SPM ≤ 0.2). In terms of satellite application, two bio-optical algorithms of POC (Tran et al. 2019) and SPM (Han et al. 2016) were processed by using the same satellite image dataset (MERIS level 3, over period 2002-2012) hereby for retrieving POC/SPM ratio to assess spatio-temporal variability. The English Channel and the Black Sea were selected to observe the spatio-temporal changes of water groups. The dynamic variation of 3 defined water groups is consistent with the general features which were documented in the literature such as the regional patterns of phytoplankton bloom and their temporal variability.

It is shown here that the water groups derived from POC/SPM ratio can be useful to observe the long and short term variability of particulate assemblage in coastal water. For future works, time-series data of hydrology and meteorology parameters such as water discharge, wave and current of some estuaries could be used in combination with POC/SPM proxy to study the coupling between physical and biological processes (e.g. river plume dispersion, re-suspension, bloom extension). It will be also interesting to study the spatio-temporal variability of the particulate assemblage using hydrodynamic models as for example Princeton Ocean Model in the Eastern English Channel (Sentchev and Korotenko 2007). The POC/SPM is available for the MERIS archive (2002-2012) over coastal waters from the ANR GlobCoast. A future study will consist in exanimating trends in terms of seasonal variability, irregular and regular variability, and long term trend using for example the Census-X-11 time series decomposition method (Loisel et al. 2014; Vantrepotte et al. 2011; Vantrepotte and Mélin 2011).

Furthermore, it would be interesting to perform comparisons of the distribution of the optical classes defined herewith that performed using another proxy (e.g. POC/SPM based approach, see chapter 4) in order to assess the complementarity in the information provided by these different partitions of the coastal water domain.

List of References

Reference List

Annick Bricaud, M.B., Andre Morel, and Herve Claustre (1995). Variability in the chlorophyll-specific absorption coefficients of natural phytoplankton: Analysis and parameterization. *Journal of Geophysical Research, 100*, 13,321-313,332

Aumont, O., Ethé, C., Tagliabue, A., Bopp, L., & Gehlen, M. (2015). PISCES-v2: an ocean biogeochemical model for carbon and ecosystem studies. *Geoscientific Model Development, 8*, 2465-2513

Babin, M., Morel, A., Fournier-Sicre, V., Fell, F., & Stramski, D. (2003a). Light scattering properties of marine particles in coastal and open ocean waters as related to the particle mass concentration. *Limnol. Oceanogr., 48*, 843–859

Babin, M., Morel, A., Fournier-Sicre, V., Fell, F., & Stramski, D. (2003b). Light scattering properties of marine particles in coastal and open ocean waters as related to the particle mass concentration. *Limnol. Oceanogr., 48(2)*, 843–859

Babin, M., & Stramski, D. (2004). Variations in the mass-specific absorption coefficient of mineral particles suspended in water. *Limnol. Oceanogr., 49(3)*, 756–767

Babin, M., Stramski, D., Ferrari, G.M., Claustre, H., Bricaud, A., Obolensky, G., & Hoepffner, N. (2003c). Variations in the light absorption coefficients of phytoplankton, nonalgal particles, and dissolved organic matter in coastal waters around Europe. *Journal of Geophysical Research, 108*

Baker, K.S., & Smith, R.C. (1982). Bio-optical classification and model of natural waters. 21*, 27*, 500-509

Barrón, C., & Duarte, C.M. (2015). Dissolved organic carbon pools and export from the coastal ocean. *Global Biogeochemical Cycles, 29*, 1725-1738

Bauer, J.E., Cai, W.J., Raymond, P.A., Bianchi, T.S., Hopkinson, C.S., & Regnier, P.A. (2013). The changing carbon cycle of the coastal ocean. *Nature, 504*, 61-70

Behrenfeld, M., & Boss, E. (2003). The beam attenuation to chlorophyll ratio: An optical index of phytoplankton physiology in the surface ocean? *Deep Sea Research Part I Oceanographic Research Papers, 50*, 1537-1549

Bélanger, S., Babin, M., & Larouche, P. (2008). An empirical ocean color algorithm for estimating the contribution of chromophoric dissolved organic matter to total light absorption in optically complex waters. *Journal of Geophysical Research, 113*

Bonato, S., Christaki, U., Lefebvre, A., Lizon, F., Thyssen, M., & Artigas, L.F. (2015). High spatial variability of phytoplankton assessed by flow cytometry, in a dynamic productive coastal area, in spring: The eastern English Channel. *Estuarine, Coastal and Shelf Science, 154*, 214-223

Boss, E., Stramski, D., Bergmann, T., Pegau, W., & Lewis, M. (2004). Why Should We Measure the Optical Backscattering Coefficient? *Oceanography (Washington D.C.), 17*

Breton, E. (2000). Annual variations of phytoplankton biomass in the Eastern English Channel: comparison by pigment signatures and microscopic counts. *Journal of Plankton Research - J PLANKTON RES, 22*, 1423-1440

Bricaud, A., Morel, A., Babin, M., Allali, K., & Claustre, H. (1998). Variations of light absorption by suspended particles with chlorophyllaconcentration in oceanic (case 1) waters: Analysis and implications for bio-optical models. *Journal of Geophysical Research: Oceans, 103*, 31033-31044

Brown, C., Huot, Y., Werdell, P., Gentili, B., & Claustre, H. (2008). The origin and global distribution of second order variability in satellite ocean color and its potential applications to algorithm development. *Remote Sensing of Environment, 112*, 4186-4203

Brunet, C., Brylinski, J.M., Bodineau, L., Thoumelin, G., Bentley, D., & Hilde, D. (1996). Phytoplankton Dynamics During the Spring Bloom in the South-eastern English Channel. *Estuarine, Coastal and Shelf Science, 43*, 469-483

Burnett, W.C., Bokuniewicz, H., Huettel, M., Moore, W.S., & Taniguchi, M. (2003). Groundwater and pore water inputs to the coastal zone. *Biogeochemistry, 66*, 3-33

Cauwet, G. (2002). Chapter 12 - DOM in the Coastal Zone. In D.A. Hansell, & C.A. Carlson (Eds.), *Biogeochemistry of Marine Dissolved Organic Matter* (pp. 579-609). San Diego: Academic Press

Claustre, H., Sciandra, A., & Vaulot, D. (2008). Introduction to the special section bio-optical and biogeochemical conditions in the South East Pacific in late 2004: the BIOSOPE program. *Biogeosciences, 5*, 679-691

Cokacar, T., Kubilay, N., & Oguz, T. (2001). Structure of Emiliania huxleyi blooms in the Black Sea surface waters as detected by SeaWIFS imagery. *Geophys. Res. Let., 28*, 4607-4610

Cokacar, T., Oguz, T., & Kubilay, N. (2003). Interannual variability of the early summer coccolithophore blooms in the Black Sea: Impacts of climatic factors. *Proceedings of SPIE - The International Society for Optical Engineering, 5155*

Cole, J.J., Prairie, Y.T., Caraco, N.F., McDowell, W.H., Tranvik, L.J., Striegl, R.G., Duarte, C.M., Kortelainen, P., Downing, J.A., Middelburg, J.J., & Melack, J. (2007). Plumbing the Global Carbon Cycle: Integrating Inland Waters into the Terrestrial Carbon Budget. *Ecosystems, 10*, 172-185

Coynel, A., Etcheber, H., Abril, G., Maneux, E., Dumas, J., & Hurtrez, J.-E. (2005). Contribution of small mountainous rivers to particulate organic carbon input in the Bay of Biscay. *Biogeochemistry, 74*, 151-171

D'Alimonte, D., Melin, F., Zibordi, G., & Berthon, J.F. (2003). Use of the novelty detection technique to identify the range of applicability of empirical ocean color algorithms. *IEEE Transactions on Geoscience and Remote Sensing, 41*, 2833-2843

Douillet, P., Ouillon, S., & Cordier, E. (2001). A numerical model for fine suspended sediment transport in the southwest lagoon of New Caledonia. *Coral Reefs, 20*, 361-372

Doxaran, D., Devred, E., & Babin, M. (2015). A 50 % increase in the mass of terrestrial particles delivered by the Mackenzie River into the Beaufort Sea (Canadian Arctic Ocean) over the last 10 years. *Biogeosciences, 12*, 3551-3565

Doxaran, D., Ehn, J., Bélanger, S., Matsuoka, A., Hooker, S., & Babin, M. (2012a). Optical characterisation of suspended particles in the Mackenzie River plume (Canadian Arctic Ocean) and implications for ocean colour remote sensing. *Biogeosciences, 9*, 3213-3229

Doxaran, D., Ehn, J., Bélanger, S., Matsuoka, A., Hooker, S., & Babin, M. (2012b). Remote sensing the dynamics of suspended particles in the Mackenzie River plume (Canadian Arctic Ocean). *Biogeosciences Discussions, 9*, 5205-5248

Duforêt-Gaurier, L., Dessailly, D., Moutier, W., & Loisel, H. (2018). Assessing the Impact of a Two-Layered Spherical Geometry of Phytoplankton Cells on the Bulk Backscattering Ratio of Marine Particulate Matter. *Applied Sciences, 8*

Duforêt-Gaurier, L., Loisel, H., Dessailly, D., Nordkvist, K., & Alvain, S. (2010). Estimates of particulate organic carbon over the euphotic depth from in situ measurements. Application to satellite data over the global ocean. *Deep Sea Research Part I: Oceanographic Research Papers, 57*, 351-367

Emmerton, C.A., Lesack, L.F.W., & Vincent, W.F. (2008). Nutrient and organic matter patterns across the Mackenzie River, estuary and shelf during the seasonal recession of sea-ice. *Journal of Marine Systems, 74*, 741-755

Evers-King, H., Martinez-Vicente, V., Brewin, R.J.W., Dall'Olmo, G., Hickman, A.E., Jackson, T., Kostadinov, T.S., Krasemann, H., Loisel, H., Röttgers, R., Roy, S., Stramski, D., Thomalla, S., Platt, T., & Sathyendranath, S. (2017). Validation and Intercomparison of Ocean Color Algorithms for Estimating Particulate Organic Carbon in the Oceans. *Frontiers in Marine Science, 4*

Falkowski, P., Scholes, R.J., Boyle, E., Canadell, J., Canfield, D., Elser, J., Gruber, N., Hibbard, K., Högberg, P., Linder, S., Mackenzie, F.T., Moore Iii, B., Pedersen, T., Rosenthal, Y., Seitzinger, S., Smetacek, V., & Steffen, W. (2000). The Global Carbon Cycle: A Test of Our Knowledge of Earth as a System. *Science, 290*, 291

Fettweis, X. (2007). Reconstruction of the 1979–2006 Greenland ice sheet surface mass balance using the regional climate model MAR. *The Cryosphere, 1*, 21-40

Garcia, V.M.T., Signorini, S., Garcia, C.A.E., & McClain, C.R. (2006). Empirical and semi-analytical chlorophyll algorithms in the south-western Atlantic coastal region (25–40°S and 60–45°W). *International Journal of Remote Sensing, 27*, 1539-1562

Gardner, W.D., Mishonov, A.V., & Richardson, M.J. (2006). Global POC concentrations from in-situ and satellite data. *Deep Sea Research Part II: Topical Studies in Oceanography, 53*, 718-740

Gomez, F., & Souissi, S. (2007). The distribution and life cycle of the dinoflagellate Spatulodinium pseudonoctiluca (Dinophyceae, Noctilucales) in the northeastern English Channel. *C R Biol, 330*, 231-236

Gower, J.F.R., Doerffer, R., & Borstad, G.A. (2010). Interpretation of the 685nm peak in water-leaving radiance spectra in terms of fluorescence, absorption and scattering, and its observation by MERIS. *International Journal of Remote Sensing, 20*, 1771-1786

Grattepanche, J.D., Breton, E., Brylinski, J.M., Lecuyer, E., & Christaki, U. (2010). Succession of primary producers and micrograzers in a coastal ecosystem dominated by Phaeocystis globosa blooms. *Journal of Plankton Research, 33*, 37-50

Grattepanche, J.D., Vincent, D., Breton, E., & Christaki, U. (2011). Microzooplankton herbivory during the diatom–Phaeocystis spring succession in the eastern English Channel. *Journal of Experimental Marine Biology and Ecology, 404*, 87-97

Han, B., Loisel, H., Vantrepotte, V., Mériaux, X., Bryère, P., Ouillon, S., Dessailly, D., Xing, Q., & Zhu, J. (2016). Development of a Semi-Analytical Algorithm for the Retrieval of Suspended Particulate Matter from Remote Sensing over Clear to Very Turbid Waters. *Remote Sensing, 8*, 211

Hu, S.B., Cao, W.X., Wang, G.F., Xu, Z.T., Lin, J.F., Zhao, W.J., Yang, Y.Z., Zhou, W., Sun, Z.H., & Yao, L.J. (2016). Comparison of MERIS, MODIS, SeaWiFS-derived particulate organic carbon, andin situmeasurements in the South China Sea. *International Journal of Remote Sensing, 37*, 1585-1600

IOCCG (2000). *Remote Sensing of Ocean Colour in Coastal, and Other Optically-Complex, Waters*. Dartmouth, Canada: IOCCG

IOCCG (2006). *Remote Sensing of Inherent Optical Properties: Fundamentals, Tests of Algorithms, and Applications*. Dartmouth, Canada: IOCCG

IOCCG (2008). *Why Ocean Colour? The Societal Benefits of Ocean-Colour Technology*. Dartmouth, Canada: IOCCG

Jamet, C., Loisel, H., Kuchinke, C.P., Ruddick, K., Zibordi, G., & Feng, H. (2011). Comparison of three SeaWiFS atmospheric correction algorithms for turbid waters using AERONET-OC measurements. *Remote Sensing of Environment, 115*, 1955-1965

Jensen, J.R. (2005). *Introductory Digital Image Processing: A Remote Sensing Perspective*. Prentice Hall

Jensen, J.R., & Lulla, K. (1987). Introductory digital image processing: A remote sensing perspective. *Geocarto International, 2*, 65-65

Keller, D.P., Lenton, A., Littleton, E.W., Oschlies, A., Scott, V., & Vaughan, N.E. (2018). The Effects of Carbon Dioxide Removal on the Carbon Cycle. *Curr Clim Change Rep, 4*, 250-265

Knap, A., Michaels, A., Close, A., Ducklow, H., & Dickson, A. (1996). Protocols for the Joint Global Ocean Flux Study (JGOFS) Core Measurements. *JGOFS Report, 19*, 170

Koestner, D., Stramski, D., & Reynolds, R. (2018). Measurements of the Volume Scattering Function and the Degree of Linear Polarization of Light Scattered by Contrasting Natural Assemblages of Marine Particles. *Applied Sciences, 8*

Koji, S., Motoaki, K., Kousei, S., Sei-ichi, S., & Toshiro, S. (1998). Chlorophyll-Specific Absorption Coefficients and Pigments of Phytoplankton off Sanriku, Northwestern North Pacific. *Journal of Oceanography, 54*, 517 to 526

Korotenko, K.A. (2018). Effects of mesoscale eddies on behavior of an oil spill resulting from an accidental deepwater blowout in the Black Sea: an assessment of the environmental impacts. *PeerJ, 6*, e5448

Le, C., Lehrter, J.C., Hu, C., MacIntyre, H., & Beck, M.W. (2016). Satellite observation of particulate organic carbon dynamics on the Louisiana continental shelf. *Journal of Geophysical Research: Oceans, 122*, 555-569

Le, C., Li, Y., Zha, Y., Sun, D., Huang, C., & Zhang, H. (2011). Remote estimation of chlorophyll a in optically complex waters based on optical classification. *Remote Sensing of Environment, 115*, 725-737

Le, C., Zhou, X., Hu, C., Lee, Z., Li, L., & Stramski, D. (2018a). A Color-Index-Based Empirical Algorithm for Determining Particulate Organic Carbon Concentration in the Ocean From Satellite Observations. *Journal of Geophysical Research: Oceans*

Le, C., Zhou, X., Hu, C., Lee, Z., Li, L., & Stramski, D. (2018b). A Color-Index-Based Empirical Algorithm for Determining Particulate Organic Carbon Concentration in the Ocean From Satellite Observations. *Journal of Geophysical Research: Oceans, 123*, 7407-7419

Leathers, R., Downes, T., & Mobley, C. (2004). Self-shading correction for oceanographic upwelling radiometers. *Optics Express, 12*, 4709-4718

Leblanc, K., Cornet, V., Rimmelin-Maury, P., Grosso, O., Hélias-Nunige, S., Brunet, C., Claustre, H., Ras, J., Leblond, N., & Quéguiner, B. (2018). Silicon cycle in the tropical South Pacific: contribution to the global Si cycle and evidence for an active pico-sized siliceous plankton. *Biogeosciences, 15*, 5595-5620

Lefebvre, A., Guiselin, N., Barbet, F., & Artigas, F.L. (2011). Long-term hydrological and phytoplankton monitoring (1992–2007) of three potentially eutrophic systems in the eastern English Channel and the Southern Bight of the North Sea. *ICES Journal of Marine Science, 68*, 2029-2043

Liu, D., Pan, D., Bai, Y., He, X., Wang, D., Wei, J.-A., & Zhang, L. (2015). Remote Sensing Observation of Particulate Organic Carbon in the Pearl River Estuary. *Remote Sensing, 7*, 8683-8704

Loisel, H. (2017). Atmospheric correction of meris for coastal water using Polymer *Presentation: validation Copernicus sentinel data using FRM 12 Jue 2017 , Plymouth UK.*

Loisel, H., Bosc, E., Stramski, D., Oubelkheir, K., & Deschamps, P.Y. (2001). Seasonal variability of the backscattering coefficient in the Mediterranean Sea based on satellite SeaWiFS imagery. *Geophysical Research Letters, 28*, 4203-4206

Loisel, H., Mangin, A., Vantrepotte, V., Dessailly, D., Dinh, D.N., Garnesson, P., Ouillon, S., Lefebvre, J.-P., XavierMériaux, & Phan, T.M. (2014). Variability of suspended particulate matter concentration in coastal waters under the Mekong's influence from ocean color (MERIS) remote sensing over the last decade. *Remote Sensing of Environment 150, 150*, 218–230

Loisel, H., Meriaux, X., Berthon, J.-F.o., & Poteau, A. (2007). Investigation of the optical backscattering to scattering ratio of marine particles in relation to their biogeochemical composition in the eastern English Channel and southern North Sea. *Limnology and Oceanography, 52-2*, 739–752

Loisel, H., & Morel, A. (1998). Light scattering and chlorophyll concentration in case 1 waters: A reexamination. *Limnology and Oceanography, 43*, 847-858

Loisel, H., Nicolas, J.-M., Deschamps, P.-Y., & Frouin, R. (2002). Seasonal and inter-annual variability of particulate organic matter in the global ocean. *Geophysical Research Letters, 29*, 49-41-49-44

Loisel, H., Stramski, D., Dessailly, D., Jamet, C., Li, L., & Reynolds, R.A. (2018). An Inverse Model for Estimating the Optical Absorption and Backscattering Coefficients of Seawater From Remote-Sensing Reflectance Over a Broad Range of Oceanic and Coastal Marine Environments. *Journal of Geophysical Research: Oceans, 123*, 2141-2171

Loisel, H., Vantrepotte, V., Jamet, C., & Ngoc Dat, D. (2013). *Challenges and New Advances in Ocean Color Remote Sensing of Coastal Waters*. INTECH

Loisel, H., Vantrepotte, V., Norkvist, K., Mériaux, X., Kheireddine, M., Ras, J., Pujo-Pay, M., Combet, Y., Leblanc, K., Dall'Olmo, G., Mauriac, R., Dessailly, D., & Moutin, T. (2011). Characterization of the bio-optical anomaly and diurnal variability of particulate matter, as seen from scattering and backscattering coefficients, in ultra-oligotrophic eddies of the Mediterranean Sea. *Biogeosciences, 8*, 3295-3317

Loisel, H., Vantrepotte, V., Ouillon, S., Ngoc, D.D., Herrmann, M., Tran, V., Mériaux, X., Dessailly, D., Jamet, C., Duhaut, T., Nguyen, H.H., & Van Nguyen, T. (2017). Assessment and analysis of the chlorophyll- a concentration variability over the Vietnamese coastal waters from the MERIS ocean color sensor (2002–2012). *Remote Sensing of Environment, 190*, 217-232

Lubac, B., & Loisel, H. (2007). Variability and classification of remote sensing reflectance spectra in the eastern English Channel and southern North Sea. *Remote Sensing of Environment, 110*, 45-58

Lubac, B., Loisel, H., Guiselin, N., Astoreca, R., Felipe Artigas, L., & Mériaux, X. (2008). Hyperspectral and multispectral ocean color inversions to detectPhaeocystis globosablooms in coastal waters. *Journal of Geophysical Research, 113*

Manolakis, D.G., Lockwood, R.B., & Cooley, T.W. (2016). *Hyperspectral Imaging Remote Sensing: Physics, Sensors, and Algorithms*. Cambridge: Cambridge University Press

Mélin, F., & Vantrepotte, V. (2015). How optically diverse is the coastal ocean? *Remote Sensing of Environment, 160*, 235-251

Miladinova, S., Adolf, S., Diego, M.M., & Elisa, G.G. (2017a). Revised Black Sea ecosystem model. *Conference Proceedings*

Miladinova, S., Garcia-Gorriz, E., Macias Moy, D., & Stips, A. (2016). Black Sea ecosystem model: Setup and validation. *JRC Technical Report, EU publications, EUR 27786*

Miladinova, S., Stips, A., Garcia-Gorriz, E., & Macias Moy, D. (2017b). Black Sea thermohaline properties: Long-term trends and variations. *J Geophys Res Oceans, 122*, 5624-5644

Mishonov, A.V., Gardner, W.D., & Jo Richardson, M. (2003). Remote sensing and surface POC concentration in the South Atlantic. *Deep Sea Research Part II: Topical Studies in Oceanography, 50*, 2997-3015

Mitchell, B.G., Bricaud, A., Carder, K., Cleveland, J., Ferrari, G., Gould, R., Kahru, M., Kishino, M., Maske, H., Moisan, T., Moore, L., Nelson, N., Phinney, D., Reynolds, R., Sosik, H., Stramski, D., Tassan, S., Trees, C., Weidemann, A., & Vodacek, A. (2000). Determination of spectral absorption coefficients of particles, dissolved material and phytoplankton for discrete water samples. *NASA Technical Memorandum*, 125-153

Mobley, C. (1994). *Light and Water: Radiative Transfer in Natural Waters.*

Mobley, C., Boss, E., & Roesler, C. (2010). Ocean Optics Web Book. http://www.oceanopticsbook.info/

Monolisha, S., Platt, T., Sathyendranath, S., Jayasankar, J., George, G., & Jackson, T. (2018). Optical Classification of the Coastal Waters of the Northern Indian Ocean. *Frontiers in Marine Science, 5*

Moore, T.S., Campbell, J.W., & Dowell, M.D. (2009). A class-based approach to characterizing and mapping the uncertainty of the MODIS ocean chlorophyll product. *Remote Sensing of Environment, 113*, 2424-2430

Moore, T.S., Campbell, J.W., & Hui, F. (2001). A fuzzy logic classification scheme for selecting and blending satellite ocean color algorithms. *IEEE Transactions on Geoscience and Remote Sensing, 39*, 1764-1776

Morel, A., & Prieur, L. (1977). Analysis of variations in ocean color1*, 22*, 709-722

Mueller, J., Morel, A., Frouin, R., Davis, C., Arnone, R., Carder, K., Lee, Z.P., Steward, R.G., Hooker, S., Mobley, C., McLean, S., Holben, B., Miller, M., Pietras, C., Knobelspiesse, K., Fargion, G., Porter, J., & Voss, K. (2003). *Ocean Optics Protocols for Satellite Ocean Color Sensor Validation, Revision 4, Volume III: Radiometric Measurements and Data Analysis Protocols.*

Nechad, B., Ruddick, K.G., & Park, Y. (2010). Calibration and validation of a generic multisensor algorithm for mapping of total suspended matter in turbid waters. *Remote Sensing of Environment, 114*, 854-866

Neukermans, G., Loisel, H., Me´riaux, X., Astoreca, R., & McKee, D. (2012). In situ variability of mass-specific beam attenuation and backscattering of marine particles with respect to particle size, density, and composition. *Limnol. Oceanogr., 57(1)*, 124–144

Neukermans, G., Reynolds, R.A., & Stramski, D. (2016). Optical classification and characterization of marine particle assemblages within the western Arctic Ocean. *Limnology and Oceanography, 61*, 1472-1494

Novoa, S., Doxaran, D., Ody, A., Vanhellemont, Q., Lafon, V., Lubac, B., & Gernez, P. (2017). Atmospheric Corrections and Multi-Conditional Algorithm for Multi-Sensor Remote Sensing of Suspended Particulate Matter in Low-to-High Turbidity Levels Coastal Waters. *Remote Sensing, 9*

O'Reilly, J.E., Maritorena, S., Mitchell, B.G., Siegel, D.A., Carder, K.L., Garver, S.A., Kahru, M., & McClain, C. (1998). Ocean color chlorophyll algorithms for SeaWiFS. *Journal of Geophysical Research: Oceans, 103*, 24937-24953

O’Reilly, J.E., Maritorena, S.e., O’Brien, M.C., Siegel, D.A., Toole, D., Menzies, D., & Smith, R.C. SeaWiFS Postlaunch Calibration and Validation Analyses. *Part 3. NASA Tech. Memo. 2000-206892, 11*

Oguz, T., & Ediger, D. (2006). Comparision of in situ and satellite-derived chlorophyll pigment concentrations, and impact of phytoplankton bloom on the suboxic layer structure in the western Black Sea during May–June 2001. *Deep Sea Research Part II: Topical Studies in Oceanography, 53*, 1923-1933

Pabi, S., & Arrigo, K.R. (2006). Satellite estimation of marine particulate organic carbon in waters dominated by different phytoplankton taxa. *Journal of Geophysical Research, 111*

Platt, T., & Sathyendranath, S. (1988). Oceanic Primary Production: Estimation by Remote Sensing at Local and Regional Scales. *Science, 241*, 1613-1620

Raymond, P.A., Hartmann, J., Lauerwald, R., Sobek, S., McDonald, C., Hoover, M., Butman, D., Striegl, R., Mayorga, E., Humborg, C., Kortelainen, P., Durr, H., Meybeck, M., Ciais, P., & Guth, P. (2013). Global carbon dioxide emissions from inland waters. *Nature, 503*, 355-359

Reynolds, R.A., & Stramski, D. (2019). Optical characterization of marine phytoplankton assemblages within surface waters of the western Arctic Ocean. *Limnology and Oceanography*

Reynolds, R.A., Stramski, D., & Neukermans, G. (2016). Optical backscattering by particles in Arctic seawater and relationships to particle mass concentration, size distribution, and bulk composition. *Limnology and Oceanography, 61*, 1869-1890

Robinson, W., Franz, B., Patt, F., Bailey, S., & Werdell, J. (2003). Masks and flags updates. *NASA Technical Memorandum - SeaWIFS Postlaunch Technical Report Series, 22*, 34-40

Rousseeuw, P.J. (1987). Silhouettes: A graphical aid to the interpretation and validation of cluster analysis. *Journal of Computational and Applied Mathematics, 20*, 53-65

Schapira, M., Vincent, D., Gentilhomme, V., & Seuront, L. (2008). Temporal patterns of phytoplankton assemblages, size spectra and diversity during the wane of a Phaeocystis globosa spring bloom in hydrologically contrasted coastal waters. *Journal of The Marine Biological Association of The United Kingdom - J MAR BIOL ASSN UK, 88*

Schlesinger, W., & Bernhardt, E. (2013). Biogeochemistry: An Analysis of Global Change, Third Edition. *Biogeochemistry: An Analysis of Global Change, Third Edition*, 1-672

Seegers, B.N., Stumpf, R.P., Schaeffer, B.A., Loftin, K.A., & Werdell, P.J. (2018). Performance metrics for the assessment of satellite data products: an ocean color case study. *Optics Express, 26*, 7404-7422

Sentchev, A., & Korotenko, K. (2007). Modelling distribution of flounder larvae in the eastern English Channel: sensitivity to physical forcing and biological behaviour. *Marine Ecology Progress Series, 347*, 233-245

Shen, Q., Li, J., Zhang, F., Sun, X., Li, J., Li, W., & Zhang, B. (2015). Classification of Several Optically Complex Waters in China Using in Situ Remote Sensing Reflectance. *Remote Sensing, 7*, 14731-14756

Snyder, W., Arnone, R., Davis, C., Goode, W., Gould, R., Ladner, S., Lamela, G., Rhea, W., Stavn, R., Sydor, M., & Weidemann, A. (2008). Optical scattering and backscattering by organic and inorganic particulates in US coastal waters. *APPLIED OPTICS, 47*, 666-677

Sohn, Y., & Rebello, N. (2002). Supervised and Unsupervised Spectral Angle Classifiers. *Photogrammetric Engineering and Remote Sensing, 68*

Son, Y.B., Gardner, W.D., Mishonov, A.V., & Richardson, M.J. (2009). Multispectral remote-sensing algorithms for particulate organic carbon (POC): The Gulf of Mexico. *Remote Sensing of Environment, 113*, 50-61

Stavn, R.H., & Richter, S.J. (2008). Biogeo-optics: particle optical properties and the partitioning of the spectral scattering coefficient of ocean waters. *Appl Opt, 47*, 2660-2679

Steinmetz, F., Deschamps, P.-Y., & Ramon, D. (2011). Atmospheric correction in presence of sun glint: application to MERIS. *Optics Express, 19*, 9783-9800

Stelmakh, L.V., & Gorbunova, T. (2018). Emiliania huxleyi blooms in the Black Sea: Influence of abiotic and biotic factors. *Botanica, 24*, 172-184

Stramska, M. (2009). Particulate organic carbon in the global ocean derived from SeaWiFS ocean color. *Deep Sea Research Part I: Oceanographic Research Papers, 56*, 1459-1470

Stramski, D., Babin, M., & Woz´niak, S.B. (2007). Variations in the optical properties of terrigenous mineral-rich particulate matter suspended in seawater. *Limnol. Oceanogr., 52(6)*, 2418–2433

Stramski, D., Boss, E., Bogucki, D., & Voss, K.J. (2004). The role of seawater constituents in light backscattering in the ocean. *Progress in Oceanography, 61*, 27-56

Stramski, D., Reynolds, R.A., Babin, M., Kaczmarek, S., Lewis, M.R., R¨ottgers, R., Sciandra, A., Stramska, M., Twardowski, M.S., Franz, B.A., & Claustre, H. (2008). Relationships between the surface concentration of particulate organic carbon and optical properties in the eastern South Pacific and eastern Atlantic Oceans. *Biogeosciences, 5*, 171–201

Stramski, D., Reynolds, R.A., Mati Kahru, & Mitchell, B.G. (1999). Estimation of Particulate Organic Carbon in the Ocean from Satellite Remote Sensing. www.sciencemag.org *SCIENCE, 285*

Świrgoń, M., & Stramska, M. (2015). Comparison of in situ and satellite ocean color determinations of particulate organic carbon concentration in the global ocean. *Oceanologia, 57*, 25-31

Toth, B., Weynants, M., Nemes, A., Mako, A., Bilas, G., & Toth, G. (2015). New generation of hydraulic pedotransfer functions for Europe. *Eur J Soil Sci, 66*, 226-238

Tran, T.K., Duforêt-Gaurier, L., Vantrepotte, V., Jorge, D.S.F., Mériaux, X., Cauvin, A., Fanton d'Andon, O., & Loisel, H. (2019). Deriving Particulate Organic Carbon in Coastal Waters from Remote Sensing: Inter-Comparison Exercise and Development of a Maximum Band-Ratio Approach. *Remote Sensing, 11*

Tranvik, L.J., Downing, J.A., Cotner, J.B., Loiselle, S.A., Striegl, R.G., Ballatore, T.J., Dillon, P., Finlay, K., Fortino, K., Knoll, L.B., Kortelainen, P.L., Kutser, T., Larsen, S., Laurion, I., Leech, D.M., McCallister, S.L., McKnight, D.M., Melack, J.M., Overholt, E., Porter, J.A., Prairie, Y., Renwick, W.H., Roland, F., Sherman, B.S., Schindler, D.W., Sobek, S., Tremblay, A., Vanni, M.J., Verschoor, A.M., von Wachenfeldt, E., & Weyhenmeyer, G.A. (2009). Lakes and reservoirs as regulators of carbon cycling and climate. *Limnology and Oceanography, 54*, 2298-2314

Twardowski, M.S., Boss, E., Macdonald, J.B., Pegau, W.S., Barnard, A.H., & Zaneveld, J.R.V. (2001). A model for estimating bulk refractive index from the optical backscattering ratio and the implications for understanding particle composition in case I and case II waters. *Journal of Geophysical Research: Oceans, 106*, 14129-14142

Vantrepotte, V. (2016). Global coastal CDOM and DOC temporal variability (MERIS 2002-2012). *Presentation: Ocean Optics conference October 23 - 28, 2016 at the Victoria in Victoria, British Columbia, Canada*

Vantrepotte, V., Brunet, C., Mériaux, X., Lécuyer, E., Vellucci, V., & Santer, R. (2007). Bio-optical properties of coastal waters in the Eastern English Channel. *Estuarine, Coastal and Shelf Science, 72*, 201-212

Vantrepotte, V., Danhiez, F.P., Loisel, H., Ouillon, S., Meriaux, X., Cauvin, A., & Dessailly, D. (2015). CDOM-DOC relationship in contrasted coastal waters: implication for DOC retrieval from ocean color remote sensing observation. *Opt Express, 23*, 33-54

Vantrepotte, V., Loisel, H., Dessailly, D., & Mériaux, X. (2012). Optical classification of contrasted coastal waters. *Remote Sensing of Environment, 123*, 306-323

Vantrepotte, V., Loisel, H., Mélin, F., Desailly, D., & Duforêt-Gaurier, L. (2011). Global particulate matter pool temporal variability over the SeaWiFS period (1997-2007). *Geophysical Research Letters, 38*

Vantrepotte, V., & Mélin, F. (2011). Inter-annual variations in the SeaWiFS global chlorophyll a concentration (1997–2007). *Deep Sea Research Part I: Oceanographic Research Papers, 58*, 429-441

Vincent, V., David, D., François, S., Didier, R., Bing, H., Xavier, M., Sylvain, O., Arand, C., & Cedric, J. Suspended particulate matter variability of the global coastal waters over the MERIS time period. *Ocen Optics XXIII, Victoria (Canada) 23-28, October 2016.*

Ward, N.D., Bianchi, T.S., Medeiros, P.M., Seidel, M., Richey, J.E., Keil, R.G., & Sawakuchi, H.O. (2017). Where Carbon Goes When Water Flows: Carbon Cycling across the Aquatic Continuum. *Frontiers in Marine Science, 4*

Willey, J.D., Kieber, R.J., Eyman, M.S., & Avery, G.B. (2000). Rainwater dissolved organic carbon: Concentrations and global flux. *Global Biogeochemical Cycles, 14*, 139-148

Woźniak, S.B. (2014). Simple statistical formulas for estimating biogeochemical properties of suspended particulate matter in the southern Baltic Sea potentially useful for optical remote sensing applications. *Oceanologia, 56*, 7-39

Woźniak, S.B., Darecki, M., Zabłocka, M., Burska, D., & Dera, J. (2016). New simple statistical formulas for estimating surface concentrations of suspended particulate matter (SPM) and particulate organic carbon (POC) from remote-sensing reflectance in the southern Baltic Sea. *Oceanologia, 58*, 161-175

Woźniak, S.B., Meler, J., Lednicka, B., Zdun, A., & Stoń-Egiert, J. (2011). Inherent optical properties of suspended particulate matter in the southern Baltic Sea. *Oceanologia, 53*, 691-729

Woźniak, S.B., Stramski, D., Stramska, M., Reynolds, R.A., Wright, V.M., Miksic, E.Y., Cichocka, M., & Cieplak, A.M. (2010). Optical variability of seawater in relation to particle concentration, composition, and size distribution in the nearshore marine environment at Imperial Beach, California. *Journal of Geophysical Research, 115*

Xing, X.-G., Zhao, D.-Z., Liu, Y.-G., Yang, J.-H., Xiu, P., & Wang, L. (2007). An overview of remote sensing of chlorophyll fluorescence. *Ocean Science Journal, 42*, 49-59

Ye, H., Li, J., Li, T., Shen, Q., Zhu, J., Wang, X., Zhang, F., Zhang, J., & Zhang, B. (2016). Spectral Classification of the Yellow Sea and Implications for Coastal Ocean Color Remote Sensing. *Remote Sensing, 8*, 321

Zhang, X., Hu, L., & He, M.-X. (2009). Scattering by pure seawater: Effect of salinity. *Optics Express, 17*, 5698-5710

Wollast, R. (1991), The coastal organic carbon cycle: Fluxes, sources, and sinks, in Ocean Margin Processes in Global Change, edited by R. F. C. Mantoura, J.-M. Martin, and R. Wollast, pp. 365–382, Wiley, Chichester, U. K.

THÈSE
DE L’UNIVERSITÉ DU LITTORAL CÔTE D’OPALE
Laboratoire d’Océanologie et de Géosciences

Présentée par
TRUNG KIEN TRAN

Pour obtenir le grade de Docteur en
SCIENCES DE LA TERRE, DE L'UNIVERS ET DE L'ESPACE: TERRE SOLIDE ET ENVELOPPES SUPERFICIELLES

Sujet de thèse

Observation du carbone organique particulaire et des assemblages de particules par télédétection dans les eaux côtières contrastées.

Soutenue le 16 Juin 2020
devant le jury composé de

Mr. David Doxaran, CNRS, LOV, France	Rapporteurs
Mr. Robert Frouin, CASPO, SIO, UC San Diego, USA	Rapporteurs
Mr. Bertrand Lubac, Université de Bordeaux, EPOC, France	Membres de jury
Mr. François Schmitt, CNRS, LOG, France	Membres de jury
Mr. Hubert Loisel, ULCO, LOG, France	Directeur de thèse
Mme. Lucile Duforêt-Gaurier, ULCO, LOG, France	Co-Directeur de thèse

Résumé

L’inversion des données satellites issues de la “couleur de l’eau” permet d’estimer depuis l’espace divers paramètres biogéochimiques dans l’océan. Différentes études ont montré la possibilité d’estimer la concentration en carbone organique particulaire (POC) dans l’océan ouvert, sur tout le globe, avec une précision satisfaisante. L’estimation de la concentration de POC dans les eaux côtières est une tâche plus complexe. En effet, les eaux côtières sont des environnements contrastés, caractérisés par des quantités importantes de particules en suspension et de matière dissoute, dont l’origine peut-être terrestre ou océanique. Le premier objectif de cette thèse était de développer une nouvelle approche pour estimer la concentration de POC dans les eaux côtières à l’échelle globale. Pour ce faire, un jeu de données in situ étendu a été utilisé. Ce jeu de données couvre une large gamme de concentrations de POC pour des environnements bio-optiques très différents. Douze algorithmes existants ont été testés. Les résultats montrent que leur performance dépend du type d’eau; elle est plus faible dans les eaux dominées par les minéraux. Aucun des algorithmes existants ne montre une performance satisfaisante sur une gamme étendue de concentration de POC. Par conséquent, une nouvelle approche a été mise au point, basée sur un rapport de réflectance (Rrs) dans plusieurs bandes spectrales. Les comparaisons entre mesures in situ et estimées de POC montrent que la performance est meilleure que les méthodes testées précédemment. Le nouvel algorithme a donc été appliqué à l’échelle régionale aux données MERIS sur les côtes de la Louisiane. Les estimations de POC sont comparables à celles obtenues avec l’algorithme de Lee et al., 2016, spécialement mis au point pour cette région. Le deuxième objectif de la thèse était d’examiner la classification des eaux côtières en utilisant différentes approches. Une classification à partir de la forme du spectre de Rrs a été proposée à partir d’un jeu de données étendu de mesures optiques, biogéochimiques et radiométriques coïncidentes. Six classes d’eau ont été définies fournissant ainsi une représentation plus fine des propriétés optiques des eaux côtières, que ce qui avait été obtenu précédemment par Vantrepotte et al., 2012. Une interprétation claire des environnements bio-optiques et biogéochimiques a été réalisée et les 6 classes ont été associées à un gradient de dilution des eaux turbides vers les eaux claires. Une autre classification des eaux côtières basée sur le rapport de la concentration de POC sur la concentration de particules en suspension (POC/SPM) (telle que proposée par Wozniak et al., 2010) a été ré-examinée. Dans la pratique, de nouveaux seuils ont été fixés sur le rapport POC/SPM pour fournir une distinction plus fine entre 3 types d’eau. Cette distinction discrimine les eaux dominées par la matière minérale, organique et les eaux mélangées. Les deux méthodes de classification ont été appliquées aux données MERIS en Manche/Mer du Nord pour la période allant de 2002-2012. La dynamique spatio-temporelle des types d’eau observée est cohérente avec celle connue dans cette région et induite par les changements saisonniers.

Mots-clés: carbone organique particulaire, couleur de l’eau, télédétection, eaux côtières, algorithmes bio-optique, classification optique, assemblages particulaires

Introduction

L'océan joue un rôle important dans le système climatique en stockant le carbone. Il permet ainsi de réguler la quantité de dioxyde de carbone (CO2) dans l'atmosphère. La quantité de carbone stockée dans l'océan est environ 50 fois plus importante que dans l'atmosphère (Siegenthaler et Sarmiento 1993). Le réservoir total de carbone à la surface de la Terre, au cours des 10 000 dernières années, est d'environ 40 000 Gt C. Environ 95 % (~ 38 000 Gt C) est stocké dans l'océan, principalement sous forme de carbone inorganique dissous (DIC) (Falkowski et al 2000 ; Schlesinger et Bernhardt 2013). Le cycle du carbone océanique est composé de processus qui échangent du carbone entre la colonne d'eau, l'atmosphère, l'intérieur de la Terre et le fond marin. Les principaux processus (ou pompes) qui assurent les échanges sont : la pompe biologique qui transfère le carbone de surface vers les fonds marins via le réseau trophique, et la pompe physique qui résulte de la circulation océanique. Les micro-organismes comme le phytoplancton sont des acteurs majeurs de la pompe biologique. Par photosynthèse, le phytoplancton fixe le carbone inorganique dissous (DIC) et les nutriments et produit, entre autres, du carbone organique particulaire (POC) et dissous (DOC). Ce processus est appelé production primaire. A noter que le POC et le DOC sont également produits par dégradation de la matière organique par la boucle microbienne. Le carbone organique particulaire contribue pour une faible part au pool de carbone océanique : 0,43 Gt C (Gardner et al. 2006) à la surface, environ 2,28 Gt C dans les premiers 200 mètres (Stramska, 2009), et 1,19 Gt C, dans la couche euphotique, respectivement (Duforêt-Gaurier et al. 2010). Malgré son stock relativement petit dans les eaux de l'océan ouvert, son taux de renouvellement élevé fait du POC un élément central du cycle du carbone océanique. La connaissance de la distribution et de la dynamique des concentrations de POC est en effet un paramètre clé pour étudier l'export biologique du carbone de la surface vers l'océan profond mais aussi le transfert de carbone à travers le réseau trophique marin.

Bien que les zones côtières ne couvrent que 7 % de la surface océanique, elles représentent des systèmes productifs et dynamiques avec environ 20 % de la production totale de matière organique océanique (Barrón et Duarte 2015). Les zones côtières sont également bien connues pour représenter 75 à 90 % du puits mondial de la charge fluviale en suspension dans laquelle se produit environ 15 % de la production primaire (Loisel et al. 2013). Les zones côtières comprennent les zones marines, estuariennes, fluviales et marécageuses. La zone côtière reçoit des apports de carbone organique des réservoirs terrestres principalement par le biais des rivières, des rejets d'eaux souterraines et de faibles apports de précipitations (Burnett et al. 2003 ; Cauwet 2002 ; Willey et al. 2000). Les apports de carbone organique fluvial dans l'océan côtier ont été estimés à environ 426 Tg C an^{-1}, dont 58,7% sont livrés sous forme de DOC et 41,3% sous forme de POC (Cauwet 2002). Le carbone organique peut être exporté de la côte vers l'océan sous forme de POC et de DOC. Les eaux côtières présentent un intérêt particulier, car elles constituent des zones d'échanges actifs entre les réservoirs terrestres et océaniques. Divers échantillonnages à bord des navires ont été effectués au cours des programmes internationaux pour mieux caractériser le stock permanent de POC et de DOC dans les eaux de l'océan ouvert ou côtières. Cependant, les mesures in situ se limitant à des prélèvements effectués dans certaines parties de l'océan, la détermination des stocks de matière organique particulaire et dissoute à l'échelle mondiale doit être établie à partir de l'extrapolation de données de terrain, réalisée à différentes échelles spatio-temporelles. Des études antérieures ont montré qu'il s'agit d'une tâche très difficile car les teneurs en carbone évaluées ne sont, dans de nombreux cas, que représentatives du contexte spatial et temporel de leur acquisition (Platt et Sathyendranath 1988).

Au cours des dernières années, des inversions de données de radiométrie par satellite (OCR) sur la couleur de l'océan ont permis de dériver des paramètres biogéochimiques depuis l'espace. L'un des principaux objectifs de la télédétection de la couleur de l'océan est de produire des champs synoptiques de concentration en chlorophylle a, un indice de la biomasse phytoplanctonique. Depuis le lancement du premier capteur de couleur de l'océan, CZCS en 1978, les capteurs de couleur de l'océan ont été augmentés en nombre et en complexité pour répondre aux demandes de la communauté scientifique. De nos jours, les capteurs satellitaires fournissent des mesures à haute fréquence avec une résolution spatiale suffisamment fine. Ce sont des outils très utiles et précieux car ils offrent une opportunité unique d'évaluer la variabilité saisonnière et interannuelle des paramètres biogéochimiques à l'échelle mondiale.

Au cours des dernières années, la communauté scientifique de la couleur de l'océan a progressé dans le développement d'algorithmes bio-optiques pour dériver des paramètres biogéochimiques, autres que la concentration en chlorophylle. Concernant le carbone organique particulaire, quelques algorithmes empiriques ou semi-empiriques ont été établis pour dériver la concentration de POC, à la fois à la surface (Gardner et al. 2006 ; Loisel et al. 2002 ; Mishonov et al. 2003 ; Pabi et Arrigo 2006 ; Son et al. al. 2009 ; Stramska 2009 ; Stramski et al. 2008 ; Stramski et al. 1999) et au sein des couches océaniques euphotiques (Duforêt-Gaurier et al. 2010) ou mixtes (Stramska 2009 ; Świrgoń et Stramska 2015). Ces algorithmes sont dédiés à l'océan ouvert et reposent sur le fait que la variabilité des propriétés optiques inhérentes est induite par le phytoplancton et son matériel associé (bactéries hétérotrophes, détritus et matière organique dissoute colorée). Les performances des différents algorithmes de POC disponibles pour les eaux océaniques ont été récemment évaluées (Evers-King et al. 2017). Les études ont montré que les approches empiriques basées sur les rapports de bandes (Stramski et al. 2008) et les approches semi-analytiques basées sur le coefficient de rétrodiffusion (bbp) et la concentration en chlorophylle-a (Chla) (Loisel et al., 2002) ont donné les meilleurs résultats. Si l'application de ces algorithmes aux observations OCR a permis d'étudier la variabilité spatio-temporelle des POC dans l'océan ouvert, de telles informations ne sont toujours pas disponibles pour les eaux côtières à l'échelle globales, qui sont des environnements bio-optiques plus complexes (Loisel et al. 2013). Pour améliorer notre compréhension de la dynamique du POC, des approches purement empiriques ont été récemment développées our estimer la concentration de POC en surface à partir de l'OCR. Elles ont été mises au point à partir de mesures in situ réalisées dans les eaux offshore et côtières (Hu et al. 2016 ; Le et al. 2018a ; Liu et al. 2015 ; Woźniak et al. 2016) ou exclusivement à partir de mesures collectées principalement dans des systèmes dominés par les rivières (Le et al. 2016) Cependant, ces algorithmes ont presque tous été développés à partir de jeux de de données limités rassemblés dans des régions spécifiques. Cela implique que les résultats et les performances de ces approches peuvent être fortement conditionnés par la représentativité du jeu de données utilisé pour leur développement lorsque ces méthodes sont appliquées à l'échelle globale. En d'autres termes, ces algorithmes peuvent ne pas être adaptés pour saisir la variabilité étendue du POC rencontrée dans les zones côtières optiquement contrastées.

Dans ce contexte, le premier objectif de cette recherche de doctorat (chapitre 2) visait à améliorer l'estimation de la concentration de POC dans les eaux côtières à l'échelle du globe (c'est-à-dire sur une large plage de concentration de POC). Comme expliqué ci-dessus, les eaux côtières présentent une complexité optique très élevée et l'analyse de la signature spectrale est une tâche fastidieuse et difficile. Par ailleurs, le développement de l'observation satellitaire des milieux côtiers doit faire face à d'autres enjeux clés comme la forte variabilité spatio-temporelle des processus hydrodynamiques et biologiques. Dans ce contexte, des algorithmes régionaux ont été développés ; chaque algorithme régional étant établi à partir de mesures in situ de paramètres optiques et biogéochimiques échantillonnés dans une zone donnée. Les approches régionales sont pratiques mais présentent des limites car elles dépendent de l'ensemble de données utilisées pour leur développement. Il en résulte que certains algorithmes développés à partir de mesures in situ échantillonnées dans des zones spécifiques peuvent montrer de bonnes performances pour certains types d'eaux et de mauvaises performances pour d'autres. Pour résumer, les algorithmes régionaux sont conditionnés à la représentativité de leur ensemble de données et ne sont potentiellement pas adaptés aux applications à l'échelle mondiale. L'influence des caractéristiques optiques de la masse d'eau sur les performances relatives des algorithmes bio-optiques a déjà été démontrée (Brown et al. 2008 ; Loisel et al. 2011 ; Woźniak et al.

2010). Une approche alternative vise à partitionner les eaux avec des caractéristiques optiques similaires et à développer un algorithme bio-optique spécifique pour chaque classe d'eau (Monolisha et al. 2018 ; Moore et al. 2009 ; Vantrepotte et al. 2012). Cela implique que les eaux côtières situées dans différentes régions peuvent présenter des caractéristiques bio-optiques similaires et ouvre potentiellement la voie à des applications à grande échelle. Des approches prometteuses ont été développées pour identifier les types d'eau optiques à partir d'un cadre dans lequel chaque type d'eau différent est automatiquement distingué, les uns des autres, en examinant des données de télédétection, comme par exemple la réflectance (Rrs) (Vantrepotte et al. 2012). Vantrepotte et al., 2012 ont développé une approche basée sur la classification basée sur Rrs pour récupérer la concentration de particules en suspension. Leur travail met en évidence le potentiel de l'approche basée sur les classes pour augmenter les performances de l'inversion de la matière particulaire en suspension (SPM). La matière particulaire en suspension est composée de particules à la fois organiques (organismes autotrophes, bactéries hétérotrophes et détritus) et minérales, d'un diamètre supérieur à 0,5-0,7 mm (Loisel et al. 2007). Dans leurs conclusions, les auteurs ont précisé que leurs résultats doivent être confirmés à partir d'un ensemble de données plus large. C'est l'objectif principal du chapitre 3. Dans ce contexte, nous avons construit un grand ensemble de données de paramètres optiques et biogéochimiques coïncidents pour appliquer une classification optique, basée sur les Rrs hyperspectrales, afin d'identifier les types d'eau optiques présents dans l'océan côtier.

Des informations sur la composition de l'assemblage de particules peuvent également être obtenues à partir du rapport POC/SPM, qui représente la fraction de la matière organique par rapport à l'assemblage total de matière particulaire en suspension (Babin et al. 2003b; Emmerton et al. 2008; Koestner et al. 2018 ; Lubac et Loisel 2007 ; Neukermans et al. 2016 ; Reynolds et Stramski 2019 ; Reynolds et al. 2016 ; Stramski et al. 2007 ; Stramski et al. 2008 ; Woźniak 2014 ; Woźniak et al. 2016 ; Woźniak et al. 2011 ; Woźniak et al. 2010). À partir de données in situ dans l'environnement marin près du rivage à Imperial Beach, en Californie, Woźniak et al. 2010 a fixé des valeurs seuils sur le rapport POC/SPM pour identifier les changements dans l'assemblage particulaire, de la dominance des particules minérales à la dominance des particules organiques, en considérant également les eaux composées de particules mixtes. Ces catégories représentent des divisions arbitraires mais fournissent un moyen utile pour classer les assemblages de particules et à partir des paramètres désormais disponibles dans les eaux côtières fournis par les mesures satellites. L'objectif du chapitre 4 est de réexaminer la pertinence des seuils POC/SPM sur un vaste ensemble de données in situ couvrant une gamme plus large de variabilité optique et biogéochimique que l'ensemble de données précédemment utilisé par Woźniak et al. 2010. Ensuite, nous étudierons la nature de l'assemblage de particules à partir des données MERIS sur deux zones côtières : la Manche et la mer Noire connues pour leur grande variabilité dans l'assemblage et la dynamique des particules. Les concentrations de POC seront dérivées à l'aide de l'algorithme développé au chapitre 2, tandis que les concentrations de SPM seront estimées à l'aide des algorithmes récemment développés de Han et al., 2016. Pour résumer, cette thèse est organisée comme suit : Le chapitre 1 introduira le formalisme utilisé en optique marine et présentera tous les paramètres utilisés dans cette étude avec leurs acronymes respectifs. Le chapitre 2 étudie les performances des algorithmes POC historiques pour les eaux côtières et présente le nouvel algorithme POC pour les eaux côtières. Dans le chapitre 3, la classification optique est appliquée pour identifier les types d'eau optiques présents dans l'océan côtier. Au chapitre 4, nous réexaminons l'utilisation du rapport POC/SPM pour la partition. Les conclusions générales et les perspectives de ce travail sont résumées dans le chapitre 5. Ce travail a donné lieu à 1 publication évaluée par des pairs, qui est disponible en libre accès :

Tran, T.K., Duforêt-Gaurier, L., Vantrepotte, V., Jorge, D.S.F., Mériaux, X., Cauvin, A., Fantond'Andon, O., &Loisel, H. (2019). Deriving Particulate Organic Carbon in Coastal Waters from Remote Sensing: Inter-Comparison Exercise and Development of a Maximum Band-Ratio Approach. Remote Sensing, 1111(23), 2849; https://doi.org/10.3390/rs11232849.

Chapitre 1 : Constituants de l'eau de mer, propriétés optiques inhérentes et apparentes : définitions

Dans ce chapitre, une brève revue de la théorie de l'optique océanique est présentée. Les définitions fondamentales des propriétés optiques inhérentes et apparentes (IOPs et AOP) et du constituant de l'eau sont présentées. Les constituants naturels de l'eau de mer sont les molécules d'eau et le sel dissous, la matière organique dissoute (également appelée gelbstoff, substance jaune ou matière organique dissoute colorée - CDOM) et la matière particulaire en suspension (SPM). Les SPM comprennent à la fois des particules inorganiques (minéraux) et organiques (phytoplancton, particules détritiques, bactéries et virus) (IOCCG 2000). Les fractions organiques et inorganiques de SPM sont respectivement POM et PIM. La présence de ces constituants et les variations de leur concentration et de leurs propriétés physico-chimiques (structure interne, composition chimique, granulométrie) modifient la couleur de l'eau. En effet, la couleur de l'eau est déterminée par la diffusion et l'absorption du champ lumineux dans la partie visible du spectre (400-700 nm) (IOCCG 2006). Les variations spectrales qui apportent des informations qualitatives et quantitatives sur les constituants de l'eau peuvent être mesurées par des radiomètres fournissant ainsi la base de la radiométrie spectrale, également appelée radiométrie de la couleur de l'océan (OCR) ou simplement couleur de l'océan (IOCCG 2008). La radiométrie de la couleur de l'océan est utilisée pour déduire des informations sur les écosystèmes marins à travers les estimations d'indicateurs, tels que la concentration en chlorophylle. Les propriétés optiques de l'eau sont divisées en deux classes : les propriétés optiques inhérentes et apparentes. Les propriétés optiques inhérentes (IOPs) sont des propriétés qui dépendent uniquement du milieu et sont donc indépendantes du champ de lumière ambiante dans le milieu. Les deux IOPs fondamentales sont le coefficient d'absorption et la fonction de diffusion volumique. Les propriétés optiques inhérentes à l'océanographie optique sont les coefficients d'absorption et de diffusion, qui sont respectivement l'absorbance et la diffusion par unité de distance. dans le milieu (Mobley 1994 ; Mobley et al. 2010). Les IOP dépendent de la concentration des particules et des substances dissoutes mais aussi de la composition chimique du pool de particules et des substances dissoutes, de la distribution granulométrique, de la structure interne et de la forme des particules. Les propriétés optiques apparentes (AOP) sont les propriétés qui (1) dépendent du milieu (les IOPs) et (2) de la structure géométrique (directionnelle) de la distribution de la luminance. Les AOPs couramment utilisées sont l'irradiance et la réflectance (Rrs), et le coefficients d'atténuation diffuse (Mobley et al. 2010).

Chapitre 2 : estimation du carbone organique particulaire dans les eaux côtières à partir de la télédétection : exercice d'intercomparaison et développement d'une nouvelle approche

Le POC est l'un des principaux réservoirs de carbone organique des océans, qui est composé de matière vivante (bactéries hétérotrophes, phytoplancton, zooplancton) et de détritus (c'est-à-dire de cellules non vivantes). Malgré son stock relativement petit dans les eaux océaniques ouvertes, son taux de renouvellement élevé fait du POC un élément central du cycle du carbone océanique. La connaissance de la distribution et de la dynamique des concentrations de POC est en effet un paramètre clé pour étudier l'export biologique du carbone de la surface vers l'océan profond mais aussi le transfert de carbone à travers le réseau trophique marin. En effet, étant le premier niveau de la chaîne trophique, la production de matière organique (et de carbone organique) par le phytoplancton soutient des niveaux trophiques et une diversité marine plus élevés. Ainsi, la quantité de POC est un indicateur de productivité dans la zone euphotique, et peut également être utilisée comme indicateur d'événements de pollution dans les zones côtières impactées par les activités humaines. Cette étude visait à améliorer l’estimation de la concentration de POC pour des applications à l'échelle mondiale dans les eaux côtières (c'est-à-dire sur une large plage de concentration de POC). À cette fin, nous avons rassemblé un vaste ensemble de données in situ représentant divers environnements côtiers bio-optiques contrastés à des latitudes basses, moyennes et élevées, avec diverses compositions chimiques de particules en vrac (à dominance minérale, 50% de l'ensemble de données, mixte, 40 %, ou à dominance organique, 10 %). L'ensemble de données comprend 606 mesures coïncidentes de la concentration de POC et de la réflectance de télédétection, Rrs, avec des concentrations de POC couvrant trois ordres de grandeur. Douze algorithmes existants ont ensuite été testés sur cet ensemble de données, et un nouveau a été proposé. Les résultats montrent que les performances des algorithmes historiques dépendent du type d'eau, avec une performance globalement faible observée pour les eaux à dominante minérale. De plus, aucun des algorithmes testés n'a fourni de résultats satisfaisants sur l'ensemble de la gamme POC.

Une nouvelle approche a ainsi été développée basée sur un ratio de bande maximum de Rrs (rapport rouge/bleu, rouge/jaune ou rouge/vert). Basé sur la métrique statistique standard pour l'évaluation des modèles inverses, le nouvel algorithme présente les meilleures performances. L'écart quadratique moyen pour les données transformées en log (RMSDlog) est de 0,25. La différence moyenne en pourcentage absolu (MAPD) est de 37,48 %. Les valeurs de biais moyen (MB) et de ratio médian (MR) sont respectivement de 0,54 µg L-1 et 1,02. Cet algorithme reproduit assez bien la distribution des données in situ. Le nouvel algorithme a également été testé sur un ensemble de données de correspondance rassemblant 154 Rrs MERIS (spectromètre d'imagerie à résolution moyenne) coïncidents et des concentrations de POC in situ échantillonnées le long de la côte française. L'analyse de correspondance a montré que les performances du nouvel algorithme sont satisfaisantes (RMSDlog = 0,24, MAPD = 34,16%, MR = 0,92). Un exercice régional appliquant ce modèle pour le plateau continental de la Louisiane montre que les concentrations moyennes mensuelles de POC dérivées de MERIS avec le nouvel algorithme sont cohérentes avec celles dérivées de l'algorithme 2016 de Le et al. qui a été spécialement développé pour cette région.

Chapitre 3 : Classification optique des eaux côtières

Ces dernières années, diverses approches visant à définir les types d'eau optiques de l'eau ont été documentées pour des applications sur les eaux ouvertes et côtières. Ces méthodes de classification optique ont été développées non seulement pour fournir une meilleure compréhension de la diversité optique de l'eau et de la variabilité des constituants dans l'eau, mais aussi pour potentiellement améliorer la précision des algorithmes de couleur de l'océan (Baker et Smith 1982 ; Garcia et al. 2006 ; Han et al. 2016 ; Le et al. 2011 ; Lubac et Loisel 2007 ; Mélin et Vantrepotte 2015 ; Monolisha et al. 2018 ; Moore et al. 2009 ; Shen et al. 2015 ; Tranvik et al. 2009 ; Vantrepotte et al. 2012 ; Ye et al. 2016). L'objectif de ce chapitre est : d'une part, de définir des types d'eaux optiques à partir d'un jeu de données étendu de spectres Rrs in situ couvrant différents écosystèmes côtiers (Manche-Sud de la mer du Nord, Gironde, Vietnam, Guyane française) et d'autre part, de mieux comprendre la signification bio-optique de chaque classe optique identifiée à partir de leurs signatures radiométriques. À cette fin, une approche de classification non supervisée a été utilisée pour répartir les spectres hyperspectraux Rrs in situ collectés dans diverses eaux côtières en classes distinctes. Le deuxième objectif est d'appliquer la classification optique aux données satellitaires dans les eaux côtières contrastées (données MERIS) afin d'évaluer l'applicabilité potentielle de nouvelles classes définies pour décrire la diversité optique des environnements côtiers. Sur la base d'une analyse groupée effectuée sur l'ensemble de données in situ étendu, 6 types d'eau optique représentant la diversité optique des eaux côtières des environnements très turbides (classe 1) aux eaux claires (classe 6) ont été définis. Ces 6 classes fournissent une description plus détaillée de la diversité optique des eaux côtières que celles obtenues à partir d'un jeu de données restreint par Vantrepotte et al. (2012), avec une classe supplémentaire correspondant au milieu d'eau claire (Classe 6) et une description plus précise des conditions de bloom phytoplanctonique (Classe 2 et Classe 4 dans les environnements d'eau peu profonde et offshore, respectivement).

Bien que les classes aient été définies à partir de spectres Rrs normalisés, elles ont montré une organisation remarquable de la classe 1 à la classe 6 avec un gradient décroissant en SPM, POC, bbp et CDOM et un gradient croissant dans les ratios aphy/ap, aCDOM/(aCDOM+ ap) et POC/ SPM. Cette définition claire des milieux bio-optiques biogéochimiques associés aux 6 classes optiques définies dans ce travail, qui peuvent être associées au premier ordre à un gradient de dilution des milieux turbides aux eaux claires, sont à cet égard plus claires que les résultats obtenus à partir de 4 classes obtenues dans l'étude de Vantrepotte et al. (2012). La classification selon ces 6 classes des données mensuelles MERIS a montré que les 6 classes suffisent à couvrir une large partie de la variabilité optique des eaux côtières, y compris sur des zones non prises en compte dans le jeu de données in situ qui a servi à développer la méthode de classification. L'examen de la distribution des classes MERIS illustre l'intérêt des classes optiques pour fournir des informations synthétiques sur la dynamique temporelle des eaux côtières optiques (et donc biogéochimiques).

Chapitre 4 : Partition optique des eaux côtières contrastées

Le présent chapitre vise à étudier la nature de l'assemblage de particules dans les eaux côtières sur la base du rapport POC/SPM. Avant d'utiliser le rapport POC/SPM pour identifier les classes d’eau (eau à dominance organique, mixte et minérale), nous avons ré-examiné les valeurs seuils à l'aide d'un vaste ensemble de données in situ couvrant une gamme plus large de variabilité optique et biogéochimique que l'ensemble de données précédent utilisé. par Woźniak et al. (2010). La pertinence des nouveaux seuils sera discutée en fonction du rapport bbp/cp dans le rouge (650 nm). Les estimations par télédétection du rapport POC/SPM ont également été testées par rapport aux mesures in situ avant les applications sur les données MERIS. Deux algorithmes bio-optiques récemment développés ont été utilisés pour dériver le POC (Tran et al. 2019, voir chapitre 2) et le SPM (Han et al. .2016)concentrations, puis rapport POC/SPM. Le rapport POC/SPM a ensuite été récupéré avec les données MERIS sur les eaux côtières mondiales. La Manche et la mer Noire ont été au centre de la discussion. Les algorithmes de Han et al. (2016) et Tran et al. (2019) ont été utilisés pour récupérer les concentrations de SPM et de POC à partir d'un ensemble de données de validation d'in situRrs, . Le rapport POC/SPM était soit surestimé, soit sous-estimé pour les eaux à dominance minérale. La surestimation peut être due aux estimations POC car une surestimation a été observée par Tran et al. (2019) sur les eaux à dominante minérale. Le RMSDlog = 0,35 est supérieur au RMSDlog (= 0,25) observé sur le POC dérivé du modèle, mais il est similaire au RMSDlog (= 0,31) observé sur les estimations SPM (Han et al., 2016). Le rapport POC sur SPM est soumis à deux sources d'erreurs car deux algorithmes bio-optiques sont utilisés, au lieu d'un seul algorithme lorsque seules les concentrations POC ou SPM sont dérivées. Cela peut expliquer pourquoi les incertitudes sur les POC/SPM sont plus élevées que les incertitudes sur les concentrations de POC ou de SPM. Une première application consistait à utiliser le rapport POC sur SPM pour diviser les assemblages de particules en groupes de base comme dans Woźniak et al. (2010). Les seuils fixés par Woźniak et al. (2010) ont été ré-examinés à partir d'un vaste ensemble de données in situ couvrant une gamme plus large de variabilité optique et biogéochimique que l'ensemble de données utilisé précédemment par Woźniak et al. (2010). La nouvelle valeur seuil pour les eaux à dominante minérale est fixée à 0,08, au lieu de 0. Pour les eaux à dominante organique, elle a été fixée à 0,2 et les eaux mixtes avec POC/SPM dans une plage de 0,08 à 0,2.

Les estimations de télédétection du rapport POC/SPM ont été dérivées des données MERIS sur la période 2002-2012 pour deux zones : la Manche orientale et le sud de la mer du Nord et la mer Noire. La dynamique spatio-temporelle des 3 types d'eau définis reste encore très pertinente face aux changements saisonniers survenant dans les masses d'eau des deux régions étudiées car elles sont cohérentes avec les caractéristiques générales précédemment documentées dans la littérature. Pour une future étude, il sera pertinent d'étudier comment la variabilité de l'assemblage particulaire et des paramètres biogéochimiques (Chla, POC et SPM) est influencée par les processus hydrodynamiques. L'idée serait d'utiliser des observations de propriétés physiques qui pourraient aider à identifier différentes masses d'eau telles que les courants océaniques et l'eau douce rejetée par les rivières, combinées à des estimations satellitaires de la température de surface de la mer. Il sera également intéressant d'étudier la variabilité spatio-temporelle de l'assemblage particulaire à l'aide de modèles hydrodynamiques tels que Princeton Ocean Model dans l'Est de la Manche (Sentchev et Korotenko 2007). Des cartes globales du rapport POC/SPM ont été générées et le coefficient de variation a été calculé pour les eaux côtières du globe. Une prochaine étape consistera à générer une climatologie POC/SPM sur des zones côtières spécifiques et à étudier les schémas de variation temporelle POC/SPM (variabilité irrégulière, variabilité saisonnière et tendance à long terme) en utilisant par exemple la méthode de décomposition des séries chronologiques Census-X-11. Les différents patrons spatio-temporels ont pu être analysés au regard des conditions océanographiques et hydrologiques régionales des zones considérées. Par exemple, une perspective intéressante sera de caractériser l'origine des processus contrôlant la saisonnalité du paramètre observé.

Conclusions générales et perspectives

Ce travail contribue aux études côtières de carbone organique particulier et vise également à contribuer à une meilleure caractérisation de la qualité optique des masses d'eau côtières à travers la classification des masses d'eau. Le premier objectif était d'estimer la concentration de POC côtiers à partir de mesures satellitaires dans les eaux côtières mondiales. La performance de 12 algorithmes historiques existants a été examinée. Grâce à l'exercice d'intercomparaison, les performances les plus élevées ont été observées pour l'algorithme du rapport des bandes bleu-vert de Hu et al. 2015 (Hu15-3). Cependant, Hu15-3 a tendance à fournir des valeurs sous-estimées pour une concentration de POC supérieure à 1000 g L-1, correspondant à des eaux à dominance minérale et des valeurs surestimées pour une concentration de POC inférieure à 1000 µg L-1. Le nouvel algorithme (CPOC) a ensuite été développé et validé à partir de deux ensembles de données in situ étendus indépendants (ensembles de données de développement et de validation) qui ont tous deux été échantillonnés dans différentes zones côtières et tous deux couvrent diverses conditions bio-optiques. Le nouvel algorithme est basé sur une relation empirique entre le POC et un rapport de bande maximum (MBR) max (Rrs(665)/Rrs(490), Rrs(665)/Rrs(510), Rrs(665)/Rrs(555)). Ces longueurs d'onde sont disponibles dans la plupart des capteurs de couleur océanique et l'utilisation de rapports de bande permet de passer d'un rapport de bande donné à un autre, évitant ainsi, dans certains cas, un rapport de bande faible et potentiellement bruyant. Ainsi, dans le contexte des applications satellitaires, il est attendu que l'utilisation du MBR au lieu d'un seul ratio de bande permette de maximiser la précision du modèle sur toute la plage de POC. En général, le nouvel algorithme POC améliore les performances sur une large gamme de concentrations POC et présente une meilleure précision (RMSDlog de 0,25, MAPD de 37,48%, MB de 0,54 g L-1 et MR de 1,02) par rapport à 12 algorithmes historiques. De plus, la classification optique des eaux côtières, selon la méthode présentée dans Vantrepotte et al., 2012, a été ré-examinée sur la base d'un ensemble de données in situ étendu couvrant diverses conditions bio-optiques et biogéochimiques. Six classes optiques d'eau ont été obtenues. Les classes 1 et 6 représentent la diversité optique des eaux côtières des milieux très turbides (classe 1) aux eaux claires (classe 6). Les classes 2 et 4 décrivent les conditions de prolifération de phytoplancton en eau peu profonde (classe 2) et en mer (classe 4). Les deux classes restantes (classes 3 et 5) sont liées à des situations optiquement mixtes avec une forte proportion de matière minérale particulaire. De plus, l'applicabilité de 6 classes a été démontrée en appliquant la présente classification sur les données mensuelles de MERIS. Les résultats ont montré que les 6 classes couvrent une large partie de la variabilité optique et fournissent non seulement des informations synthétiques sur la dynamique temporelle de la qualité optique des eaux côtières mais montrent également la variation de l'extension du panache fluvial. L'étude précédente de Vantrepotte et al., 2012 a démontré le potentiel de récupérer SPM à partir d'algorithmes d'inversion basés sur les classes. Il serait intéressant de définir si les classes optiques correspondantes peuvent fournir un cadre pertinent pour dériver des algorithmes d'inversion basés sur les classes prenant en compte la variabilité optique de l'environnement côtier dans le cadre de la procédure de développement de l'algorithme.

Une autre contribution clé de cette thèse de doctorat est qu'elle offre une approche globale pour évaluer le rapport POC/SPM en tant que proxy pour les masses d'eau. La relation entre le rapport POC/SPM et bbp/cp a été étudiée sur la base d'une large gamme de données POC/SPM in situ (0,001 – 0,87) qui ont été collectées dans diverses régions géographiques. L'ensemble de données in situ a été classé en 3 groupes : à dominante minérale (POC/SPM < 0,08), à dominante organique (POC/SPM > 0,2) et la masse d'eau mixte (0,08 mixed POC/SPM 0,2). En termes d'application satellitaire, deux algorithmes bio-optiques de POC (Tran et al. 2019) et SPM (Han et al. 2016) ont été traités en utilisant le même jeu de données d'images satellitaires (MERIS niveau 3, sur la période 2002-2012). pour récupérer le rapport POC/SPM pour évaluer la variabilité spatio-temporelle. La Manche et la Mer Noire ont été choisies pour observer les changements spatio-temporels des groupes d'eau. La variation dynamique de 3 groupes d'eau définis est cohérente avec les caractéristiques générales qui ont été documentées dans la littérature telles que les modèles régionaux de bloom phytoplanctonique et leur variabilité temporelle. Il est montré ici que les groupes d'eau dérivés du rapport POC/SPM peuvent être utiles pour observer la variabilité à long et à court terme de l'assemblage de particules dans les eaux côtières. Pour les travaux futurs, les données de séries chronologiques des paramètres hydrologiques et météorologiques tels que le débit d'eau, les vagues et le courant de certains estuaires pourraient être utilisées en combinaison avec le proxy POC/SPM pour étudier le couplage entre les processus physiques et biologiques (par exemple, la dispersion du panache des rivières, la re -suspension, extension de floraison). Il sera également intéressant d'étudier la variabilité spatio-temporelle de l'assemblage particulaire à l'aide de modèles hydrodynamiques comme par exemple le Princeton Ocean Model dans l'Est de la Manche (Sentchev et Korotenko 2007). Le POC/SPM est disponible pour les archives MERIS (2002-2012) sur les eaux côtières de l'ANR GlobCoast. Une future étude consistera à examiner les tendances en termes de variabilité saisonnière, de variabilité irrégulière et régulière, et de tendance à long terme en utilisant par exemple la méthode de décomposition des séries chronologiques Census-X-11 (Loisel et al. 2014 ; Vantrepotte et al. 2011 ; Vantrepotte et Mélin 2011). Par ailleurs, il serait intéressant d'effectuer des comparaisons de la distribution des classes optiques définies ci-après avec celle réalisée à l'aide d'un autre proxy (ex : approche basée sur POC/SPM, voir chapitre 4) afin d'évaluer la complémentarité des informations fournies par ces différentes partitions de le domaine des eaux côtières.